SMALL MOLECULE ACTIVATION BY IRIDIUM COMPLEXES SUPPORTED BY A MONOANIONIC *NNN*-PINCER LIGAND

SAM L. DRESCHER
Bachelor of Science, University of Lethbridge, 2020

A thesis submitted
in partial fulfillment of the requirements for the degree of

MASTER OF SCIENCE

in

CHEMISTRY

Department of Chemistry and Biochemistry
University of Lethbridge
LETHBRIDGE, ALBERTA, CANADA

SMALL MOLECULE ACTIVATION BY IRIDIUM COMPLEXES SUPPORTED BY A MONOANIONIC *NNN*-PINCER LIGAND

SAM L. DRESCHER

Date of Defence: May 26th, 2023

Dr. Paul G. Hayes Thesis Supervisor	Professor	PhD
Dr. René T. Boeré Thesis Examination Committee Member	Professor	PhD
Dr. Peter W. Dibble Thesis Examination Committee Member	Associate Professor	PhD
Dr. Robert Morris External Examiner University of Toronto Toronto, Ontario	Professor	PhD
Dr. Michael Gerken Chair, Thesis Examination Committee	Professor	PhD

DEDICATION

For Emily and Jesse, for others who lost the battle to mental illness, and for anyone who is fighting against their own brain:

It gets better.

ABSTRACT

The synthesis of iridium 1,5-cyclooctadiene and cyclooctene complexes supported by a monoanionic *NNN*-pincer ligand is described. The 1,5-cyclooctadiene complexes, ^{Ar}LIr(COD) (L = 2,5-(^{i}Pr$_2$P=NAr)$_2$C$_4$H$_2$N, Ar = Pipp, Dipp, Mes, COD = 1,5-cyclooctadiene) did not react with dihydrogen or silanes, precluding further work into catalytic processes, such as alkane dehydrogenation and hydrosilylation. As such, a more reactive species was sought. ^{Pipp}LIr(COE) (COE = cyclooctene) reacted with dihydrogen and silanes, allowing the synthesis of ^{Pipp}LIr(H)$_2$ and ^{Pipp}LIr(H)(SiR$_3$) (R$_3$ = Et$_3$, HPh$_2$, H$_2$Ph). These complexes were characterized by multinuclear (^{1}H, ^{13}C{^{1}H}, ^{29}Si, ^{31}P{^{1}H}) and 2-dimensional NMR spectroscopy, X-ray crystallography, and elemental analysis. Alternatives to ^{Pipp}LIr(COE), including ^{Pipp}LIr(CO), ^{Pipp}LIr(PPh$_3$), and others were investigated. This was undertaken to avoid competing reactivity with free COE in solution.

The efficacy of ^{Pipp}LIr(H)$_2$ and ^{Pipp}LIr(H)(SiR$_3$) (R$_3$ = Et$_3$, HPh$_2$, H$_2$Ph) as catalysts for alkene hydrogenation and alkane dehydrogenation, and hydrosilylation, respectively, was explored.

PREFACE

The work in this thesis could not have been completed alone. Shou-Jen Hsiang and Dr. Dylan Webb performed all elemental analyses of the newly reported iridium complexes in this thesis, the data for which is included in Chapter 6. Dr. Connor MacNeil acquired the X-ray crystal structure of ^{Pipp}LIr(COD) presented in section 2.1.1. Ash Aborawi first synthesized and characterized ^{Pipp}LIr(COD). All other work in this thesis was performed by the author, Sam L. Drescher.

ACKNOWLEDGEMENTS

To my mom: without your support I would not have made it this far. You helped me get back up through every cycle, every burn out, and every failure.

To my dad: despite the physical distance you supported me and pushed me to keep going when everything seemed impossible.

To my friends, Daisy, Dylan, Desmond, Ed, Jackson, Taylor, Taylor 2.0 (which one is which?), Felix, and Craig. Thank you for keeping me sane, even if we often consumed above the recommended weekly limit of alcohol. For all the much-needed distractions: Dungeons and Dragons, “cheeky pints”, ice cream, and so much more. Without all of you, this would not have been possible.

To the synthetic floor: thank you for letting me wander on over and distract you for who knows how long when I did not have the energy to do anything.

To my lab mates, past and current: thank you for helping me through a massive career change. For your help and support when I felt like I had no idea what organometallic chemistry was, I am thankful. Special shout out to Dylan; your patience throughout the learning process during my undergraduate research in chemistry allowed me to continue through to my M.Sc. I would not be the chemist I am today if it was not for you.

To the University of Lethbridge and the National Science and Engineering Council of Canada for funding and a Michael Smith Foreign Study Supplement, allowing me to go to UW – Madison for four months.

To everyone at UW – Madison, special shout out to Prof. J.M. Schomaker, Logan, Bob, Emily, Hillary, and Mahzad: thank you for the opportunities, friendship, and laughing at my weird Canadian mannerisms.

To my supervisor, Prof. Paul Hayes: Thank you for listening to my persistence and taking me on in my undergraduate degree, despite being in an entirely different program. Thank you for letting me continue through to my M.Sc., without these opportunities everything would be very different (and not for the better).

I would like to thank the MR Facility staff (Tony Montina, Michael Opyr, and Vincent Weiler) for the training and assistance in all of my not so complex and also complex experimentation. I would also like to thank Prof. René Boeré for the training, patience, and assistance with X-ray crystallography. Lastly, I would like to thank my committee members, Prof. René Boeré and Prof. Peter Dibble, as well as my external examiner Prof. Robert Morris.

TABLE OF CONTENTS

LIST OF TABLES

LIST OF FIGURES

LIST OF SCHEMES

LIST OF NEW COMPOUNDS

Chapter 2 Complexes

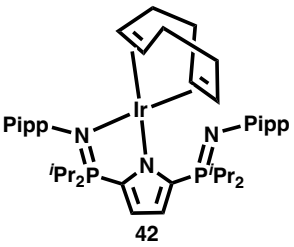

42

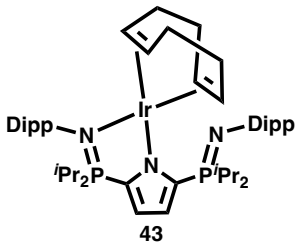

43

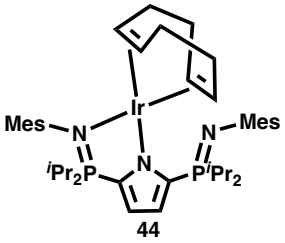

44

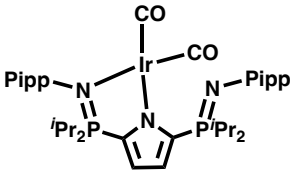

50

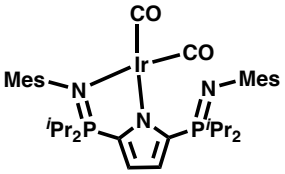

51

Chapter 3 Complexes

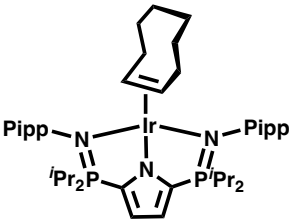

52

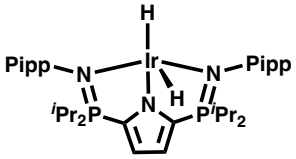

53

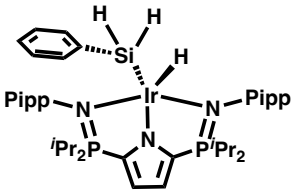

55

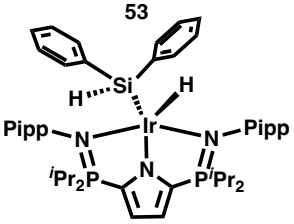

56

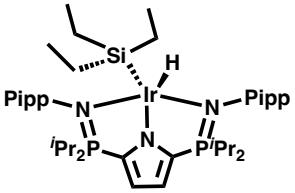

57

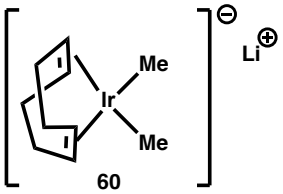

60

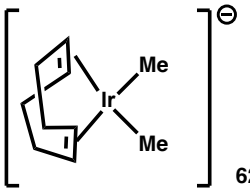

62

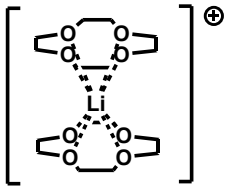

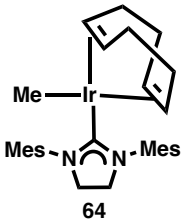

64

Chapter 4 Complexes

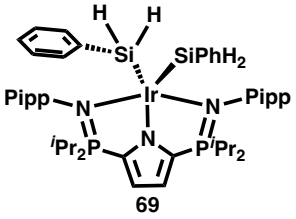

69

LIST OF SYMBOLS AND ABBREVATIONS

a, b, c, α, β, γ = crystallographic unit cell parameters
Ad = adamantyl
Anal. Cald. = analysis calculated
APT = attached proton test
Ar = aryl
cat. = catalyst
COA = cyclooctane
COD = 1,5-cyclooctadiene
COE = cyclooctene
COSY = correlated spectroscopy
DEPT = distortionless enhancement by polarization transfer
Dipp = 2,6-diisopropylphenyl
ee = enantiomeric excess
equiv = equivalent
g = gram(s)
h = hour(s)
HMBC = heteronuclear multiple bond coupling
HSQC = heteronuclear single quantum coherence
Hz = Hertz
^{i}Pr = isopropyl
IR = infrared
$^{n}J_{A\text{-}B}$ = coupling constant in Hertz between nuclei A and B separated by n bonds
K = Kelvin
k = reaction rate constant
L = ligand
ln = natural logarithm
Me = methyl
Mes = 2,4,6-trimethylphenyl
mg = milligram(s)
MHz = megaHertz
min = minutes
mL = millilitres
mmol = millimoles
mol% = percent of molar equivalents
nacnac = β-dikitiminato
NHC = *N*-heterocyclic carbene
^{n}Bu = *n*-butyl
NMR = nuclear magnetic resonance
°C = degrees Celcius
° = degrees
Pipp = *para*-isopropylphenyl
ppm = parts per million
RBF = round bottomed flask
R_1 = conventional agreement index
R^2 = coefficient of determination

SPS = solvent purification system
TBE = *tert*-butylethylene
^{t}Bu = *tert*-butyl
THF = tetrahydrofuran
TMS = tetramethylsilane
TOF = turnover frequency
TON = turnover number
Trip = 2,4,6-triisopropylphenyl
whh = width at half height in Hertz
wR_2 = weighed agreement index
Z = number of formula units per unit cell
Å = Angstroms
$\{^1H\}$ = proton decoupled
δ = chemical shift in parts per million
κ^n = denticity to order n
π = pi
σ = sigma
μ = micro
τ^n = geometry index for n-coordinate complexes
% = percent

CHAPTER 1 – INTRODUCTION AND RELEVANT LITERATURE

1.1 Introduction to Iridium

Iridium is a group 9 transition metal that has access to fewer oxidation states than other transition metals, such as manganese or osmium.[1] When considering the +I oxidation state iridium typically disobeys the 18-electron rule and is a 16-electron square planar complex.[1] Iridium has found many uses in catalysis over the years. For example, Vaska's complex (*trans*-$(PPh_3)_2Ir(Cl)(CO)$, **1**) has been found to be useful in catalytic processes because of its propensity to oxidatively add bonds, such as H–H, and participate in facile Ir(I)/Ir(III)/Ir(I) cycles (Figure 1).[2, 3]

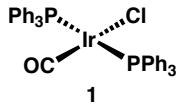

1

Figure 1 Vaska's complex

1.2 Pincer Ligands

1.2.1 General Introduction to Pincer Ligands

Pincer ligands are tridentate donors that bind in a meridional fashion (Figure 2) and have found uses in catalysis and small molecule activation (*vide infra*).[4-9] The central donor (E, Figure 2) can be neutral or anionic. The other two donors are typically neutral and identical

(Y, Figure 2). Although this is the typical structure of pincer ligands, there are many other permutations. One of the benefits of pincer ligands is that the complexes resulting from coordination of a metal most often show high thermal stability which is useful for endothermic processes.[10]

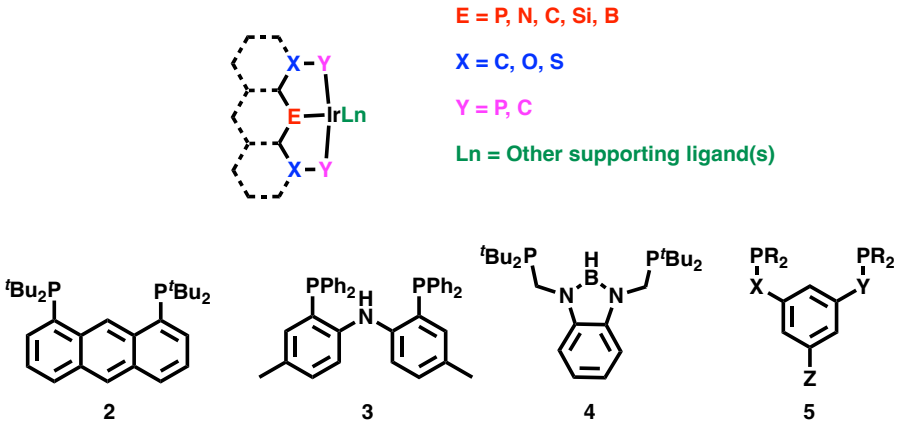

Figure 2 Basic pincer ligand scaffold and example pincer ligands used with iridium[11-14]

1.2.2 Pincer and Other Supporting Ligand Modification

The steric and electronic properties of pincer ligands can be easily modified which renders them appealing for catalytic processes. In particular, ligand **5** (Figure 2) could be synthetically modified at R, X, Y, or Z. The steric environment may be altered by modifying R, whereas the electron donating capacity of the pincer ligand can be adjusted by X, Y, and Z. In turn, this changes the steric and electronic properties about the coordinated metal centre.

One example of pincer ligand modification to optimize catalytic activity is shown in Figure 3. Goldman *et al*. computationally and experimentally investigated replacing the phosphine *tert*-butyl substituents in a stepwise fashion (*i.e.* replacing one *tert*-butyl group with a methyl group until all *tert*-butyl substituents were replaced).[15] Each iridium complex with a different number of phosphine methyl substituents was computationally investigated for the dehydrogenation of *n*-octane. The best results were tested experimentally. Simply changing one of the four *tert*-butyl groups to a methyl moiety showed an increase from 29 mM to 190 mM of octenes after 30 minutes. The study exhibits how simple modification of the pincer ligand can drastically change catalytic activity.

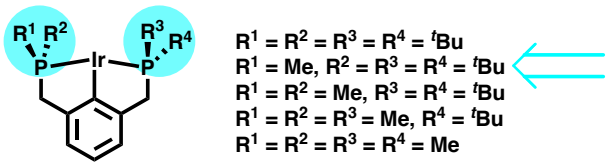

Figure 3 Modification of iridium PCP-pincer complex

In addition to modification of the pincer ligand, the choice of other supporting ligand(s) is also important. A study by Goswami *et al*. revealed that altering the non-pincer supporting ligand changed the redox non-innocence of the reported pincer ligand (A, Figure 4).[16] Using different supporting ligands also affected the isolated yields in the dehydrogenation of alcohols. Complex **6d** possessed the greatest catalytic activity, which they explained to be due to the electron accepting nature of the supporting ligand, rendering the metal centre more electron deficient.

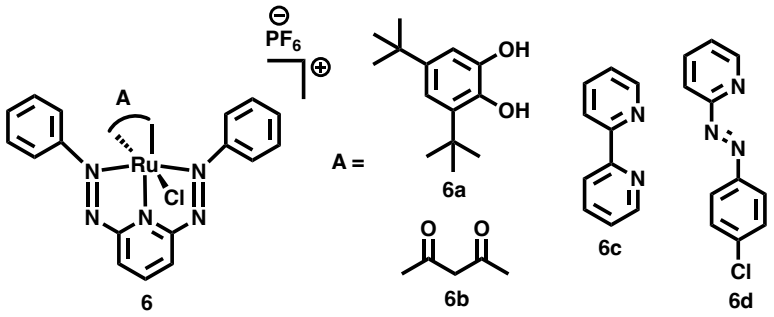

Figure 4 Redox non-innocent ruthenium pincer complex

1.3 Iridium Pincer Complexes

1.3.1 Preface

Iridium pincer complexes are an extensively researched topic, and a comprehensive review is beyond the scope of this thesis. There are numerous reviews that can be referenced,[4, 5, 7, 17, 18] although even this list is not exhaustive. In this section, selected examples of iridium(I) and iridium(III) complexes and their transformations are discussed.

1.3.2 Iridium(I) Complexes Supported by Pincer Ligands

Iridium(I) complexes readily participate in oxidative addition reactions because of the electron-rich nature of the metal centre and access to the +III oxidation state. Accordingly, they are often useful in catalytic processes that include oxidative addition/reductive elimination steps, such as E–H and/or small molecule activation. Hartwig and Goldman investigated N–H activation by the oxidative addition of ammonia and anilines.[19] Scheme

1 shows an example of the oxidative addition and reductive elimination of NH_2R by a T-shaped, 14-electron intermediate (*PCP*-Ir, **7**). The NH_2R unit can be released by reaction with an isocyanide or CO to form *PCP*-Ir(CX) (X = N^{t}Bu, O; **9**). Although the process is non-constructive (oxidative addition and reductive elimination of the same molecule), it exhibits that the oxidative addition of the N–H bond of ammonia is possible with iridium(I) complexes, which was viewed at the time only as an ancillary ligand.

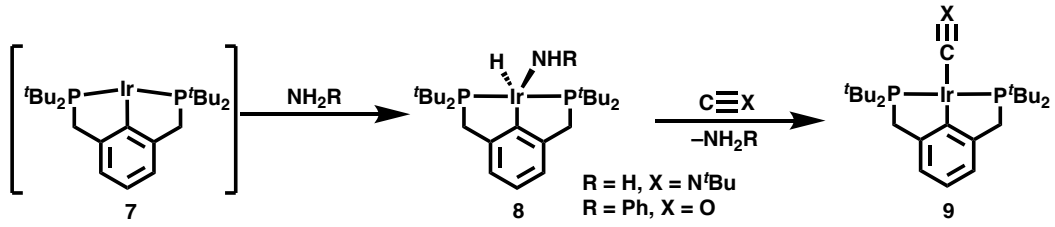

Scheme 1 Oxidative addition and reductive elimination of NH_2R

Another example of iridium(I) complexes participating in stoichiometric transformations is provided in Scheme 2.[20] A formal stoichiometric hydrogenation of nitrous oxide was achieved using *PC$_{carbene}$P*-IrCl (**10**) and dihydrogen, releasing dinitrogen and water. Cooperation with the double bond between the iridium=carbene facilitated this process.

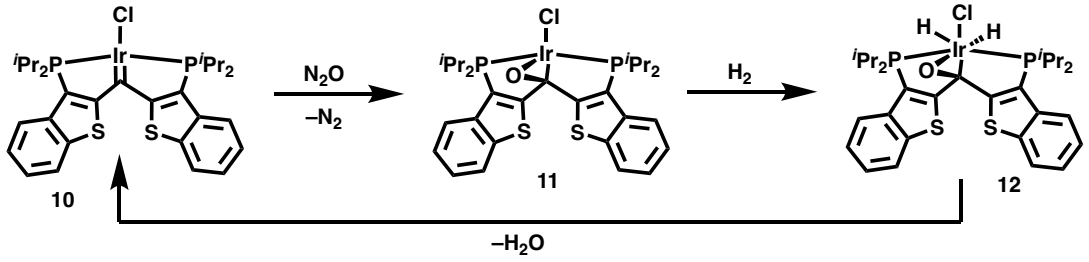

Scheme 2 Hydrogenation of nitrous oxide by iridium pincer complex PC$_{carbene}$P-IrCl

1.3.3 Iridium(III) Complexes Supported by Pincer Ligands

Iridium(III) complexes are less commonly known to undergo oxidative addition, although there have been unanticipated examples, such as reported by Goldman *et al*.[21] Despite the fact that E–H oxidative addition at iridium(III) centres is less facile than iridium(I) complexes, there are numerous examples of small molecule activation, as well as catalytic processes that have been reported for iridium(III) complexes.[22-24] An example of iridium(III) pincer complexes in stoichiometric reactions and catalytic processes is by iridium silyl hydrides and silylenes. Figure 5 shows examples of iridium silyl hydride (*PNP*-Ir(H)(SiRR'X), **13**) and silylene ([*PNP*-Ir(H)(SiRR')]$^{+}$[B(C_6F_5)$_4$]$^{-}$, **14**) complexes reported by Tilley *et al*.[25] Iridium silyl hydrides are typically synthesized through oxidative addition of an Si–H bond, and the corresponding silylene may be made by hydride abstraction. Both iridium silyl hydrides and silylenes have shown success in hydrosilylation processes (*vide infra*).

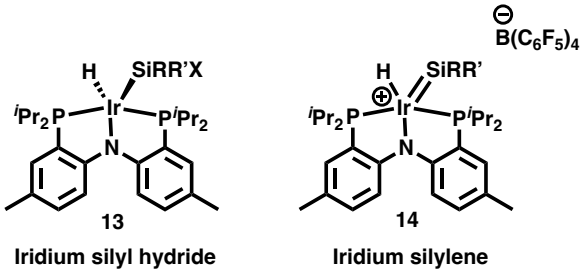

Figure 5 Examples of iridium silyl hydride and silylene complexes

Iridium complexes have also shown success in a variety of different catalytic processes such a H/D exchange,[26] hydroarylation,[27] allylic amination,[28] photoredox catalysis,[29] and

dehydrogenative borylation.[30] These processes are beyond the scope of this thesis and will not be discussed further.

1.4 Alkane Dehydrogenation Mediated by Iridium Pincer Complexes

Alkane dehydrogenation is a challenging, but crucial transformation that converts alkanes into value-added alkenes which can be readily functionalized by well-established protocols.[31, 32] Alkane dehydrogenation is extremely challenging because of the endothermic nature of the reaction.[33] Industrial processes for alkane dehydrogenation typically use heterogenous catalysts, but they often provide poor selectivity and require significantly elevated temperatures (500–900 °C).[34] One way the challenges can be overcome is by using homogenous catalysts in the presence of *tert*-butylethylene (TBE). Using TBE generates a 3-coordinate, 14-electron intermediate that is presumably able to oxidatively add C(sp^3)–H bonds (Scheme 3). This does not entirely negate the challenges, as elevated temperature is often still required (typically 150–250 °C) and the turnover numbers (TON) are still not excellent (total of 5901 turnovers by Huang *et al*.).[35]

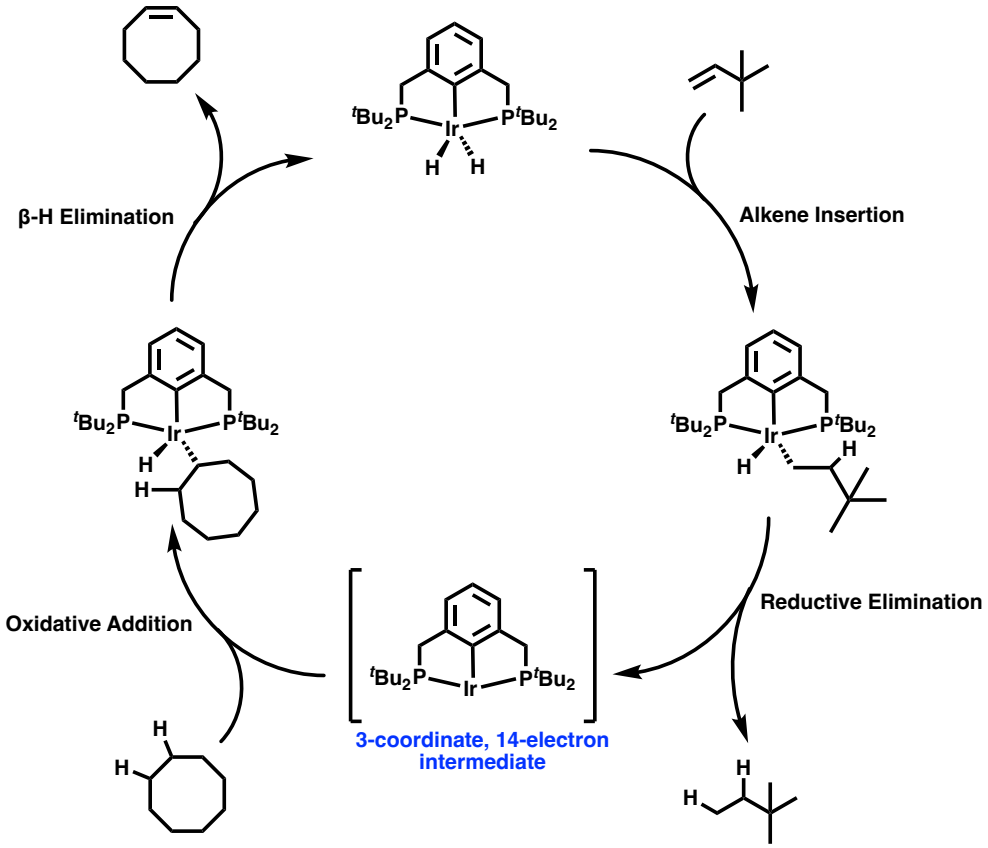

Scheme 3 Mechanism for homogenous alkane dehydrogenation

Crabtree *et al*. reported the first example of stoichiometric alkane dehydrogenation in 1979 using an iridium complex of the formula $[Ir(H)_2(olefin)_2(PPh_3)_2]$, but the substrate was not released.[36] Felkin *et al*. followed with a rhenium heptahydride that was able to dehydrogenate cyclopentane, but was plagued with the same problem in that the substrate was not released.[37] In 1984, however, their group achieved catalytic alkane dehydrogenation with iridium and ruthenium polyhydrides in the presence of *tert*-butylethylene, with 45–70 turnovers.[38]

In 1996, Jensen *et al*. introduced the thermally robust complexes $^{t\text{Bu}}$*PCP*-Rh(H)$_2$ (**15**) and $^{t\text{Bu}}$*PCP*-Ir(H)$_2$ (**16**) (Scheme 4).[14] The rhodium analogue **15** was essentially inactive for alkane dehydrogenation, even at 200 °C. In contrast, the iridium complex **16** was able to catalyze alkane dehydrogenation at 150 °C; 82 turnovers were achieved in the first hour. This complex showed stability for up to one week at 200 °C and was active if TBE was present. The stability at elevated temperature is important because of the endothermic nature of the reaction, requiring consistently high temperature to allow the reaction to proceed. Further work also proved this complex was capable of acceptorless alkane dehydrogenation, in which no TBE was present.[39]

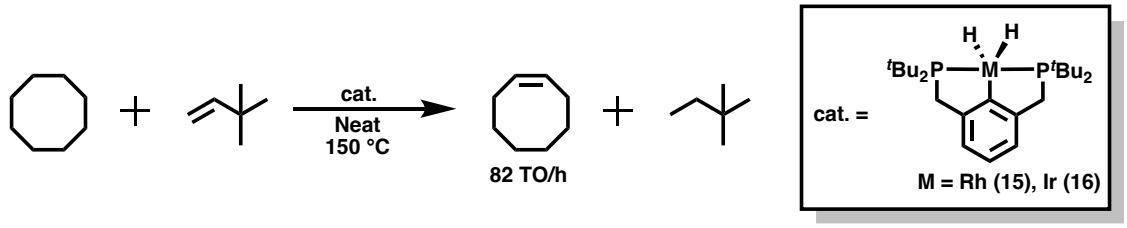

Scheme 4 First example of alkane dehydrogenation catalyzed by PCP-pincer iridium complex

Numerous groups have altered the *PCP*-pincer ligand in attempts to realize improved reactivity. For example, Goldman *et al*. modified Jensen's *PCP*-pincer ligand by changing the *tert*-butyl substituents on phosphorus to isopropyl groups.[40] COA was dehydrogenated with a turnover frequency (TOF) of 47 turnovers in the first 30 minutes (94 per hour), in the absence of TBE. Cyclodecane was dehydrogenated even faster (460 per hour). Moving to more sterically demanding adamantyl moieties did not improve the TOF, but did enhance thermal stability.[41] Lastly, when one of the *tert*-butyl substituents was replaced with a

methyl group, catalytic activity increased substantially (TOF of $^{t\text{Bu4}}$*PCP*-Ir(H)$_4$: 78 h^{-1}; TOF of $^{t\text{Bu3Me}}$*PCP*-Ir(H)$_4$: 570 h^{-1}).[15]

Changes to the central donor and ligand backbone of the *PEP*-pincer scaffold have also been investigated. Table 1 summarizes the results of the selected iridium catalysts. In 2001 Hall *et al*. discovered a highly robust anthropos catalyst, *PC$_{anthropos}$P*-Ir(H)$_2$ (**17**) which gave a TOF of 40 per hour for cyclodecane.[11] The catalyst was stable up to 250 °C. Another alteration to the ligand backbone was undertaken by Yamamoto *et al*. in 2013 when they reported a 7-6-7 ring backbone ($^{\text{Ph}}$*PC$_{7\text{-}6\text{-}7}$P*-Ir(H)(Cl), complex **18**).[42] With phenyl substituents on phosphorus a TOF of 201 per hour (total TON of 4820) was observed at 230 °C.

Table 1 Summary of alkane dehydrogenation activity of selected iridium catalysts

Author, Year	Complex	Substrate	Temperature	TOF (h^{-1})
Hall, 2001	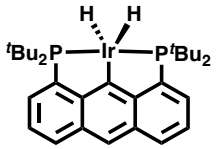 17	Cyclodecane	250 °C	40
Yamamoto, 2013	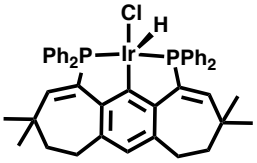 18	COA	230 °C	201
Brookhart, 2004	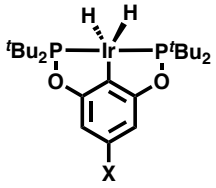 19	COA	200 °C	51
Huang, 2016	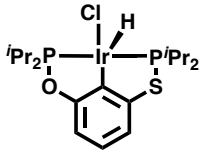 20	COA	200 °C	393
Yamashita, 2018	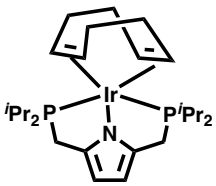 21	COA	220 °C	5
Goldman, 2022	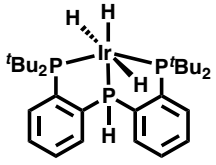 22	*n*-octane	100 °C	30

When two oxygen atoms were installed on a tether, a TOF of 51 per hour (total TON 2070) was achieved, when X = Ar^F (^{tBu}*POCOP*-Ir(H)$_2$, complex **19**).[43] Replacing one of the oxygen atoms with a sulfur (^{iPr}*POCSP*-Ir(H)(Cl), complex **20**) led to a TOF of 393 per hour (total TON of 5901), which is one of the highest activities reported up to 2018.[44, 45] Substituting the carbon donor with a nitrogen (^{iPr}*PNP*-Ir(COD), complex **21**) provided a low TOF of 5 per hour.[45] When the carbon atom was replaced with a phosphorus atom (complex **22**), as reported by Goldman *et al*. in 2022, a substantial improvement in catalytic activity was observed, and is one of the most active catalysts for the dehydrogenation of *n*-octanes, especially at lower temperature (100 °C).[46]

Although a review of some of the catalysts active for alkane dehydrogenation have been provided in this section, a clear trend between structure and activity cannot be made. This is because different temperatures, activators, and substrates have been used. This is one of the current challenges of the literature that needs to be addressed.

1.5 Iridium-Catalyzed Hydrosilylation

The activation of Si–H bonds by transition metals has gained interest because of the possible use in catalytic processes such as hydrosilylation.[47] Hydrosilylation is the addition of an Si–H bond across a multiple bond, and is a safer, more efficient, and atom-economic way to reduce C–C and C–heteroatom multiple bonds compared to the use of dihydrogen gas.[48, 49] For example, hydrosilylation of ketones could be an alternative route to chiral alcohols.[50-53] Furthermore, hydrosilylation of alkenes and alkynes is one of the most efficient routes to C–Si bond formation, which can produce commercially valuable fine

chemicals and reaction intermediates.[47] After the hydrosilylation of alkenes, a saturated silyl-containing product, which can be further transformed, is generated (Scheme 5).[54] Hydrosilylation of alkynes produces vinylsilanes that are useful because of their versatility, ease of handling, low toxicity, and general stability.[55]

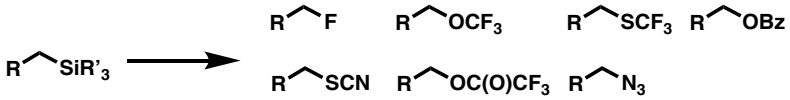

Scheme 5 Further transformations possible after hydrosilylation of alkenes

Hydrosilylation is also one of the most important reactions in the silicone industry, as it is needed to prepare silicon elastomers, adhesives, sealing materials, silicon polymers, and organofunctionalized silanes.[56] Industrial processes typically use platinum catalysts, such as Karstedt's catalyst (**23**, Figure 6).[56] One drawback to platinum-based catalysts is that multiple competing mechanistic pathways exist often resulting in low selectivity.[56, 57]

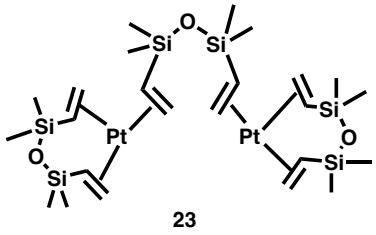

23

Figure 6 Karstedt's catalyst used in industrial hydrosilylation

Most hydrosilylation catalysts produce anti-Markovnikov selectivity products (*i.e.* the silyl ends up on the least substituted carbon, Scheme 6). The selectivity can be explained by the

Chalk-Harrod/Modified Chalk-Harrod mechanism (Scheme 6).[58, 59] The first step includes the oxidative addition of an Si–H bond, followed by coordination of the alkene to iridium. The Chalk-Harrod and Modified Chalk-Harrod mechanisms diverge at the proceeding step (insertion of the alkene). Insertion of the alkene is the key step in selectivity. In the Chalk-Harrod mechanism, the alkene is inserted in a 1,2-fashion whereby the large R group is oriented so as to avoid the metal centre. In contrast, in the Modified Chalk-Harrod mechanism the alkene is inserted in a 2,1-fashion. Both mechanisms afford the same anti-Markovnikov products. Despite the typical mechanism and selectivity, there have been some examples wherein Markovnikov selectivity prevails. The selectivity is promoted by modifying the catalyst, as well as the steric and electronic properties of the hydrosilane and alkyne.[60] Markovnikov selectivity is especially valuable when considering the hydrosilylation of alkynes; production of vinylsilanes can be important building blocks in organic synthesis.[61] There are a variety of reasons why one selectivity would be preferred by chemists, depending on what functionalization is desired in the next step. Therefore, having access to systems that favour Markovnikov selectivity and others that afford anti-Markovnikov products is important.

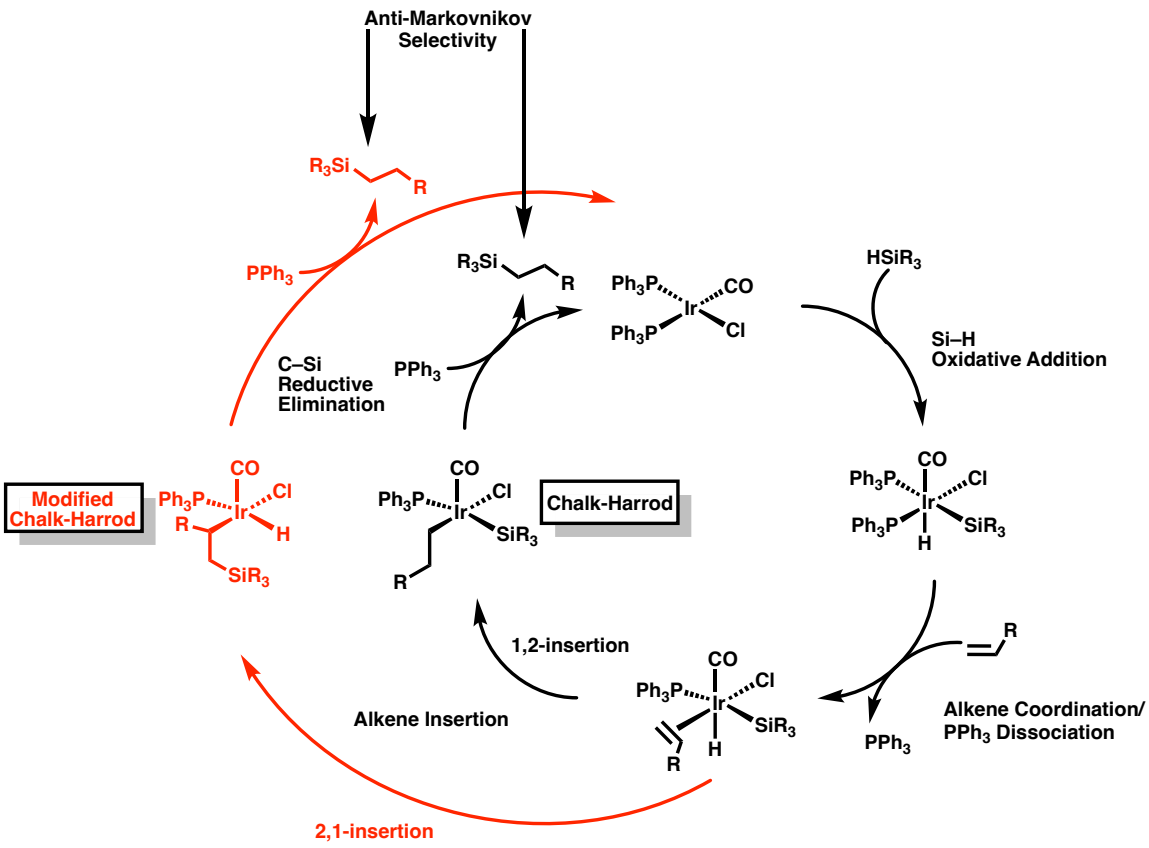

Scheme 6 Chalk Harrod and Modified Chalk-Harrod mechanisms for iridium-catalyzed hydrosilylation of alkenes

In addition to C–C multiple bonds, hydrosilylation of C–O double bonds gives promise into the production of chiral alcohols as an alternative to dihydrogen reduction, or one-step alcohol protections.[50] Figure 7 shows three examples of iridium complexes that can catalyze the hydrosilylation of ketones, albeit with no enantioselectivity.[48, 50, 62] On the contrary, the examples in Figure 8 hydrosilylate ketones with moderate to excellent (66–96%) enantiomeric excess (*ee*).[49, 63-65]

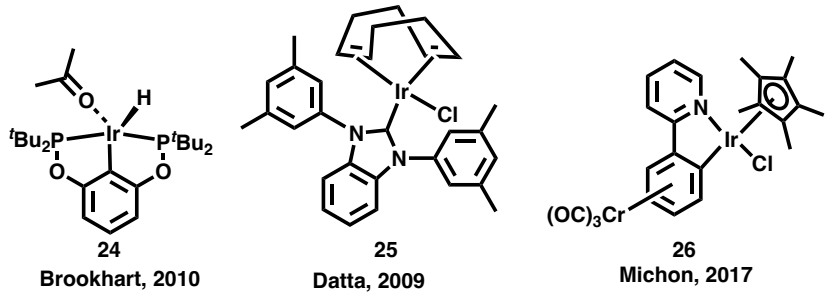

Figure 7 Three examples of iridium complexes that catalyze C–O multiple bond hydrosilylation

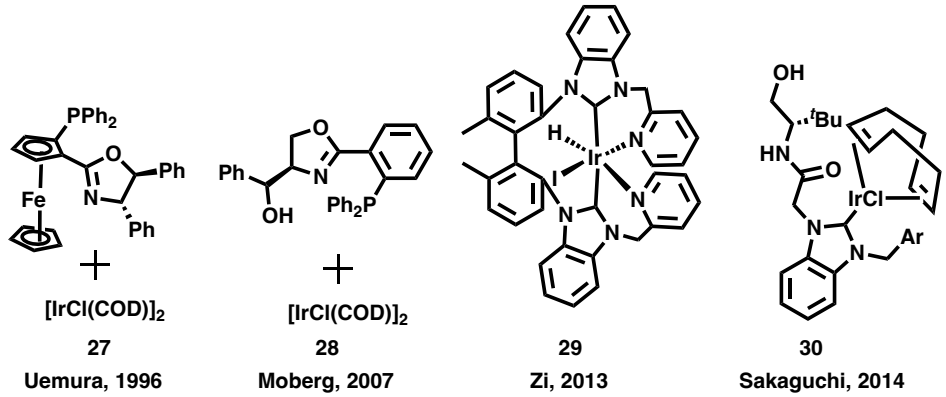

Figure 8 Examples of iridium complexes that catalyze asymmetric ketone hydrosilylation

The hydrosilylation of amides and nitriles is one route to the synthesis of amines.[66] Reduction of nitriles without harsh reaction conditions is rare.[67] One example of the reduction of nitriles to amines is shown in Scheme 7.[67] At 1 mol% catalyst loading of **31**, 95% conversion to product was observed after 72 hours at 80 °C.

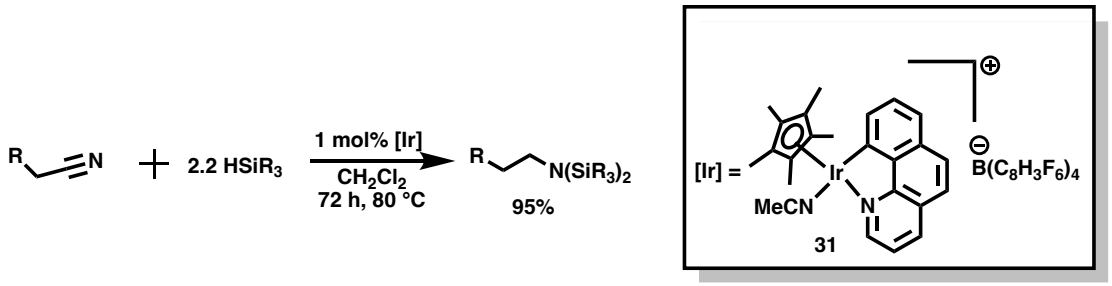

Scheme 7 Hydrosilylation of nitriles by cationic iridium complex

Iridium has gained much less attention than rhodium in the hydrosilylation of C–heteroatom multiple bonds, likely because compared to its rhodium counterpart, enantioselectivity and isolated yields are typically lower.[68, 69] More work into efficiency and enantioselectivity with iridium complexes may lead to a less expensive alternative than rhodium-catalyzed hydrosilylation.

1.6 Relevant Hayes Group Chemistry

1.6.1 Pincer Ligand Scaffold

The Hayes group has produced extensive work with bisphosphinimine-based pincer ligand scaffolds, the first of which was reported 14 years ago.[70] That particular variant employed a carbazole backbone; however, destructive cyclometallation was observed with organolutetium complexes.[71, 72] Further work changed the carbazole backbone to pyrrole, decreasing the chelate ring from six to five. The organometallic rare earth complexes supported by this pincer ligand demonstrated far greater thermal stability.[71, 73]

The phosphinimine functionality ($R_3P{=}NR'$) is highlighted in red in Figure 9. Although a double bond between nitrogen and phosphorus is drawn for convenience, a more chemically appropriate representation is $R_3P^{(+)}–N^{(-)}R'$. Notably, phosphinimines are strong σ- and π-donors.[74] The ylidic character also makes them less prone to nucleophilic attack than imines. They also provide ^{31}P NMR chemical shifts that are highly sensitive to the local chemical environment; hence, metal coordination causes substantial downfield shifts in the ^{31}P NMR spectrum. The bisphosphinimine-pincer framework also has the key benefits of other pincer ligands: the complexes generally show thermal stability[71] and can easily be fine-tuned, allowing systematic changes to the steric[75] and electronic properties of the corresponding metal complex (Ar and R in Figure 9).

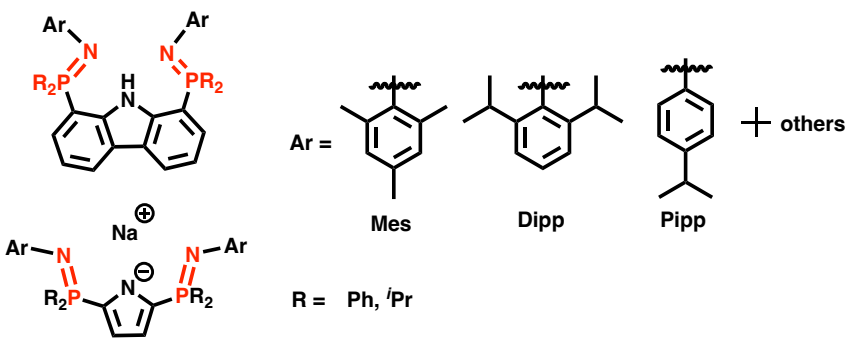

Figure 9 Hayes group pincer ligand scaffold

1.6.2 Group 9 Chemistry Explored by the Hayes Group

1.6.2.1 Hydrogenation by NNN-Pincer Ligand Supported Rhodium Complex

The Hayes group work with group 9 transition metals has predominantly focused on rhodium. Using the previously mentioned pyrrole-based bisphosphinimine ligand system

(2,5-(^{i}Pr$_2$P=NPipp)$_2$C$_4$H$_2$N, Pipp = *para*-isopropylphenyl), small molecule activation and metal-ligand cooperation have been explored. Reaction of ^{Pipp}LRh(COE) (COE = cyclooctene) with an atmosphere of dihydrogen led to the hydrogenation of COE.[76] However, the catalyst was deactivated likely due to a 14-electron species, ^{Pipp}LRh, after ejection of COA. The deactivation product is complex **32** (Scheme 8). To reactivate the rhodium species for further hydrogenation, reaction with ethylene could promote the loss of dihydrogen and production of ^{Pipp}LRh(H$_2$C=CH$_2$) (**33**). Hydrogenation of phenylacetylene was also achieved under an atmosphere of dihydrogen.

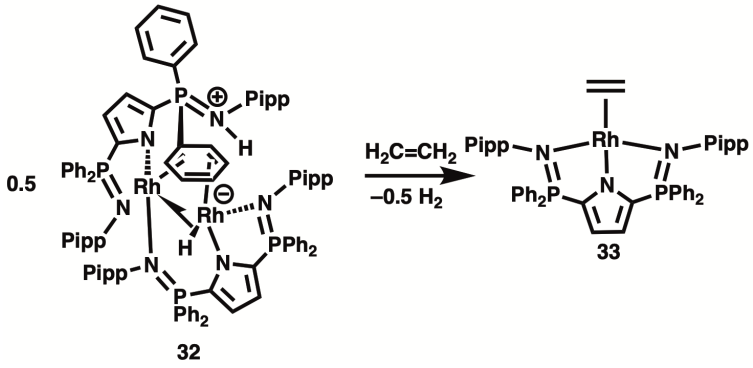

Scheme 8 Deactivation and reactivation of rhodium hydrogenation catalyst

1.6.2.2 CO Bond Scission at an NNN-Pincer Ligand Supported Rhodium Complex

Deoxygenative coupling of CO was investigated with rhodium supported by ^{Pipp}L.[77] The complex ^{Pipp}LRh(CO)$_2$ (**34**) was reacted with B(C$_6$F$_5$)$_3$ resulting in the activation of CO through metal-ligand cooperation to yield ^{Pipp}L^{+}Rh^{-}(CO)(C=O→B(C$_6$F$_5$)$_3$) (**35**, Scheme 9). The complex decomposes ($t_{1/2}$ = three hours) into three different units. The monocarbonyl complex, ^{Pipp}LRh(CO) (**36**), and ^{O}LRh(CO)$_2$ (^{O}L = 2-(^{i}Pr$_2$P=NPipp)-5-(^{i}Pr$_2$P=O→B(C$_6$F$_5$)$_3$)C$_4$H$_2$N, **37**), were the phosphorus containing products. In addition, the

para-isopropylphenyl isocyanide with a dative bond to $B(C_6F_5)_3$ was observed. There did not appear to be a substantial contribution from the metal centre; rather, the rhodium was the "encounter complex" (**35**) and the phosphinimine and Lewis acid promote the deoxygenation.

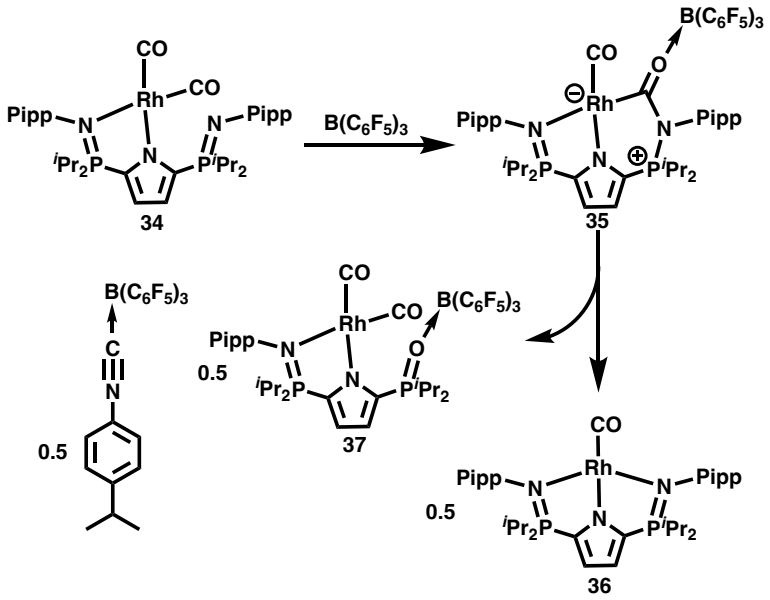

Scheme 9 CO activation and bond scission at rhodium facilitated by $B(C_6F_5)_3$

1.6.2.3 E–H (E = Si, B) Bond Activations by NNN-Pincer Ligand Supported Rhodium Complex

Activation of E–H bonds has also been explored with rhodium complexes supported by ^{Pipp}L, such as for the synthesis of rhodium silylene and silyl hydride complexes.[78] Specifically, reaction of ^{Pipp}LRh(CO) (**36**) with primary and secondary aryl silanes led to extrusion of dihydrogen, producing the formally base-stabilized rhodium silylene

(^{Pipp}LRh(SiRR')(CO), complex **38**, Scheme 10). On the contrary, when cyclooctene (COE), rather than CO, was *trans* to the anionic pyrrole nitrogen, only Si–H oxidative addition occurred.

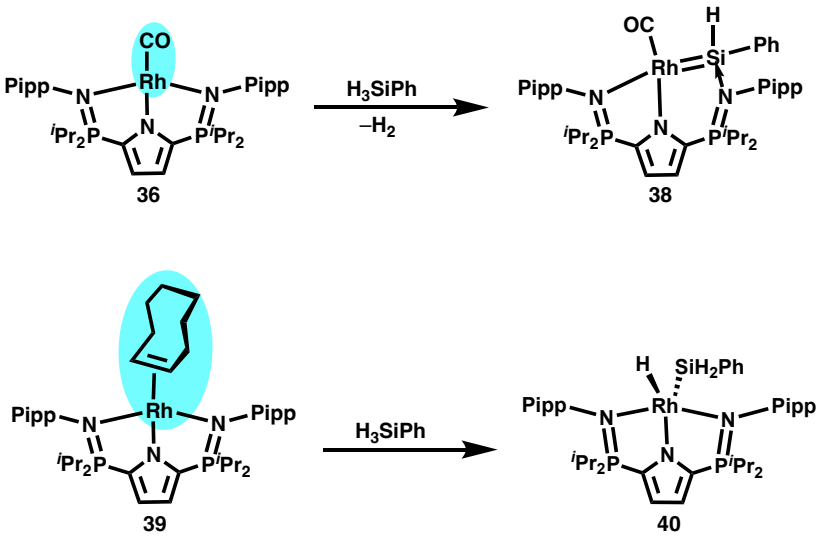

Scheme 10 Difference in reactivity of rhodium CO and COE complexes

Analogous to the work with hydrosilanes, the formally base-stabilized borylenes were prepared *via* dehydrogenation of primary aryl boranes (Scheme 11).[77] A formal borylene transfer to pinacol was also achieved with the regeneration of **36**.

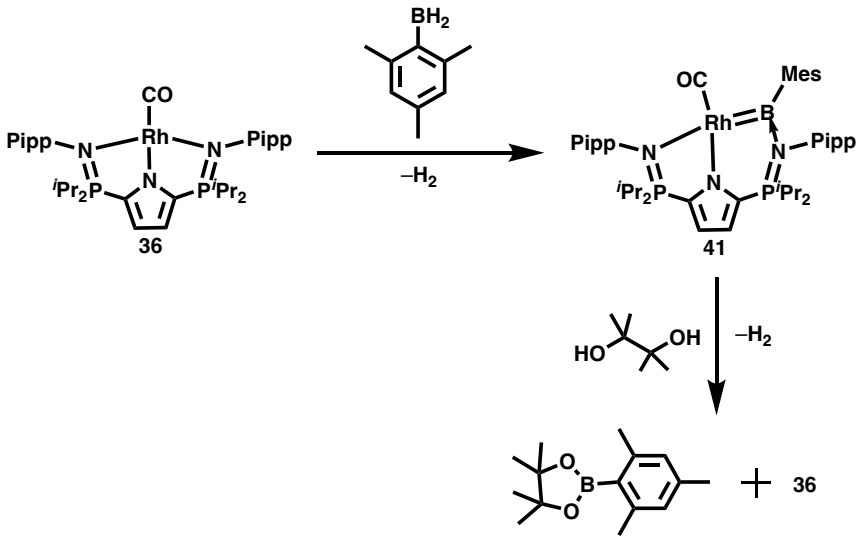

Scheme 11 Synthesis of base-stabilized rhodium borylene

1.7 Project Goals

1.7.1 General Project Goals

Previous work with rhodium has given evidence for ^{Ar}L (L = 2,5-(^{i}Pr$_2$P=NAr)$_2$C$_4$H$_2$N) to support group 9 transition metals. The project goals included comparing the structure and reactivity between the corresponding rhodium and iridium complexes. Analogous complexes for a direct comparison between the two metals supported by an *NNN*-pincer ligand were desired. Possible target reactions included Si–H bond activation, which has potential in catalytic or stoichiometric hydrosilylation. In addition, activation of dihydrogen could allow access to the iridium dihydride complex, ^{Ar}LIr(H)$_2$, in which reaction with TBE would produce a 3-coordinate, 14-electron species. In the presence of an appropriate substrate, such as cyclohexane, alkane dehydrogenation may be observed.

1.7.2 Goals of Chapter 2

In initial attempts at finding a balance between stability and reactivity, the synthesis of iridium 1,5-cyclooctadiene complexes, ^{Ar}LIr(COD) (Ar = *para*-isopropylphenyl, 2,6-diisopropylphenyl, 2,4,6-trimethylphenyl; COD = 1,5-cyclooctadiene) was pursued. Reaction with small molecules such as silanes, dihydrogen, CO, and triphenylphosphine were executed to probe the lability of the COD ligand, and to reveal new iridium complexes that could undergo different catalytic or stochiometric processes.

1.7.3 Goals of Chapter 3

An iridium cyclooctene complex, ^{Ar}LIr(COE) (COE = cyclooctene), was the next synthetic target. Reaction with small molecules, as with ^{Ar}LIr(COD), was pursued. The target complexes from ^{Ar}LIr(COE) were ^{Ar}LIr(H)(SiR$_3$), ^{Ar}LIr(H)$_2$, ^{Ar}LIr(CO)$_n$ (n = 1, 2), and ^{Ar}LIr(PPh$_3$). In addition, a new iridium starting material, [Li]$^+$[(COD)Ir(Me)$_2$]$^-$, was explored with different mono- and multi-dentate ligands for direct access to different organoiridium complexes.

1.7.4 Goals of Chapter 4

The efficacy of the newly synthesized complexes, ^{Ar}LIr(H)(SiR$_3$) and ^{Ar}LIr(H)$_2$, to promote hydrosilylation, and alkene hydrogenation and alkane dehydrogenation, respectively, was explored. A semiquantitative kinetic analysis of the reactions was undertaken.

CHAPTER 2 – SYNTHESIS AND REACTIVITY OF 1,5-CYCLOOCTADIENE COMPLEXES OF IRIDIUM

2.1 Synthesis and Characterization of Iridium Cyclooctadiene Complexes Supported by a Monoanionic NNN-Pincer Ligand

2.1.1. Synthesis from $Na^{Ar}L$ (L = 2,5-($^{i}Pr_2P$=NAr)$_2C_4H_2N$)

In a general procedure, the 1,5-cyclooctadiene (COD) complexes **42**, **43**, and **44** were synthesized *via* a salt metathesis reaction between one equivalent of $Na^{Ar}L$ (L = 2,5-($^{i}Pr_2P$=NAr)$_2C_4H_2N$, Ar = *para*-isopropylphenyl (Pipp), 2,6-diisopropylphenyl (Dipp), 2,4,6-trimethylphenyl (Mes)) and 0.5 equivalents of $[IrCl(COD)]_2$ (Scheme 12). Initial reactions on an NMR tube scale in 0.5 mL of benzene-d_6, monitored by ^{1}H and $^{31}P\{^{1}H\}$ NMR spectroscopy, indicated that the reactions required between 10 minutes (**42** and **44**) and two hours (**43**) to proceed to completion. For larger scale reactions in toluene, however, the mixtures were allowed to stir for 16 hours to ensure complete conversion. With all variants of the ligand, the reactions afforded yellow powders in 84%–94% yield.

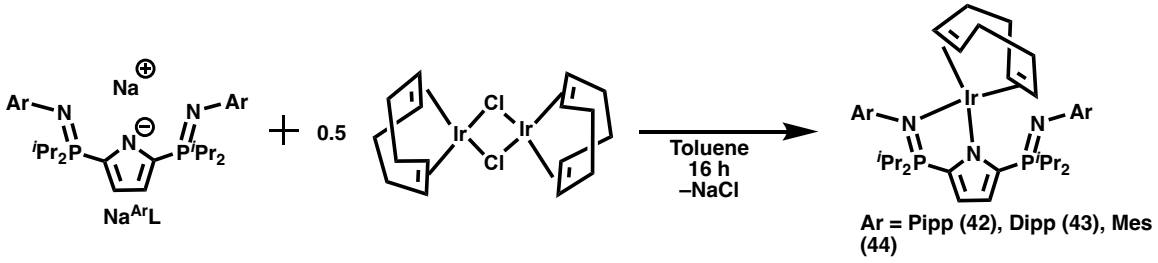

Scheme 12 Synthesis of $^{Ar}LIr(COD)$ (Ar = Pipp, Dipp, Mes)

In all cases, the ligand adopts a κ^2-coordination mode to iridium, evidenced by two resonances in the $^{31}P\{^1H\}$ NMR spectrum (δ 58.7 (bound), 13.3 (free) (**42**); 50.0 (bound), –2.9 (free) (**43**); 52.0 (bound), –0.9 (free) (**44**)), as the iridium atom is coordinated to only one phosphinimine donor (Table 2). Additionally, all ^1H NMR and $^{13}C\{^1H\}$ NMR resonances which correspond to the ligand display two signals for each environment. The expected κ^2-coordination mode was also observed for COD. In both the ^1H and $^{13}C\{^1H\}$ NMR spectra, there are two resonances that correspond to the alkene hydrogen (δ 4.94, 3.23 (**42**); 5.22, 4.17 (**43**); 5.15, 3.10 (**44**)) and carbon atoms (δ 61.9, 59.6 (**42**); 67.5, 61.7 (**43**); 62.3, 60.3 (**44**)), respectively. There are two resonances for each because of the atoms *trans* in the predicted square planar geometry. Specifically, one of the double bonds is *trans* to the pyrrole nitrogen atom, whereas the other is coordinated *trans* to the phosphinimine moiety.

*Table 2 Selected ^1H, ^{13}C, and ^{31}P NMR data for **42**, **43**, and **44***

Compound	***H*C=C*H* (^{1}H, δ)**	**H*C*=*C*H ($^{13}C^1$, δ)**	**$^{31}P^1$ (δ)**
42	4.94, 3.23	61.9, 59.6	58.7, 13.3
43	5.22, 4.17	67.5, 61.7	50.0, –2.9
44	5.15, 3.10	62.3, 60.3	52.0, –0.9

Both signals corresponding to the alkene hydrogens in the ^1H NMR spectrum are shifted substantially upfield when compared to free COD (δ 5.58 for free COD versus 4.94, 3.23 (**42**); 5.22, 4.17 (**43**); 5.15, 3.10 (**44**)). The same is true in the $^{13}C\{^1H\}$ NMR spectrum

[1]The ^{13}C and ^{31}P NMR spectra of complexes **42**, **43**, and **44** were ^1H decoupled.

(δ 128.9 for free COD versus 61.9, 59.6 (**42**); 67.5, 61.7 (**43**); 62.3, 60.3 (**44**)).[79] The upfield shifts were expected, due to π-backbonding interactions from iridium, rendering the alkene carbons more sp^3-like .

X-ray quality, yellow crystals for all three complexes were grown from saturated toluene solutions at –30 °C over periods between one day and one week. The displacement ellipsoid plots (50% probability) for complexes **42**, **43**, and **44** are depicted in Figure 10, Figure 11, and Figure 12, respectively.

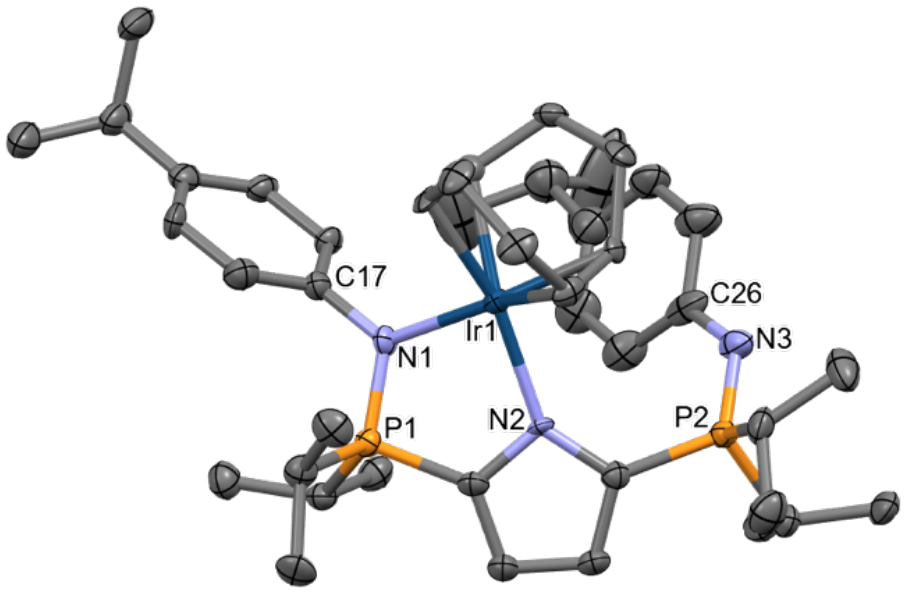

*Figure 10 Displacement ellipsoid plot (50% probability) of complex **42**. See Table 3 for selected bond distances and angles. Hydrogen atoms were removed for clarity. Space group = Pn. R_1 = 3.08%. Credit to A. A. Aborawi and C. S. MacNeil*[80]

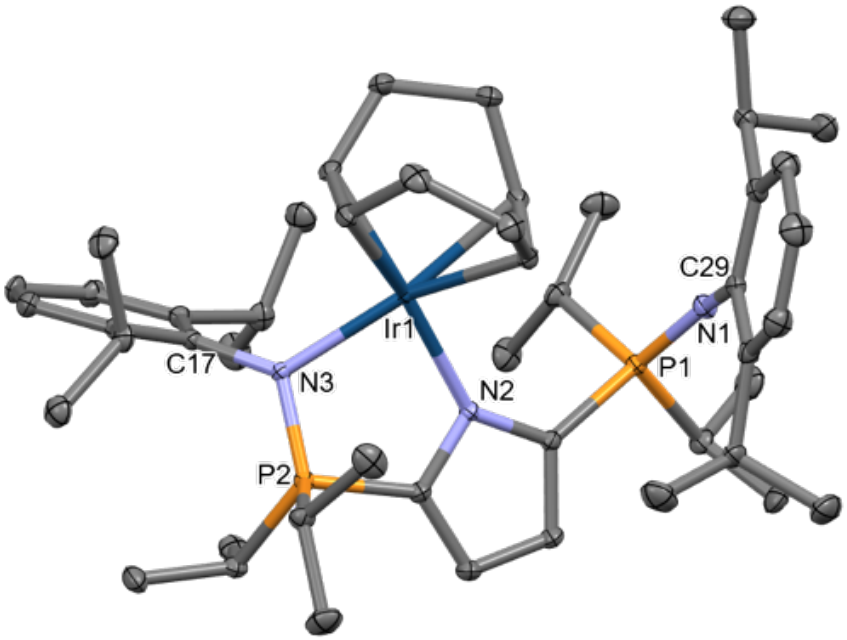

*Figure 11 Displacement ellipsoid plot (50% probability) of complex **43**. Hydrogen atoms were removed for clarity. See Table 3 for selected bond distances and angles. Space group = $P2_1/n$. R_1 = 3.34%*

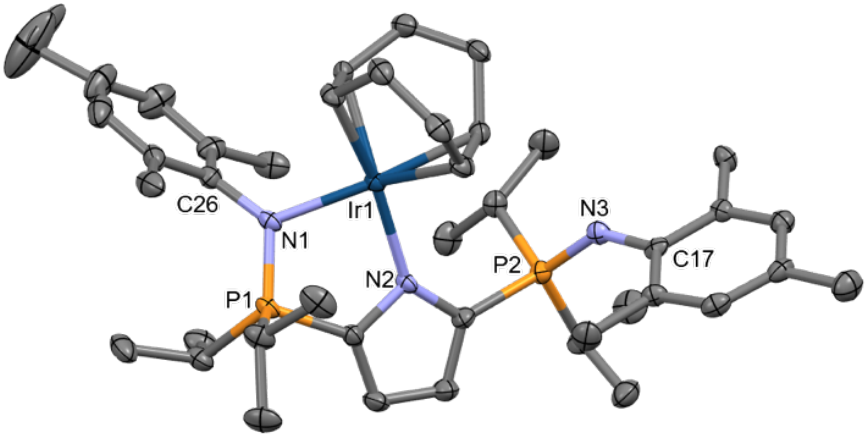

*Figure 12 Displacement ellipsoid plot (50% probability) of complex **44**. Hydrogen atoms were removed for clarity. See Table 3 for selected bond distances and angles. Space group = $P2_1/n$. R_1 = 5.57%*

The X-ray crystal structures of complexes **42**, **43**, and **44** confirmed the expected κ^2-coordination mode of both COD and the supporting *NNN*-ligand. In all cases, iridium exhibits a distorted square planar geometry (τ^4 = 0.24 (**42**); 0.074 (**43**); 0.27 (**44**), Table 3). The geometry index for four-coordinate complexes ($\tau^4 = \frac{360° - (\alpha + \beta)}{360° - 2\theta}$, where α, β = largest angles; $\theta \approx 109.5°$) was used to distinguish between square planar (τ^4 = 0) and tetrahedral (τ^4 = 1) geometries, as was its intended use when introduced in 2007.[81] Coordination to iridium elongates the P=N distance when compared to $H^{Ar}L$ and the free phosphinimine donor (1.618(7) Å (**42**); 1.6177(14) Å (**43**); 1.623(4) Å (**44**) compared to <1.6 Å for $H^{Ar}L$ and free phosphinimine, Table 3). Furthermore, the P=N–Ar angle of the free phosphinimine follows a steric trend; as the Ar group increases in size (Pipp < Mes < Dipp), the angle becomes larger (128.3(6)° (**42**); 139.9(3)° (**44**); 145.52(13)° (**43**); Table 3). This phenomenon was not observed in $H^{Ar}L$, and is likely a consequence of accommodating the large iridium atom and COD ligand, although in solution this may be quite flexible as there would be free bond rotation. Differences in the phosphinimine donor angles and bonding was also seen by the Hayes group in $^{Ar}LAl(Me)_2$.[82] When there are Pipp substituents on nitrogen, the ligand displays a κ^3-coordination mode; however, when Mes moieties are present, the ligand coordinates to the aluminium in a κ^2-fashion. The P=N–Ar angle of the free phosphinimine in $^{Ar}LAl(Me)_2$ (125.4(2)°) was also larger than that of the bound group (119.9(2)°).

*Table 3 Selected bond distances (Å) and angles (°) for complexes **42**, **43**, and **44** with $H^{Ar}L$ (Ar = Pipp, Dipp, Mes) included for comparison.[77, 82] Note: the P=N distances and P=N–Ar angles of $H^{Ar}L$ represent averaged values*

Atoms	42	$H^{Pipp}L$	43	$H^{Dipp}L$	44	$H^{Mes}L$
P=N (Bound)	1.618(7)	—	1.6177(14)	—	1.623(4)	—
P=N (Free)	1.569(6)	1.578(1)	1.5516(15)	1.551(1)	1.564(4)	1.562(1)
N–Ir–N	82.2(2)	—	83.25(5)	—	83.32(14)	—
P=N–Ar (Bound)	120.5(5)	—	123.29(11)	—	126.2(3)	—
P=N–Ar (Free)	128.3(6)	133.4(1)	145.52(13)	134.4(2)	139.9(3)	134.0(1)

*2.1.2 Alternative Synthesis of Complex **43***

In an attempt to synthesize ^{Dipp}LIr(H)(Cl) (**45**) by N–H oxidative addition, $[IrCl(COD)]_2$ was reacted with $H^{Dipp}L$ in 0.5 mL of benzene-d_6 at ambient temperature (Scheme 13). The initial orange-brown solution became yellow-brown within 16 hours. Unexpectedly, the $^{31}P\{^1H\}$ NMR spectrum exhibited signals at δ 50.0 and –2.9 in a 1:1 ratio. After 64 hours, 80% of the starting materials had been converted to the new compound. No free COD was observed in solution, and the ^1H NMR spectrum between δ 0.0 and –60.0 did not reveal a

hydride resonance. Careful analysis of the NMR data discovered that the product of the reaction was complex **43** (Table 2).

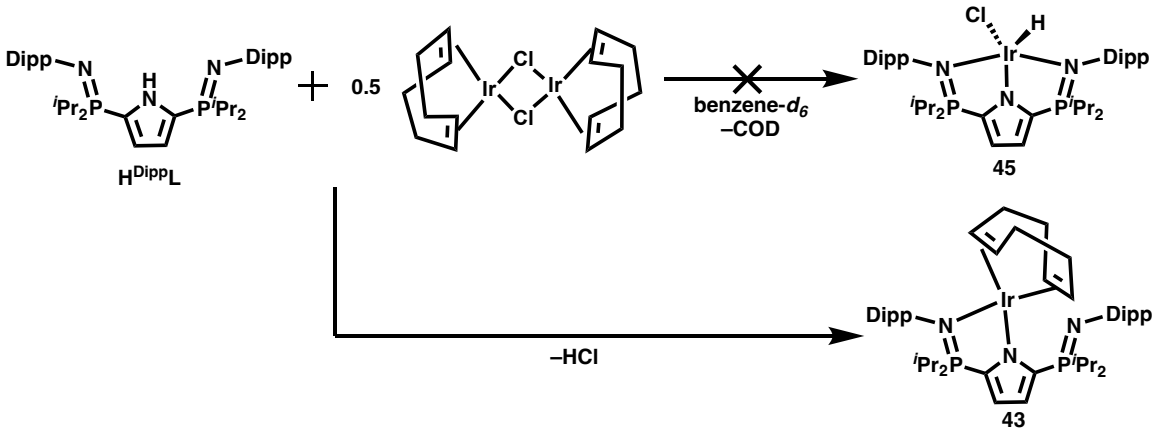

Scheme 13 Attempted synthesis of ^{Dipp}*LIr(H)(Cl)*

X-ray quality crystals from the reaction mixture were grown from a saturated pentane solution stored at –30 °C for three days. The structure confirmed that the asymmetric product was indeed complex **43**. The metrical parameters for this species were discussed in section 2.1.1.

Hydridochloride complexes, such as **45**, are often isolable and usually require a base to promote reductive elimination of HCl.[83] In fact, there are only a few examples of reductive elimination of HCl from iridium.[84-87] Scheme 14 shows the proposed intermediate from which reductive elimination of HCl would form complex **43**. The intermediate is hypothesized to be dimeric, as that would be the product of N–H oxidative addition. The dimeric species would be sterically crowded, which could promote HCl reductive elimination to form two molecules of **43**. The presence of free phosphinimine nitrogen

atoms could also assist this process, by allowing a base-assisted reductive elimination of HCl. Another argument could be that the process occurs through complex **45**; however, the only observable product throughout the reaction is complex **43**. More work would be required to determine the mechanism. This could include low temperature NMR spectroscopy experiments to observe any intermediates in solution.

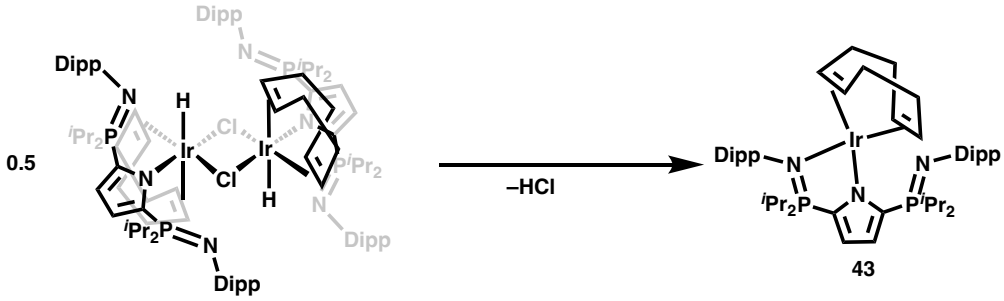

*Scheme 14 Proposed intermediate to produce **43** through reductive elimination of HCl*

With knowledge that **43** can be synthesized from $H^{Dipp}L$, the same reaction was undertaken with both $H^{Mes}L$ and $H^{Pipp}L$. When Ar = Mes, the reaction proceeded smoothly to give **44** within 10 minutes, as indicated by both NMR spectroscopy ($^{31}P\{^1H\}$ NMR spectrum: δ 52.0 and –0.9) and X-ray crystallography. In contrast, reaction of $H^{Pipp}L$ with 0.5 equivalents of $[IrCl(COD)]_2$ for one hour yielded three products. Within this mixture, 30% was assigned as **42**. Another 30% of the mixture was an unknown asymmetric product, resonating at δ 59.4 and 44.9 in the $^{31}P\{^1H\}$ NMR spectrum. The remaining portion gave rise to one ^{31}P NMR signal at δ 46.3. After two days at ambient temperature, the major product was the signal at δ 46.3. Although the identity of the product cannot be confirmed by NMR spectroscopy, complex **42** may be the initial product of the reaction. If **42** was formed during the reaction, a new product, such as $^{Pipp}H^+LIr(COD)$ (H^+L = [2-

(^{i}PrP=NPipp)-5-(^{i}PrP=NHPipp)$C_4H_2N]^+[Cl]^-$, **46**, Scheme 15), may be quickly produced from the release of HCl. Studies investigating the robustness of **42**, **43**, and **44** should be conducted with HCl in diethylether to determine whether it was **42** reacting with reductively eliminated HCl.

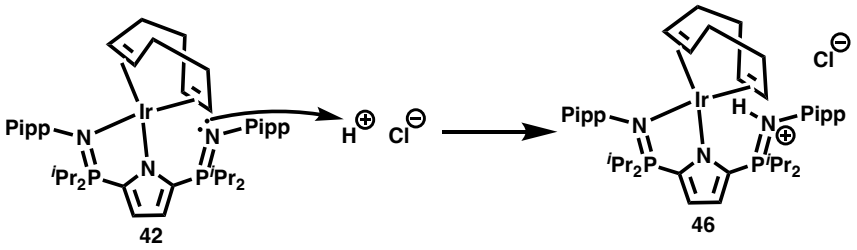

*Scheme 15 Reaction of **42** with HCl*

2.2 Reactivity of ^{Ar}LIr(COD)

2.2.1 Reactivity of ^{Pipp}LIr(COD) and ^{Mes}LIr(COD) with Dihydrogen and Silanes

With small molecule activation and alkane dehydrogenation in mind, ^{Ar}LIr(H)$_2$ (complex **47**, Scheme 16) is desired since extrusion of dihydrogen would provide access to a highly reactive T-shaped, 14-electron species ^{Ar}LIr. One common route to dihydride complexes of iridium is reaction with dihydrogen gas. Addition of an atmosphere of dihydrogen to **42** showed no reaction at ambient temperature in 0.5 mL of benzene-d_6 (Scheme 16). Increasing the temperature incrementally by 10 °C up to 90 °C failed to reveal any reactivity. Addition of dihydrogen to **44** also did not lead to a reaction even at 75 °C for 24 hours.

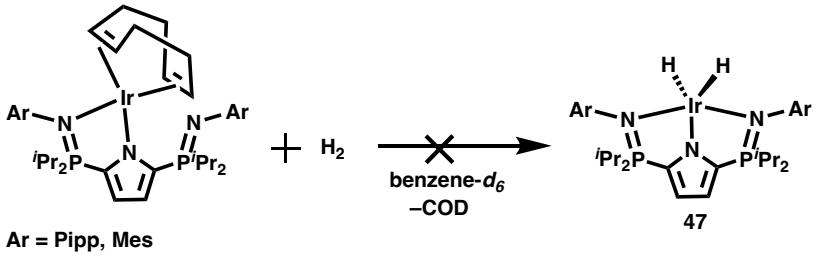

Scheme 16 Attempted synthesis of ^{Ar}LIr(H)$_2$

Since no reaction was observed between either **42** or **44** with dihydrogen, silanes were employed. No reaction was observed between **42** and one equivalent of $HSiEt_3$ at ambient temperature or upon heating to 70 °C for 4 hours (Scheme 17**)**.

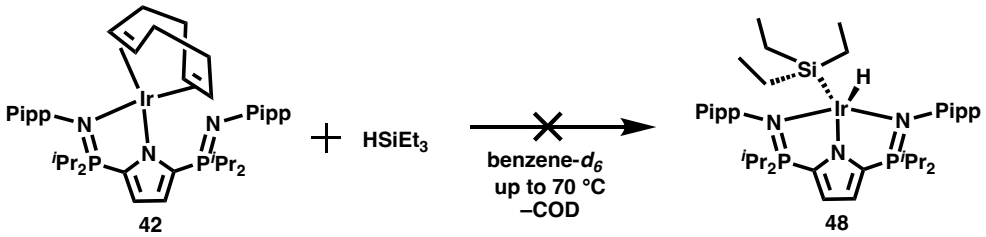

Scheme 17 Attempted synthesis of ^{Pipp}LIr(H)(SiEt$_3$)

Since $HSiEt_3$ is a tertiary silane, and hence, more sterically demanding than some other silanes, **44** was combined with one equivalent of H_3SiPh (Scheme 18). Unfortunately, only starting materials were observed, even after the mixture was heated to 70 °C for 24 hours.

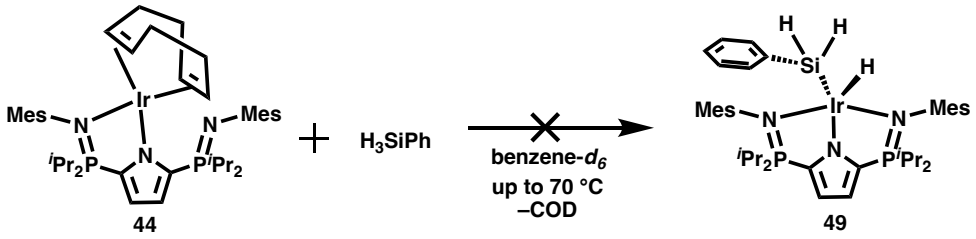

Scheme 18 Attempted synthesis of ^{Mes}LIr(H)(SiH$_2$Ph)

One of the likely culprits preventing reaction of complexes **42** and **44** with dihydrogen and silanes is the chelate effect.[88] The chelate effect describes the phenomenon that multidentate ligands readily replace monodentate ligands and form more stable complexes, explained by entropy. Since COD is a κ^2 ligand, release of COD and addition of two separate monodentate ligands is not entropy favoured.

2.2.2 Reactivity of ^{Pipp}LIr(COD) and ^{Mes}LIr(COD) with Strong σ-Donors

In an attempt to probe the lability of the COD ligand, an atmosphere of CO was added to complexes **42** and **44** (Scheme 19). The bright yellow solutions became pale yellow within 16 hours after the addition of CO. ^{Pipp}LIr(CO)$_2$ (**50**) was isolated as a brown powder in a 98% yield when volatiles were removed under reduced pressure, and ^{Mes}LIr(CO)$_2$ (**51**) was obtained as an off-white powder in 97% yield. Despite clean conversion in a J. Young NMR tube, extended periods of reduced pressure generated *minor* quantities of monocarbonyl complex ^{Ar}LIr(CO).

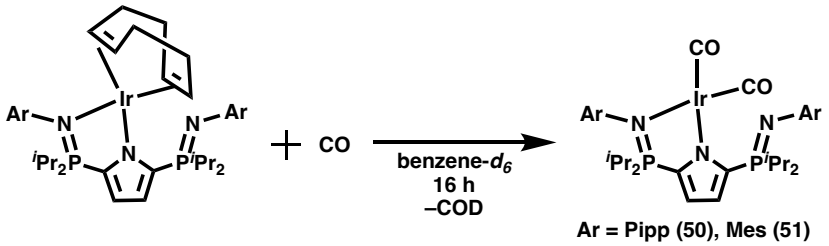

Scheme 19 Synthesis of ^{Ar}LIr(CO)$_2$ (Ar = Pipp, Mes)

Complex **50** exhibits two resonances in the $^{31}P\{^{1}H\}$ NMR spectrum (δ 58.3 and 10.2), which are slightly shifted from complex **42** (δ 58.7, 13.3). In the $^{13}C\{^{1}H\}$ NMR spectrum, there are two resonances assigned as *C*O at δ 174.3 and 172.7. Complex **51** displayed similar changes as **50**, with $^{31}P\{^{1}H\}$ chemical shifts at δ 53.7 and –2.0. The $^{13}C\{^{1}H\}$ resonances assigned as *C*O were observed at δ 173.9 and 170.9.

When compared to the rhodium analogue, ^{Pipp}LRh(CO)$_2$ (L = 2,5-(^{i}Pr$_2$P=NPipp)$_2$C$_4$H$_2$N), reported by Hayes *et al*., the $^{31}P\{^{1}H\}$ NMR spectrum of **50** is only slightly different (δ 58.9 and 13.8 for ^{Pipp}LRh(CO)$_2$; δ 58.3 and 10.2 for **50**).[77] The $^{13}C\{^{1}H\}$ *C*O resonances, however, are substantially more upfield in complex **50** (δ 186.3 and 184.7 for ^{Pipp}LRh(CO)$_2$; δ 174.3 and 172.7 for **50**). The CO stretching frequencies are approximately 30 cm^{-1} lower for the iridium complex **50** (^{Pipp}LRh(CO)$_2$: 2071, 1994; **50**: 2048, 1963). Others that have reported rhodium and iridium complexes with the same ligand also found a difference in the CO stretching frequencies and an upfield shift in the ^{13}C NMR for iridium, likely explained by more π-backdonation from iridium.[89-92] For example, with a bidentate, phosphine functionalized *N*-heterocyclic carbene the *C*O resonance in the $^{13}C\{^{1}H\}$ NMR spectra (M

= Rh: δ 190.4; M = Ir: $^{13}C\{^{1}H\}$ *C*O: δ 181.1, 180.0) and *C*O stretching frequencies in the IR spectra (M = Rh: 2079, 2008 cm^{-1}; M = Ir: 2067, 1997 cm^{-1}) are substantially different.[90]

Evidence for greater π-backdonation from iridium (*c.f.* rhodium) was provided by the X-ray crystal structure of **50**. Figure 13 shows the displacement ellipsoid plot (50% probability) of complex **50**. Iridium exhibits distorted square planar geometry ($\tau^4 = 0.11$) and κ^2-coordination of the *NNN*-ligand. Compared to $^{Pipp}LRh(CO)_2$, the M–C distances are shorter (M = Rh, 1.848(3) and 1.847(4) Å; M = Ir, 1.841(3), 1.839(3) Å) and the C–O distances are longer (M = Rh, 1.139(4), 1.149(4) Å; M = Ir, 1.147(4), 1.158(4) Å). The shortening of the M–C bond and corresponding elongation of the C–O bond can be explained by more π-backdonation from iridium to the CO ligand. Figure 14 shows typical donation and acceptance of CO ligands. The metal donates into the empty CO π* orbital, which reduces the CO bond order, elongating the C–O distance.

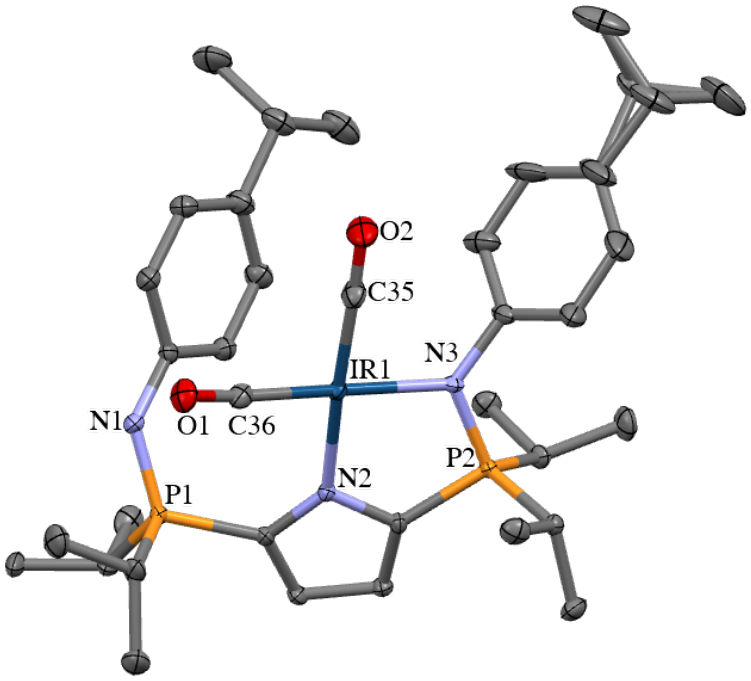

*Figure 13 Displacement ellipsoid plot (50% probability) of complex **50**. Hydrogen atoms were removed for clarity. Space group = P-1, R_1 = 3.42%. Selected bond distances (Å) and angles (°): Ir1–C35: 1.841(3), Ir1–C36: 1.839(3), Ir1–N2: 2.091(2), Ir1–N3: 2.081(2), C35–O2:1.147(4), C36–O1:1.158(4), P1–N1: 1.567(2), P2–N3: 1.621(2), N2–Ir1–N3: 82.91(9)*

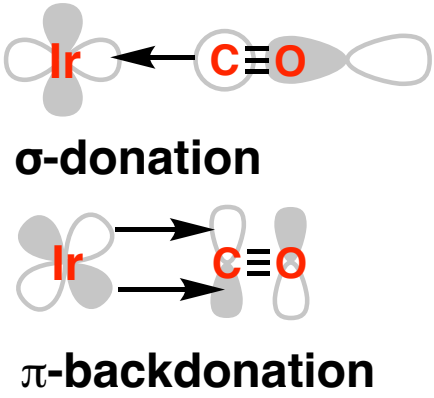

Figure 14 Graphical representation of the sigma donation and π-backdonation in Ir–CO bonding

With the knowledge that a strong σ-donor and good π-acceptor, such as CO, was able to replace COD, triphenylphosphine was added to a benzene-d_6 solution of complex **44**. Even after 3.5 hours at 50 °C, no reaction was observed. One possible explanation for the contrast in reactivity between CO and triphenylphosphine is that triphenylphosphine is more sterically demanding. Triphenylphosphine is larger than CO and therefore, if substitution occurs *via* an associative or interchange associative mechanism, the incoming phosphine may not be able to access the iridium centre. Differences in reactivity could also be attributed to the electronic differences between CO and triphenylphosphine.

2.3 Summary and Concluding Remarks

Three 1,5-cyclooctadiene iridium complexes, ^{Ar}LIr(COD) (Ar = Pipp, Dipp, Mes), were prepared from Na^{Ar}L and [IrCl(COD)]$_2$. Unexpectedly, when Ar = Mes and Dipp, these complexes could be generated with H^{Ar}L, presumably *via* the reductive elimination of HCl. All of the complexes were characterized by X-ray crystallography and multinuclear NMR spectroscopy. Steric trends were observed in the crystal structures, in which the free phosphinimine P=N–Ar angle increased with greater size of the N–Ar group.

The complexes ^{Pipp}LIr(COD) and ^{Mes}LIr(COD) did not react with dihydrogen or silanes; however, carbonyl complexes ^{Pipp}LIr(CO)$_2$ and ^{Mes}LIr(CO)$_2$ were generated through exposure to an atmosphere of CO. The iridium carbonyl complexes have been compared to the rhodium analogue, ^{Pipp}LRh(CO)$_2$. In contrast, ^{Mes}LIr(COD) did not react with triphenylphosphine.

Due to the chemical inertness of **42 – 44**, a more reactive species was sought. The synthesis, characterization, and reaction chemistry of a cyclooctene complex, ^{Pipp}LIr(COE), will be described in detail.

CHAPTER 3 – AN IRIDIUM CYCLOOCTENE COMPLEX: THE KEY TO FURTHER REACTIVITY

Chapter 2 described the synthesis, characterization, and reactivity of ^{Ar}LIr(COD). The complexes did not react with dihydrogen or various silanes under the experimental conditions studied, precluding further work. Given the increased lability of cyclooctene compared to 1,5-cyclooctadiene (monodentate versus bidentate alkene ligand; the chelate effect referred to in Chapter 2), an iridium cyclooctene complex was the next synthetic target. This chapter describes the synthesis, characterization, and reaction chemistry of the iridium cyclooctene complex, ^{Pipp}LIr(COE) (L = 2,5-(^{i}Pr$_2$P=NPipp)$_2$C$_4$H$_2$N, Pipp = *para*-isopropylphenyl).

3.1 Synthesis and Characterization of ^{Pipp}LIr(COE)

3.1.1 Synthesis and Characterization

In order to synthesize the iridium cyclooctene (COE) complex ^{Pipp}LIr(COE) (L = 2,5-(^{i}Pr$_2$P=NPipp)$_2$C$_4$H$_2$N, Pipp = *para*-isopropylphenyl, **52**), one equivalent of Na^{Pipp}L and 0.5 equivalents of the dimer [IrCl(COE)$_2$]$_2$ were reacted for 16 hours in toluene at ambient temperature (Scheme 20). The initial orange-yellow suspension became reddish-brown within five minutes. After 16 hours, volatiles were removed under vacuum, using pentane (4 × 4 mL) to assist removal of free COE, leaving a reddish-brown powder.

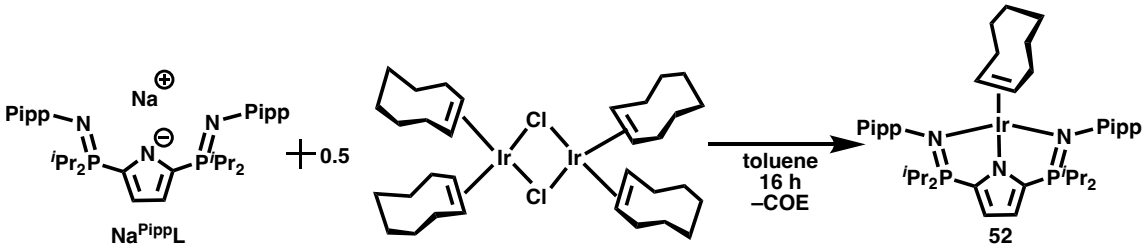

*Scheme 20 Synthesis of iridium cyclooctene complex ^{Pipp}LIr(COE) (**52**)*

The $^{31}P\{^{1}H\}$ NMR spectrum of ^{Pipp}LIr(COE) showed a major signal at δ 56.1. The ^{1}H NMR spectrum revealed a single alkene resonance at δ 3.16, shifted substantially upfield from free COE (δ 5.62). The $^{13}C\{^{1}H\}$ NMR spectrum contains an upfield shifted alkene resonance at δ 45.7 (δ 130.2 for free COE). Furthermore, there were only a single set of resonances for each environment of the pincer ligand in the ^{1}H NMR spectrum, and a single resonance in the $^{31}P\{^{1}H\}$ NMR spectrum suggesting C_s molecular symmetry, as well as a κ^3-coordination mode of the supporting pincer ligand. Despite the use of multiple solvents and temperatures, repeated attempts to grow X-ray quality crystals of **52** were unsuccessful.

3.1.2 Challenges of ^{Pipp}LIr(COE)

Although the method described in the previous section provided one *major* product (complex **52**), the NMR spectra did not suggest an analytically pure sample. Typically, the $^{31}P\{^{1}H\}$ NMR spectrum indicated ~65-70% purity based off the relative integrations of the signals in the spectrum. It was unclear what the remaining portion of the mixture contained, but they did lie within the range of iridium complexes for this system (δ 55.0–70.0). To elucidate which aspect of the reaction conditions posed problems (*e.g.* time, temperature,

or exposure to vacuum), the reaction of $Na^{Pipp}L$ and $[IrCl(COE)_2]_2$ was performed at an NMR scale. The reaction indicated that a 48-hour reaction time led to an increase in purity (~85-90%), as demonstrated by the relative integrations of the signals in the $^{31}P\{^1H\}$ NMR spectrum. When the sample was left in solution at ambient temperature for 50 hours, no decomposition of **52** was observed. When all solvent and excess COE were removed under vacuum, however, a decrease in purity to ~65-70% was indicated by the $^{31}P\{^1H\}$ NMR spectrum, with all resonances lying within the range of iridium complexes for this system. It was determined that the product is not stable under low pressure, presumably due to loss of COE. Accordingly, the complex was generated *in situ* for further reaction chemistry. The optimal reaction conditions for the *in situ* synthesis of **52** was determined to be 48 hours at ambient temperature in an aromatic solvent (benzene-d_6 or toluene-d_8).

With the intention of changing the steric and electronic properties of **52**, reactions of $Na^{Ar}L$ (Ar = Mes, Dipp) with $[IrCl(COE)_2]_2$ were attempted (Scheme 21). In both instances, $H^{Ar}L$ was one of the products of the reaction. When Ar = Mes, a new iridium containing species appeared at δ 54.7 in the $^{31}P\{^1H\}$ NMR spectrum within 15 minutes. Over the course of the reaction, the complex never exceeded 3% of the mixture, while $Na^{Mes}L$ was slowly being consumed. However, the reaction was not monitored longer than 10% consumption of $Na^{Mes}L$. It was hypothesized that **52** is not vacuum stable, because COE is presumably labile. Introducing additional steric bulk about the metal centre was anticipated to drive the equilibrium towards free COE + ^{Mes}LIr. Once COE has dissociated, the resultant 14-electron species, ^{Mes}LIr, likely decomposes quickly affording $H^{Mes}L$ and various unidentified iridium-containing species. The 14-electron intermediate would be very

reactive, and solvent may be the source of H^+ or, although all solvents were rigorously dried, adventitious water may be the source of H^+.

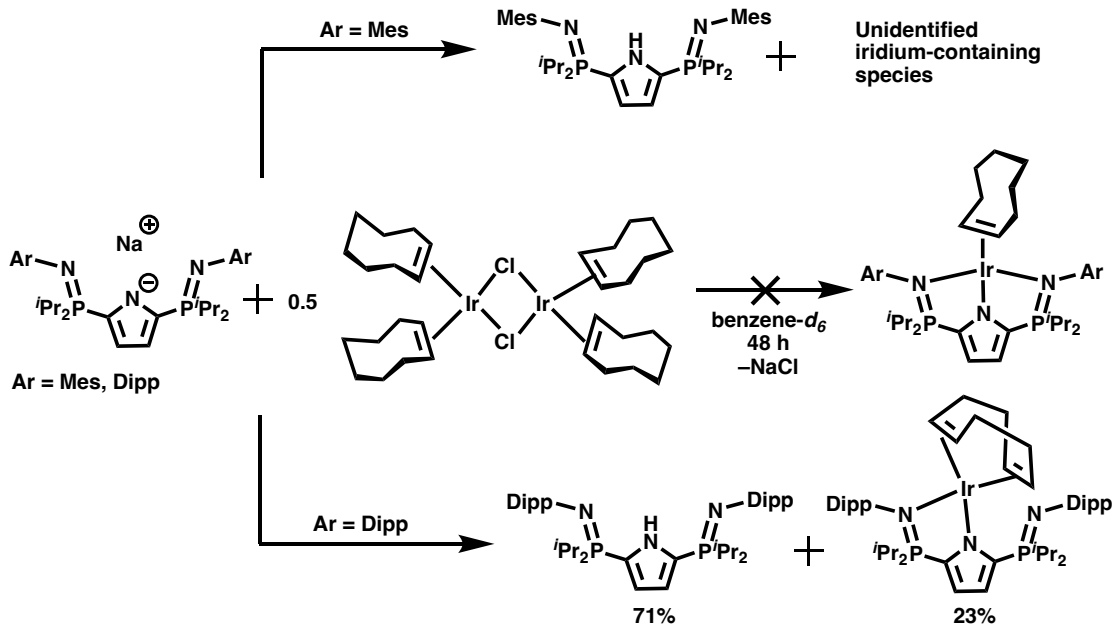

Scheme 21 Attempted synthesis of ^{Mes}LIr(COE) and ^{Dipp}LIr(COE)

When Ar = Dipp, different reactivity was observed (Scheme 21). Within 15 minutes, 5% of the phosphorus-containing portion of the mixture was $H^{Dipp}L$ and the remaining portion was $Na^{Dipp}L$. With heating to 50 °C for 17 hours, more of $Na^{Dipp}L$ was converted to $H^{Dipp}L$. However, in addition to this change, a new asymmetric product which gave rise to signals at δ 49.9 and δ –3.0 in the $^{31}P\{^1H\}$ NMR spectrum was observed, which corresponds to ^{Dipp}LIr(COD) (**43**), that was reported in Chapter 2. There was a multiplet at δ 5.65 in the ^1H NMR spectrum assigned as free COE. After 113 hours at 50 °C, 23% of the mixture was **43**. The ^1H NMR spectrum did not have any resonances that could be assigned as coordinated COD. However, the ^1H NMR spectrum of ^{Dipp}LIr(COD) is broad and the

coordinated COD resonances could not be observed at ambient temperature. In addition, the resonances assigned as COE no longer appeared as a multiplet, but as a small, broad singlet. Since no internal standard was used it cannot be confirmed whether the amount of COE in solution had decreased. The mechanism for the conversion to ^{Dipp}LIr(COD) is unknown but it may involve dehydrogenation of COE. Free dihydrogen would be expected in solution, but this was not observed. Further experimentation, such as testing higher temperatures for the reaction to observe full conversion would need to be undertaken.

3.2 Reaction of ^{Pipp}LIr(COE) with Dihydrogen

3.2.1 Synthesis and Characterization of an Iridium Dihydride

With the goal of bond activation and alkane dehydrogenation in mind, ^{Pipp}LIr(COE) (**52**) was reacted with an excess of dihydrogen at ambient temperature (Scheme 22). Within 10 minutes, a new resonance at δ 59.8 was observed in the $^{31}P\{^{1}H\}$ NMR spectrum, as well as a signal corresponding to H^{Pipp}L at δ 15.2. Furthermore, a signal attributed to a hydride appeared at δ –29.45 in the ^{1}H NMR spectrum. Although this resonance is more upfield than might be expected, Iluc *et al*. reported *PCOP*-Ir(H)$_2$ (**54**), which exhibited two hydride resonances at δ –11.39 and –31.85 in the ^{1}H NMR spectrum (Figure 15).[93] In addition, numerous other reports of iridium dihydride complexes supported by pincer ligands have ^{1}H NMR signals that range between δ –18.81[87] and –22.14[94].

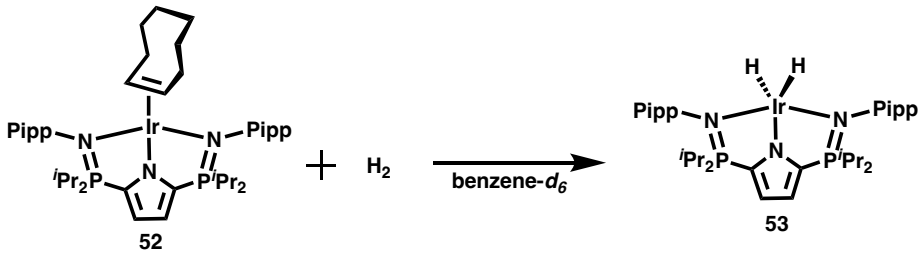

Scheme 22 Attempted synthesis of ^{Pipp}LIr(H)$_2$

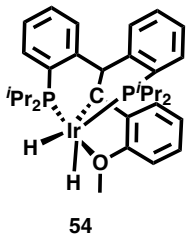

*Figure 15 PCOP-Ir(H)$_2$ (**54**) used as comparison to ^{Pipp}LIr(H)$_2$*

Two hours after the addition of dihydrogen, a mixture of products was observed in the $^{31}P\{^{1}H\}$ NMR spectrum, as well as multiple new hydride resonances between δ –20 and –40 in the ^{1}H NMR spectrum. By this point, the signal at δ 59.8 in the $^{31}P\{^{1}H\}$ NMR spectrum contributed only approximately 5% of the mixture.

Since initial attempts to synthesize ^{Pipp}LIr(H)$_2$ (**53**) at ambient temperature led to a number of products, it was concluded that complexes such as **53** may be thermally sensitive. Accordingly, dihydrogen was added at –53 °C to a solution of **52** in 0.5 mL of toluene-d_8 in a J. Young NMR tube (Scheme 23). There were no immediate visible changes to the solution. The J. Young NMR tube containing the sample was then injected into a pre-cooled

NMR probe at –30 °C; necessary precautions were taken to ensure the sample was not warmed above this temperature before measurements were obtained.

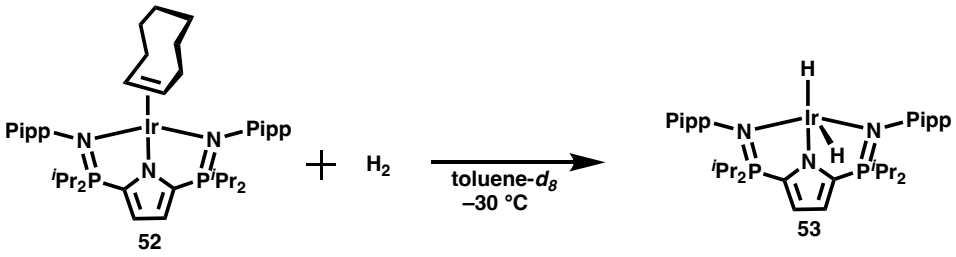

*Scheme 23 Synthesis of ^{Pipp}LIr(H)$_2$ (**53**)*

The ^{31}P{^{1}H} NMR spectrum indicated ~62% of the mixture had been converted to a new complex that gave rise to a signal at δ 60.2, which was attributed to ^{Pipp}LIr(H)$_2$ (complex **53**, Scheme 23). The assignment of the signal in the ^{31}P{^{1}H} NMR spectrum as a dihydride species was corroborated by two broad hydride resonances, each integrating to 1H, at δ –6.90 and –14.62, in the ^{1}H NMR spectrum (Figure 16). Analysis of the ^{1}H NMR spectrum did not reveal free dihydrogen at δ 4.46. Further additions of dihydrogen (five times) to the J. Young NMR tube converted all of **52** to **53**.

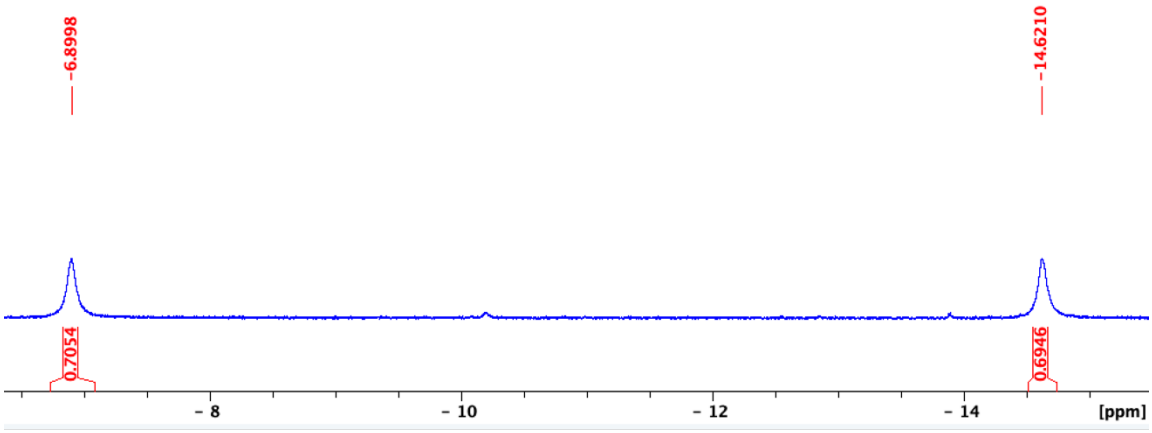

*Figure 16 Iridium hydride resonances in the ^{1}H NMR spectrum (300.13 MHz) of complex **53** in toluene-d_8 at –30 °C*

In-depth analysis of the ^{1}H NMR spectrum revealed that although there was no free dihydrogen in solution, there was a broad resonance at δ 4.10 that did not exhibit crosspeaks in the ^{1}H-^{1}H COSY NMR spectrum. The signal was assigned as dihydrogen, likely in dynamic equilibrium with $^{Pipp}LIr(H)_2$. For example, an equilibrium between $^{Pipp}LIr(H)_2$ and $^{Pipp}LIr + H_2$ is one possibility. Another possibility would be an equilibrium between $^{Pipp}LIr(H)_2$ and $^{Pipp}LIr(H)_2(H_2)$, or even $^{Pipp}LIr(H)_4$. With the data acquired, a definitive conclusion could not be drawn.

Most iridium species of the formula $LIr(H)_2$ only have one Ir–*H* signal in the ^{1}H NMR spectrum.[11, 41, 43, 87] Accordingly, it is unusual that two hydride resonances were observed for complex **53**. This finding is attributed to the complex exhibiting square pyramidal geometry and slow, if any, fluxionality on the NMR time scale. One report by Wendt *et al*. discussed solvent dependent differences in the geometry of *PCP*-$Ir(H)_2$ complexes.[95] They suggested that iridium dihydride species supported by *PCP*-based pincer ligands are often

trigonal bipyramidal in non-polar solvents and square pyramidal in polar solvents. This is different than what was observed for complex **53**, as this species displays square pyramidal geometry in the hydrocarbon solvent toluene-d_8.

An early report on the discussion of trigonal bipyramidal and square pyramidal geometries in d^6 five-coordinate complexes suggested that the ligand in the basal site has an influence on which geometry is favoured.[96] If the ligand is a weak σ-donor and π-donor, the complex typically displays trigonal bipyramidal geometry. In contrast, if the ligand is a σ-donor and π-acceptor, the complex tends to exhibit square pyramidal geometry. In the case of complex **53**, the ligand in the basal site is an anionic pyrrole. Pyrrole is a strong σ-donor and weak π-donor, which would suggest, based on the aforementioned report, that trigonal bipyramidal geometry would prevail, which is not the case. Furthermore, dihydride species supported by *PCP*-pincer ligands that have been used for alkane dehydrogenation are often highly thermally stable (sometimes up to 200 °C or higher), which is not the case for complex **53** (*vide infra*). Given that there are very few iridium pincer complexes supported by monoanionic *NNN*-pincer ligands (as is the case for those described in this thesis), it is not surprising that they possess unusual structural properties and reaction patterns. Continued and comprehensive studies on this unique and exciting class of iridium complexes are warranted.

Another observation was that free COE was hydrogenated to cyclooctane (COA) as **53** was formed. Details of the hydrogenation, as well as catalytic hydrogenation, will be discussed in Chapter 4.

To gain further insight into the structure and stability of **53**, a larger scale reaction was undertaken in an effort to isolate $^{Pipp}LIr(H)_2$. Dihydrogen was added to a frozen solution of **52** in toluene. The reaction mixture was then allowed to warm to ambient temperature. Volatiles were removed under vacuum and the ^1H and $^{31}P\{^1H\}$ NMR spectra were acquired in benzene-d_6. No evidence of reaction was observed; complex **52** was the only phosphorus-containing iridium complex in the mixture. It is peculiar that no decomposition was observed as the reaction mixture was allowed to warm to ambient temperature. One possible explanation is that if a rapid equilibrium between $^{Pipp}LIr(H)_2$ and $^{Pipp}LIr + H_2$ exists, dihydrogen could easily be removed and replaced by COE when the mixture is exposed to dynamic vacuum. It may be argued that because free COE is hydrogenated in solution as **53** forms, decomposition should be observed as the equilibrium is pushed towards free dihydrogen with increasing temperature. Therefore, it could be suggested that dihydrogen was not added in an appropriate quantity to the reaction mixture. However, NMR analysis of the reaction mixture did show free COA (δ 1.50 with absence of a resonance at δ 5.62) in solution suggesting that some, but not all, of the COE was hydrogenated during the reaction.

3.2.2 Effect of Increasing Temperature on $^{Pipp}LIr(H)_2$

The complex $^{Pipp}LIr(H)_2$ (**53**) was stable at –30 °C for 16 hours. The mixture was then monitored as the temperature was increased incrementally. When the temperature was changed to –20 °C, the hydride resonances immediately became substantially broader (Figure 17, whh: 119.7 Hz and 111.0 Hz from 26.5 Hz and 25.8 Hz for δ –6.90 and –14.62,

respectively). At 0 °C, the hydride signals were no longer observed. The signal corresponding to complex **53** was still present in the $^{31}P\{^{1}H\}$ NMR spectrum, however. After 45 minutes at 0 °C, conversion back to complex **52** was observed at a ratio of 4:1 (**53**:**52**) based on the relative integrations observed in the $^{31}P\{^{1}H\}$ NMR spectrum (Figure 18). The temperature was further increased to 15 °C. After 2 hours and 45 minutes the ratio of **53**:**52** changed to 1:4. There were also numerous decomposition products observed in the $^{31}P\{^{1}H\}$ NMR spectrum, such as resonances at δ 63.1 (unknown), 55.1 (unknown), and 15.0 ($H^{Pipp}L$). When the reaction mixture was cooled back to –30 °C, a portion of the mixture converted back to **53** (3:7, **53**:**52**), evidenced by a return of the hydride resonances and $^{31}P\{^{1}H\}$ NMR signal. If the temperature was increased again to 15 °C, the signals corresponding to the hydride ligands were no longer present and further decomposition was observed.

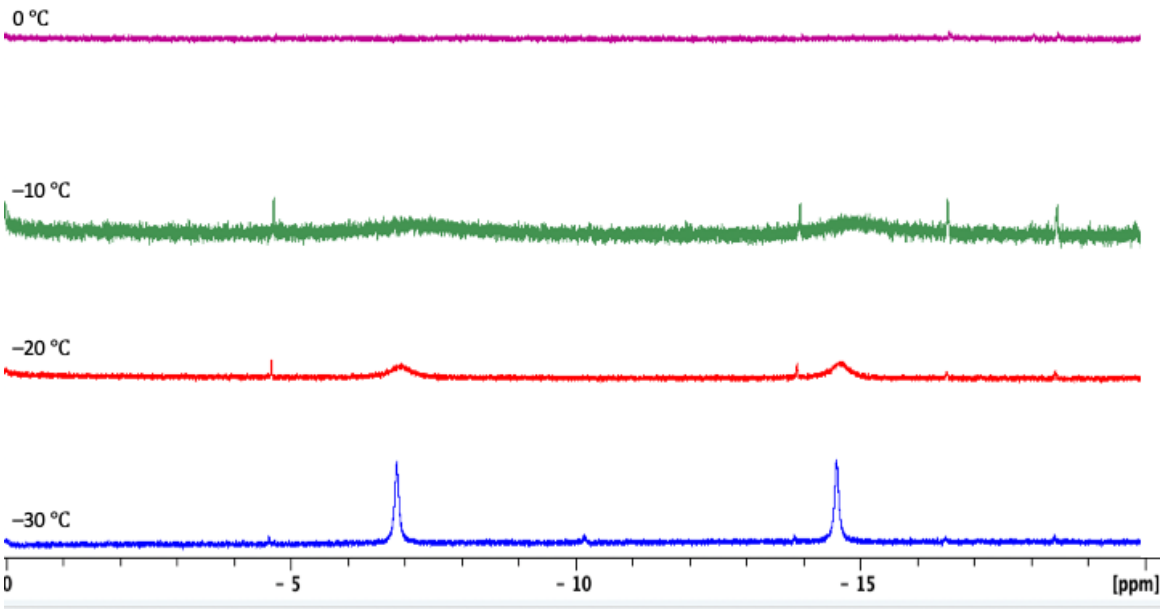

*Figure 17 Hydride region of the ^{1}H NMR spectrum (300.13 MHz) of complex **53** at different temperatures (–30 °C, –20 °C, –10 °C, and 0 °C) in toluene-d_8*

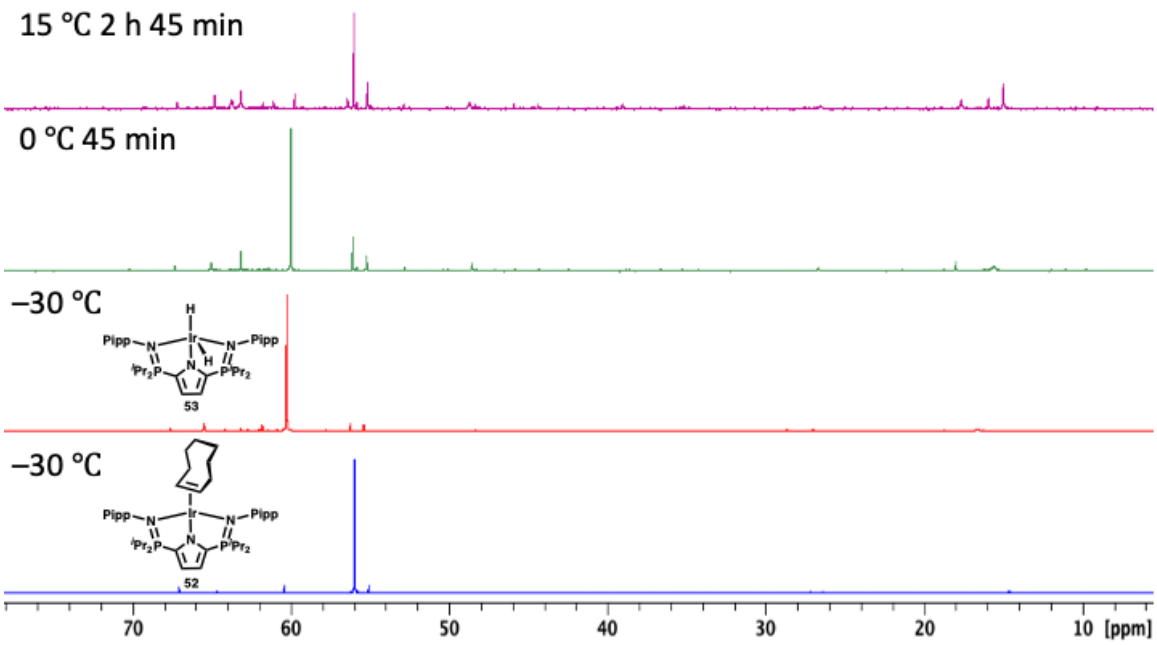

*Figure 18 $^{31}P\{^1H\}$ NMR spectra (121.495 MHz) in toluene-d_8 of complexes **52** and **53**, and the effect of increasing temperature on complex **53***

For alkane dehydrogenation to occur, C(sp^3)–H oxidative addition is often required. Goldman *et al*. reported experimental and computational studies on two possible pathways for acceptorless alkane dehydrogenation.[97] The associative pathway involves an Ir(V) intermediate after C(sp^3)–H oxidative addition, followed by reductive elimination of dihydrogen (Scheme 24). The dissociative pathway begins with reductive elimination of dihydrogen, resulting in a complex which could presumably undergo C(sp^3)–H oxidative addition.

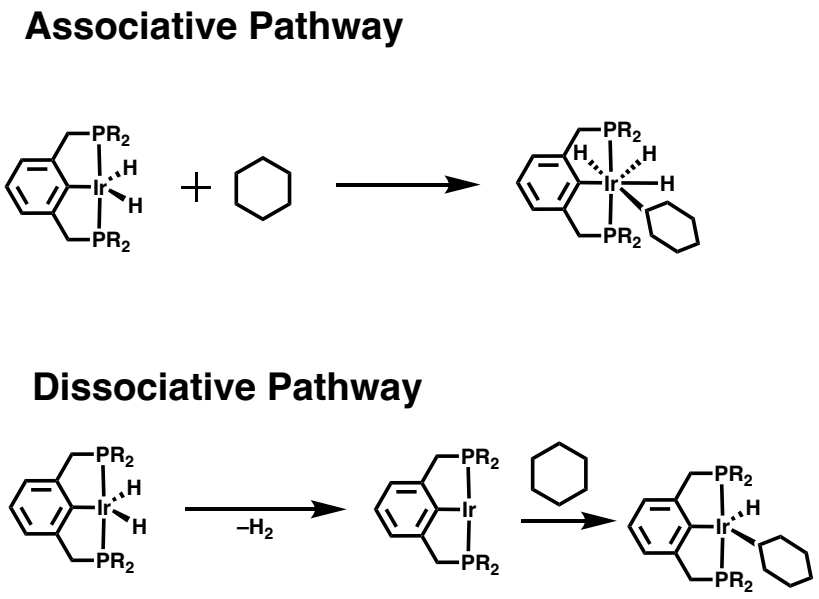

Scheme 24 Associative and dissociative alkane dehydrogenation mechanisms proposed by Goldman et al.[97]

Considering these two pathways, it could be that with an increase in temperature the equilibrium between $^{Pipp}LIr(H)_2$ and $^{Pipp}LIr + H_2$ either begins to favour the latter or becomes more rapid. If the process is faster than the NMR time scale, this may explain why the hydride resonance are not observed at 0 °C. In addition, it could provide insights into the decomposition of complex **53**. The highly reactive, T-shaped, 14-electron species (^{Pipp}LIr) generated by dihydrogen reductive elimination would presumably react with any solvent or other molecules in solution, but this is not readily apparent by NMR spectroscopy.

3.3 Reaction of ^{Pipp}LIr(COE) with Silanes (H_3SiPh, H_2SiPh_2, $HSiEt_3$)

3.3.1 Synthesis and Characterization of Iridium Silyl Hydride Complexes

Oxidative addition of an Si–H bond is the first step in the Chalk-Harrod mechanism for catalytic hydrosilylation of alkenes (Scheme 25).[58] Reactions between ^{Pipp}LIr(COE) (**52**) and primary, secondary, and tertiary silanes were conducted. Reaction of **52** with R_3SiH (R_3 = H_2Ph, HPh_2, Et_3) in sealed J. Young NMR tubes produced bright red solutions (Scheme 26). The reaction was complete within one hour when using H_3SiPh and H_2SiPh_2, but required 16 hours when $HSiEt_3$ was employed, likely due to the additional steric demand of three ethyl substituents.

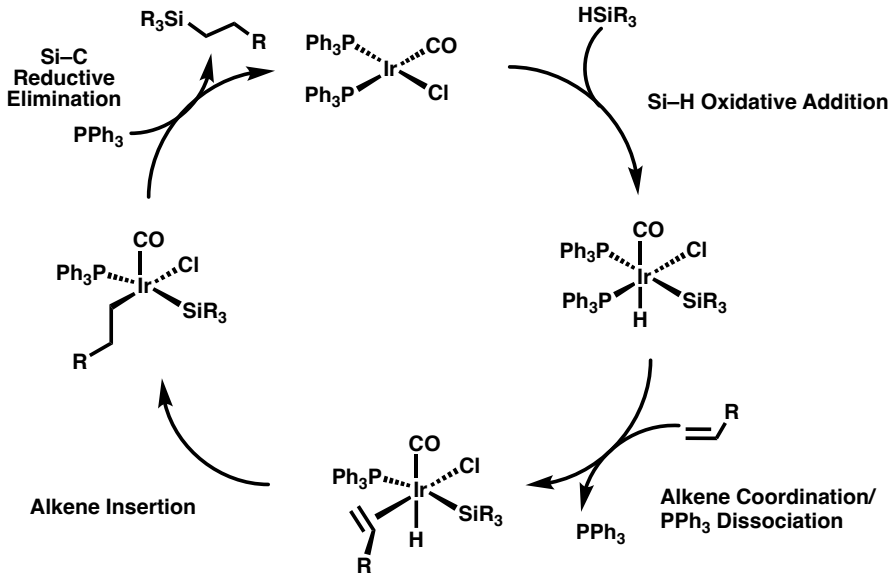

Scheme 25 Chalk-Harrod mechanism for hydrosilylation[58]

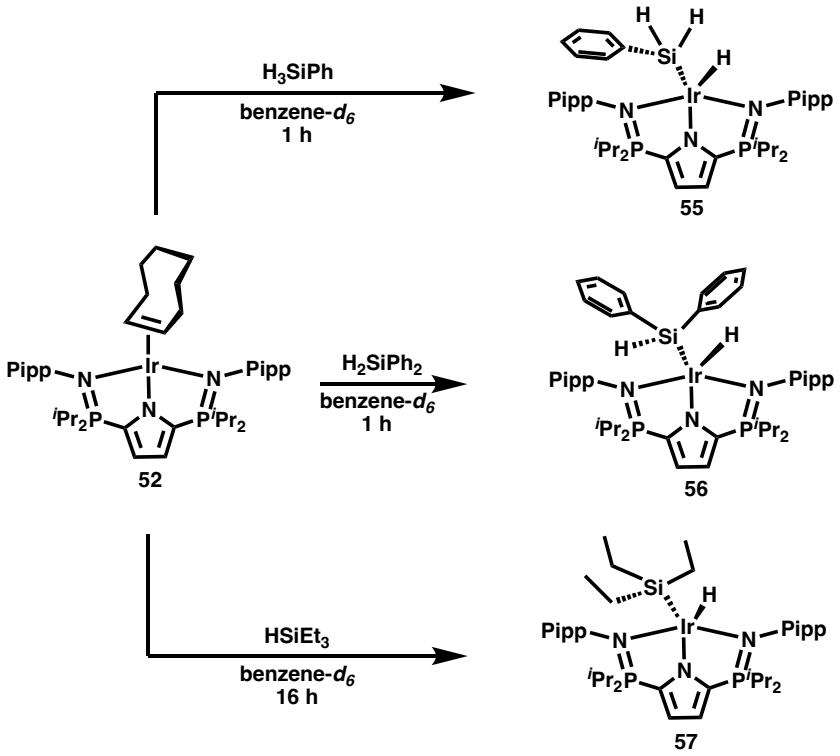

*Scheme 26 Synthesis of ^{Pipp}LIr(H)(SiR$_3$) (R$_3$ = H$_2$Ph (**55**), HPh$_2$ (**56**), Et$_3$ (**57**))*

Reaction of **52** with H$_3$SiPh in benzene-d_6 at ambient temperature led to a species that exhibited a downfield shifted signal in the ^{31}P{^{1}H} NMR spectrum (δ 56.1 to 62.6). The upfield region (δ 0 to –60) of the ^{1}H NMR spectrum contains a broad triplet ($^3J_{H\text{-}H}$ = 2.8 Hz, δ –16.16) that integrates to approximately 1H and is attributed to a terminal iridium hydride. The SiH_2 signal appeared at δ 4.96 with ^{29}Si satellites but coupling to the hydride was not observed. The ^{29}Si NMR spectrum exhibited a triplet of triplets ($J_{Si\text{-}H}$ = 175.9 Hz, $^3J_{Si\text{-}H}$ = 6.0 Hz) centred at δ –42.9, due to coupling to the directly attached hydrogen atoms, as well as the *ortho* hydrogens of the phenyl group. All signals corresponding to the supporting ligand in the ^{1}H and ^{13}C{^{1}H} NMR spectra were symmetric, suggesting a κ^3-coordination mode to iridium and C_s molecular symmetry. The complex ^{Pipp}LIr(H)(SiH$_2$Ph)

(**55**) was isolated in 99% yield as a red powder. Numerous attempts to grow X-ray quality crystals of **55** were unsuccessful.

Reaction of **52** with H_2SiPh_2 in a sealed J. Young NMR tube in benzene-d_6 at ambient temperature revealed a new resonance at δ 63.1 (from δ 56.1) in the $^{31}P\{^1H\}$ NMR spectrum, corresponding to $^{Pipp}LIr(H)(SiHPh_2)$ (**56**). A new broad resonance attributed to an iridium hydride was observed at δ –15.37 in the ^1H NMR spectrum. A doublet with ^{29}Si satellites also emerged at δ 5.16 which was assigned as the hydrogen directly attached to silicon ($^3J_{H\text{-}H}$ = 2.6 Hz). A doublet was observed in the ^{29}Si NMR spectrum ($J_{Si\text{-}H}$ = 176.9 Hz), due to coupling to the directly attached hydrogen, was observed at δ –10.3. As discussed for complex **55**, the ligand resonances are symmetric, suggesting a κ^3-coordination mode and C_s molecular symmetry. Complex **56** was isolated in a 92% yield as a pale red powder.

The reaction of **52** with $HsiEt_3$ in a sealed J. Young NMR tube in benzene-d_6 produced $^{Pipp}LIr(H)(SiEt_3)$ (**57**) in 16 hours at ambient temperature. A new singlet in the $^{31}P\{^1H\}$ NMR spectrum was observed at δ 60.0 from δ 56.1. There was a singlet hydride resonance at δ –16.79 in the ^1H NMR spectrum. The ^{29}Si NMR spectrum revealed one singlet resonating at δ 9.0. Complex **7** was isolated in a 58% yield after crystallization from pentane.

With all NMR data considered, there are some comparisons to be made (Table 4). Complex **55** gave rise to the most upfield (δ –42.9) ^{29}Si resonance. A trend was observed in that there was a more downfield shift with increased substitution (**56**: δ –10.3; **57**: δ 9.0). Others have

also found that increasing the steric bulk at silicon resulted in a more downfield shift in the ^{29}Si NMR spectrum (Figure 19).[98, 99] For both rhodium(V) and iridium(V) bis(silyl)dihydride complexes, the complexes with three ethyl substituents give rise to the most downfield signals in the ^{29}Si NMR spectrum. As the steric bulk decreases, the resonances shift further upfield. This comment, however, does not consider the electronic differences between phenyl and ethyl substituents. Phenyl moieties are electron withdrawing, and ethyl functionalities are electron donating. This would cause an opposite effect than what was observed. There was no obvious trend in the location of the hydride resonances. Complex **57** displayed the most upfield ^{31}P{^{1}H} NMR resonance (δ 60.0), likely due to the greater electron-donating capacity of the ethyl substituents compared to phenyl moieties.

*Table 4 NMR spectral data of silyl hydride complexes **55**, **56**, and **57***

Complex	**^{31}P[2] (δ)**	**^{1}H: Ir–*H* (δ)**	**^{29}Si (δ)**
55	62.6	–16.2	–42.9
56	63.1	–15.4	–10.3
57	60.0	–16.8	9.0

[2] The ^{31}P NMR spectra of complexes **55**, **56**, and **57** were ^{1}H decoupled.

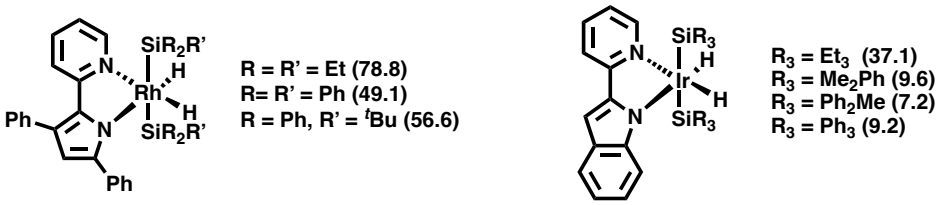

Figure 19 Rhodium(V) and Iridium(V) bis(silyl)dihydride complexes. The values in brackets are the ^{29}Si NMR chemical shift in ppm

Bright red blocks were grown out of a concentrated toluene solution of **56** stored at –30 °C for one week. During the mounting procedure, the bright red crystals (under Paratone oil) became black within 10 minutes, exhibiting the extreme air sensitivity of **56**. The X-ray crystal structure of **56** is shown in Figure 20. The hydride ligand could not be located in a difference Fourier map.

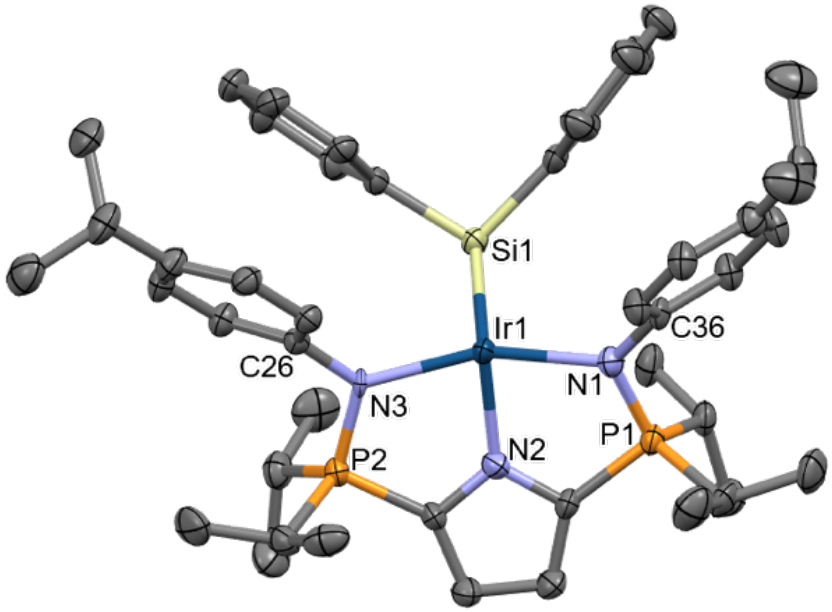

*Figure 20 Displacement ellipsoid plot (50% probability) of **56**. See Table 5 for selected bond distances and angles. Hydrogen atoms were removed for clarity. The hydride ligand was not located in the difference Fourier map. Space group = P2/c. R_1 = 3.31%*

Large, bright red blocks of **57** were grown from a concentrated pentane solution stored at –30 °C for two days. During the mounting procedure, the bright red crystals (under Paratone oil) became black within 10 minutes, exhibiting the extreme air sensitivity of **57**. The X-ray crystal structure of complex **57** is shown in Figure 21. The hydride ligand was located by in the difference Fourier maps, but the Si–Ir–H angle was restrained to 120 °. Two molecules of **57** and one pentane solvent molecule crystallized in the asymmetric unit. In-depth comparison of the bond distances and angles did not reveal a significant difference between the two molecules of complex **57** (e.g. Ir–Si: 2.2781(7) and 2.2828(7) Å).

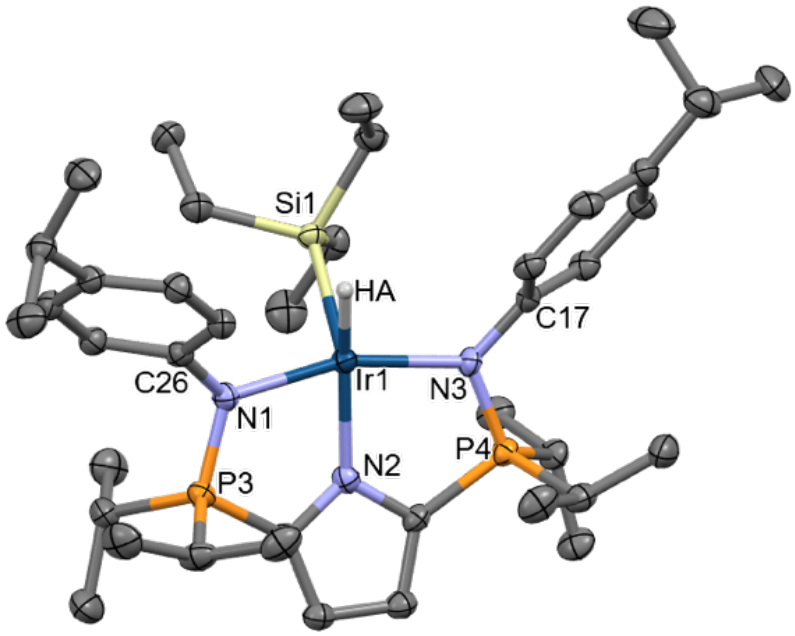

*Figure 21 Displacement ellipsoid plot (50% probability) of **57**. See Table 5 for selected bond distances and angles. One pentane solvent molecule and most hydrogen atoms were removed for clarity. Two molecules of **57** crystallized in the asymmetric unit, but only one is shown for clarity. Space group = $P2_1/c$. R_1 = 2.61%*

The X-ray crystal structures of complexes **56** and **57** confirmed the κ^3-coordination mode of the supporting ligand in the solid state. The P=N distances were elongated upon coordination to iridium (**56**: 1.6313(16) Å; **57**: 1.629(2) Å; *c.f.* $H^{Pipp}L$: 1.578(1) Å[77]). The hydride ligand was not located in **56**, but was found in the difference Fourier maps for **57**. When considering the N–Ir–N (**56**: 81.64(6)°; **57**: 82.48(9)°) and N–Ir–Si (**56**: 122.15(5)°; **57**: 131.87(6)°) angles, the geometry at iridium can be considered distorted trigonal bipyramidal (Table 5); however, a reliable τ^5 value could not be calculated as the hydride ligand was not located for **56** and the H–Ir–Si angle was restrained for **57**. The N–Ir–Si angle was significantly larger for **57** than **56** (**56**: 122.15(5) °; **57**: 131.87(6) °), likely for the larger ethyl substituents to avoid the isopropyl groups on phosphorus. When comparing complexes **56** and **57** to other Ir–Si containing complexes found in the Cambridge Structural Database, the Ir–Si distances were shorter than the average reported distance of 71 other complexes (**56**: 2.2397(5) Å; **57**: 2.2805(7) Å; literature average: 2.3741 Å).[100]

*Table 5 Selected bond distances (Å) and angles (°) of silyl hydrides complexes **56** and **57***

Atoms	56	57†
P=N‡	1.6313(16)	1.629(2)
Ir–Si	2.2397(5)	2.2805(7)
N–Ir–Si	122.15(5)	131.87(6)
N–Ir–N‡	81.64(6)	82.48(9)

†*The asymmetric unit contains two molecules of **57** and one pentane solvent molecule. Reported distances and angles are an average of both molecules.*

‡*These values are an average of the two distances/angles, respectively.*

3.4 Alternatives to ^{Pipp}LIr(COE) for Catalytic Applications

3.4.1 Preface

Although ^{Pipp}LIr(COE) (**52**) reacted with $HSiR_3$ (R_3 = Et_3, H_2Ph, HPh_2) and dihydrogen leading to further exploration into catalytic processes (see Chapter 4), cyclooctene (COE) presented a likely competitor. Since neither **52** nor ^{Pipp}LIr$(H)_2$ (**53**) can be isolated as analytically pure solids and COE is hydrogenated to cyclooctane (COA) during the synthesis of **53**, there is free COE/COA in solution during catalytic runs. During alkane dehydrogenation, COA would compete with any other alkane substrates for dehydrogenation. For this reason, it was considered important to discover an alternative to ^{Pipp}LIr(COE) for catalytic or chemical applications.

3.4.2 Attempted Synthesis of the Monocarbonyl Complex ^{Pipp}LIr(CO)

A revised synthesis of an analogous rhodium monocarbonyl complex, ^{Pipp}LRh(CO), was reported by the Hayes group in 2019.[78] The original synthesis involved heating ^{Pipp}LRh$(CO)_2$ with periodic evacuation of the headspace.[77] The complex ^{Pipp}LIr$(CO)_2$ (**50**) showed vacuum stability, and therefore, the aforementioned route was not considered feasible. The revised preparation involved a comproportionation reaction by which ^{Pipp}LRh$(CO)_2$ was reacted with one equivalent of the ^{Pipp}LRh(COE) to afford ^{Pipp}LRh(CO). The reaction was complete within one hour.

In order to synthesize ^{Pipp}LIr(CO)$_2$ (**50**), **52** in 0.5 mL of benzene-d_6 was exposed to an atmosphere of CO at ambient temperature in a J. Young NMR tube (Scheme 27). The reaction mixture immediately turned pale yellow-brown from dark reddish-brown. Within one hour, only two signals (in a 1:1 ratio) were observed in the ^{31}P{^{1}H} NMR spectrum (δ 58.3 and 10.2, from δ 56.1), assigned as complex **50**. For an in-depth discussion of **50**, see Chapter 2.

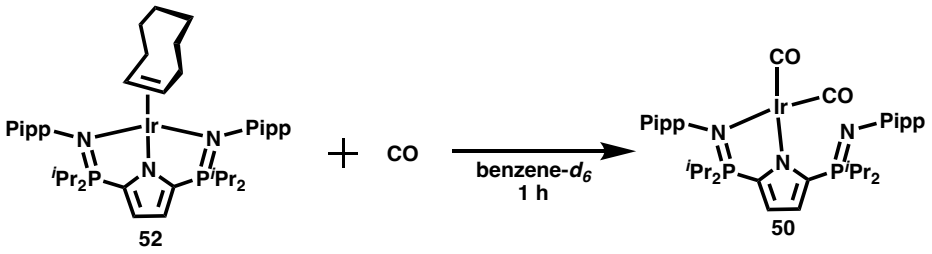

Scheme 27 Synthesis of ^{Pipp}LIr(CO)$_2$ from ^{Pipp}LIr(COE)

Combination of **52** with one equivalent of **50** in benzene-d_6 indicated no reaction occurred at ambient temperature within two hours (Scheme 28). After 18 hours at 40 °C, however, two new signals were observed in the ^{31}P{^{1}H} NMR spectrum at δ 58.2 and 58.0 comprising approximately 5% and 3.5% of the mixture, respectively. The temperature was then increased to 60 °C. The two new resonances increased in intensity over two hours at this temperature, as did multiple other signals (δ 67.3, 64.9, and 60.5). Complex **52** was fully consumed after 20 hours at 70 °C, but **50** was not. It was hypothesized that **52** was not stable at 60–70 °C, and the new resonances correlated to decomposition products. A control experiment heating **52** to 60–70 °C would need to be conducted to confirm this hypothesis.

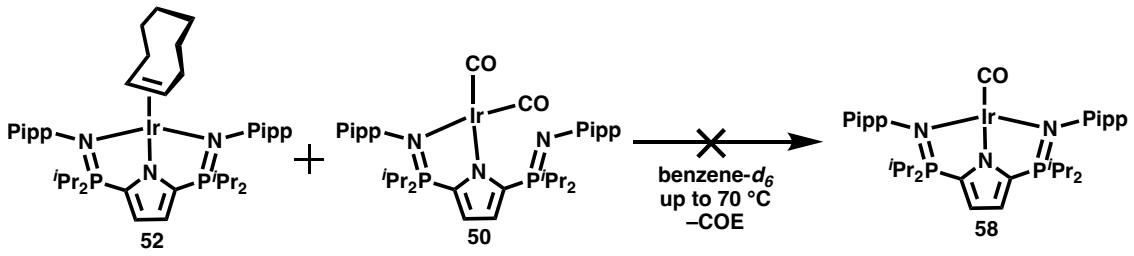

*Scheme 28 Attempted comproportionation reaction to synthesize ^{Pipp}LIr(CO) (**58**)*

Figure 22 shows some examples of iridium monocarbonyl complexes supported by pincer ligands.[101-103] The complexes by Bernskoetter[101] and Morales-Morales[102] were synthesized by addition of one atmosphere of CO, and there was no competition for the formation of the dicarbonyl complexes. On the contrary, in a related system Piers often found a mixture of monocarbonyl and the dicarbonyl complexes, even when one equivalent of CO was added.[103] They were able to successfully isolate the monocarbonyl complex by only brief exposure to CO. It may also be the case with **58** that reaction of **52** with a stoichiometric amount of CO with short exposure time and reduced temperatures may allow isolation of **58**. This work needs to be further explored.

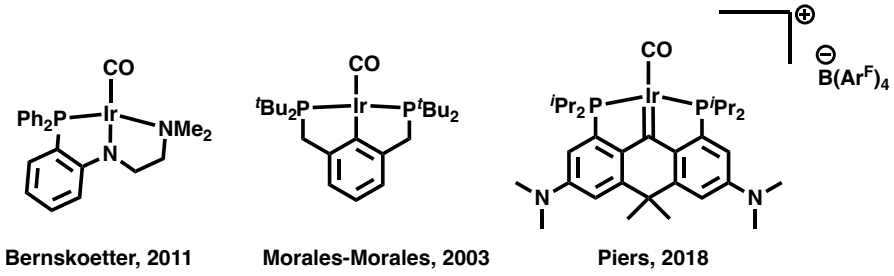

Figure 22 Some examples of iridium monocarbonyl complexes supported by pincer ligands

3.4.3 Attempted Synthesis of ^{Pipp}LIr(PPh$_3$)

3.4.3.1 Reaction with Triphenylphosphine

In Chapter 2, attempted synthesis of ^{Mes}LIr(PPh$_3$) by reaction of ^{Mes}LIr(COD) with triphenylphosphine was described, but no reaction was observed even at 50 °C. Since **52** showed reactivity with other small molecules, similar efforts as with ^{Mes}LIr(COD) at the synthesis of ^{Pipp}LIr(PPh$_3$) (**59**) were undertaken (Scheme 29). Others in the Hayes group have also found success substituting COE with triphenylphosphine.[104]

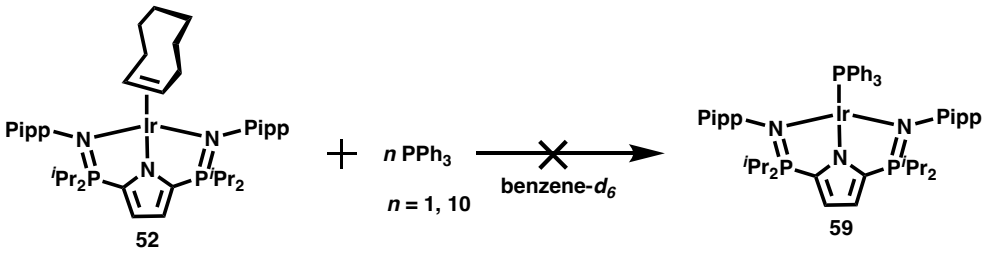

*Scheme 29 Attempted synthesis of ^{Pipp}LIr(PPh$_3$) (**59**)*

Reaction of one equivalent of triphenylphosphine with **52** in benzene-d_6 at ambient temperature for four hours led to multiple phosphorus-containing products. The ^{31}P{^{1}H} NMR spectrum showed a doublet at δ 68.1 ($J_{P\text{-}P}$ = 5.7 Hz), a singlet at δ 61.3, and a doublet at δ 23.2 ($J_{P\text{-}P}$ = 23.4 Hz) in a 1:2:2 ratio, respectively. There was no evidence of free triphenylphosphine in ^{31}P{^{1}H} NMR spectrum. Accordingly, another 10 equivalents of triphenylphosphine were added to the reaction mixture. After 3 hours at ambient temperature, the ^{31}P{^{1}H} NMR spectrum contained signals at δ 60.5, 55.3, 28.1, and 18.4

(doublet, $J_{P\text{-}P}$ = 5.8 Hz). The resonances at δ 68.1, 61.3, and 23.2 also remained. At this point, **52** constituted only approximately 16% of the mixture.

3.4.3.2 Reaction of $Na^{Pipp}L$ with $(PPh_3)_3IrCl$

Combination of one equivalent of $Na^{Pipp}L$ and one equivalent of $(PPh_3)_3IrCl$ in benzene-d_6 for 1.5 hours at ambient temperature did not lead to a reaction (Scheme 30, top). The reaction mixture was then warmed to 40 °C. Two new resonances were observed in the $^{31}P\{^1H\}$ NMR spectrum after 20 hours, at δ 68.1 (doublet; $J_{P\text{-}P}$ = 6.1 Hz) and a singlet at δ 27.9. An accurate integration for the signal at δ 27.9 could not be determined as it overlaps with $Na^{Pipp}L$ (δ 28.4, broad). The resonance at δ 68.1, however, was approximately 1% of the phosphorus-containing products. In addition, o*rtho*-cyclometallation of $(PPh_3)_3IrCl$ was detected after one hour and complete by 20 hours (Scheme 30, bottom). Evidence of cyclometallation included the presence of a multiplet resonance at δ –18.35 in the ^1H NMR spectrum that was attributed to an iridium hydride. Furthermore, three doublet of doublets, in an AMX coupling pattern, were observed in the $^{31}P\{^1H\}$ NMR spectrum. The reported coupling pattern and hydride resonance have been reported by others with cyclometallation of $(PPh_3)_3IrCl$ by refluxing in cyclohexane for 2 hours.[105]

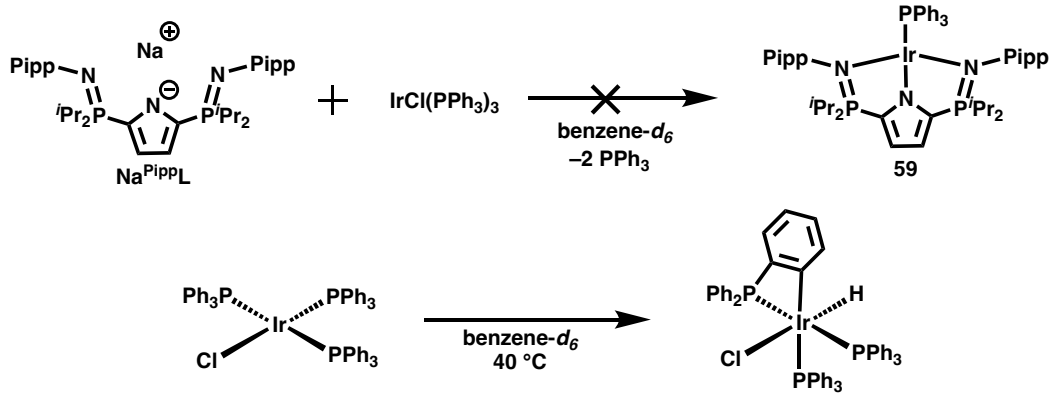

Scheme 30 Attempted synthesis of ^{Pipp}LIr(PPh$_3$) and cyclometallation of (PPh$_3$)$_3$IrCl

The reaction mixture containing *ortho*-cyclometallated $(PPh_3)_3IrCl$ and $Na^{Pipp}L$ was heated to 70 °C in an effort to promote a reaction. After 48 hours, a new signal was observed at δ 65.1 (doublet; $J_{P\text{-}P}$ = 6.0 Hz) in the $^{31}P\{^1H\}$ NMR spectrum. The resonances at δ 68.1 and 27.9 remained. There were also seven new signals between δ 28.0 and 17.4. A new resonance was also observed at δ –5.4, attributed to free triphenylphosphine. Further attempts at this reaction should be conducted, possibly maintaining the reaction at 40 °C for a longer time period. Keeping the mixture at a lower temperature may prevent a complex mixture, as was observed at 70 °C.

3.4.4 Synthesis, Characterization, and Reaction Chemistry of $[Li]^+[(COD)Ir(Me)_2]^-$

3.4.4.1 Synthesis and Characterization of $[Li]^+[(COD)Ir(Me)_2]^-$

Through a modified literature procedure, $[IrCl(COD)]_2$ was reacted with four equivalents of methyllithium at –94 °C for one hour in diethylether (Scheme 31).[106] After that point the diethylether was removed *in vacuo* at approximately –50 °C. The bright orange residue was

brought into a glove box, filtered through Celite, and recrystallized from toluene at –30 °C. The supernatant was decanted and the crystals dried under vacuum. The relevant NMR spectra were acquired in benzene-d_6 at ambient temperature. In the prior report of $[Li]^+[(COD)Ir(Me)_2]^-$ (**60**), only elemental analysis and the COD resonances in the ^1H NMR spectrum were provided. In the ^1H NMR spectrum acquired here, the COD alkene resonance was observed as a broad signal at δ 3.06, which is substantially upfield from free COD (δ 5.58). The COD methylene protons are diasteriotopic, with two resonances at δ 2.06 and 1.52 each integrating to 4H. One signal at δ 0.77 corresponded to both methyl groups. The presence of lithium was confirmed by the $^7Li\{^1H\}$ NMR spectroscopy; one broad singlet was detected at δ 0.1. The reaction was low yielding (~30%) but repeated recrystallization improves the yield (43.9% for two recrystallizations).

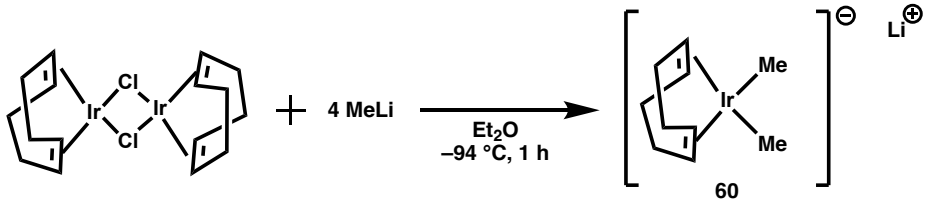

Scheme 31 Synthesis of $[Li]^+[(COD)Ir(Me)_2]^-$

Preliminary attempts of the aforementioned reaction removed the diethylether at ambient temperature, as described by Kulzick *et al.*[106] However, this method produced a dark brown solid that remained in solution when crystallization from toluene was attempted. The ^1H NMR spectrum contained four broad resonances at δ 4.63, 2.07, 1.36, and 0.81. It is hypothesized that the product was not stable in solution at ambient temperature in the presence of excess methyllithium.

Although **60** was previously reported[106], a solid-state structure had not been acquired. Bright orange, X-ray quality crystals of **60** were grown from a concentrated toluene solution stored at –30 °C for one week. Two independent molecules crystallized in the asymmetric unit. An in-depth analysis of the two molecules revealed that there was not a significant difference in the bond distances and angles between the two molecules (*e.g.* Ir–Me: 2.115(9) and 2.119(10) Å). Complex **60** is dimeric in the solid state, bridging the two iridium atoms by two lithium cations (Figure 23). The iridium center exhibits square planar geometry (τ^4 = 0.042 for Ir1; τ^4 = 0.046 for Ir2). The average Ir–Me distance was 2.113(10) Å. A search of the Cambridge Structural Database indicated that the Ir–Me distance was similar to the average of 178 other Ir–Me containing compounds, in which the average is 2.128 Å.[100]

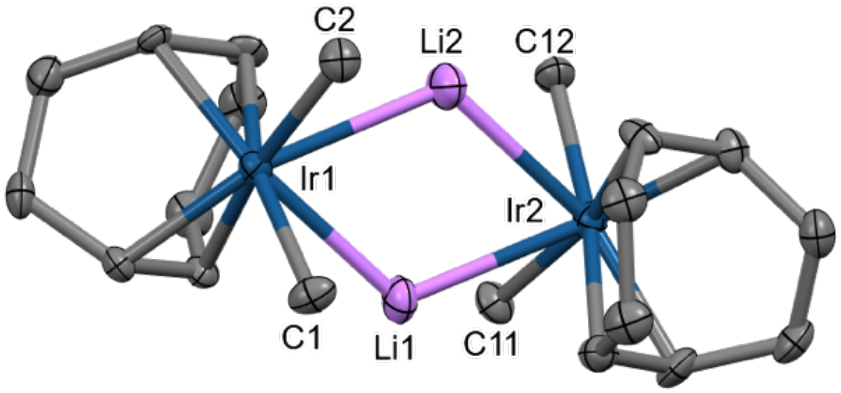

*Figure 23 Displacement ellipsoid plot (50% probability) for complex **60**. Two molecules crystallized in the asymmetric unit, but only one is shown for clarity. Hydrogen atoms were removed for clarity. Space group = P-1. R_1 = 4.94%. Selected bond distances (Å) and angles (°): Ir1–Li1: 2.555(19); Ir1–Li2: 2.62(2); Ir1–C1: 2.119(10); Ir1–C2: 2.109(10); C1–Ir1–C2: 88.4(4)*

3.4.4.2 Reaction Chemistry of $[Li]^+[(COD)Ir(Me)_2]^-$

3.4.4.2.1 Reaction of $[Li]^+[(COD)Ir(Me)_2]^-$ with $H^{Mes}L$

To investigate the potential of **60** to be used as an iridium starting material, one equivalent of $H^{Mes}L$ was reacted with one equivalent of **60** (Scheme 32). $H^{Mes}L$ was chosen to increase the steric influence, compared to Pipp, as the methyl groups in the *ortho*-position provide steric bulk about the metal centre. The hope was to thermodynamically stabilize the product, $[Li]^+[^{Mes}LIr(Me)]^-$ as it was hypothesized to be unstable (**61**, Scheme 32). When THF-d_8 was added to the two solids at ambient temperature the solution immediately bubbled and turned dark brown. Ten minutes after the start of the reaction, the $^{31}P\{^1H\}$ NMR spectrum showed a major resonance at δ 17.1, which is not in the typical range for an iridium complex with this ligand system (δ 50.0 to 70.0). There was also a singlet at δ 0.19 in the ^1H NMR spectrum that was assigned as methane. Notably, there were no resonances that could be assigned as coordinated COD or methyl ligands. It was thus hypothesized that the product was lithiated ligand ($Li^{Mes}L$) as $Na^{Mes}L$ (δ 16.8) appears in a very similar range in the $^{31}P\{^1H\}$ NMR spectrum.

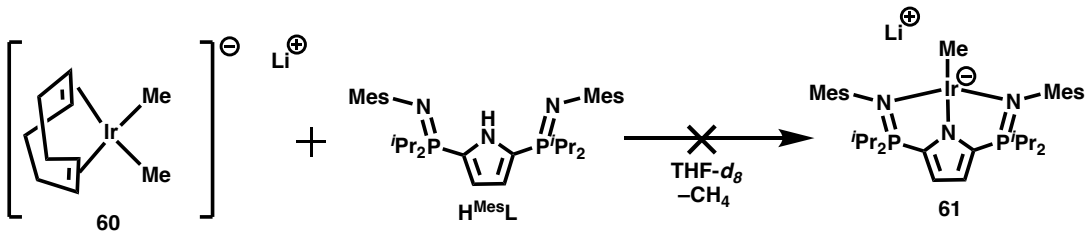

Scheme 32 Attempted synthesis of complex $[Li]^+[^{Mes}LIr(Me)]^-$

To prevent formation of Li^{Mes}L, **60** was reacted with 12-crown-4 to sequester Li^+ prior to the addition of H^{Mes}L. Preliminary attempts used one equivalent of 12-crown-4; however, the ^{1}H NMR suggested that there were two 12-crown-4 molecules trapping the lithium atom, as the resonance attributed to the crown ether integrated to 32H. Accordingly, subsequent reactions used 2 equivalents of 12-crown-4 (Scheme 33). Specifically, 12-crown-4 was added to a toluene solution of **60**, and the flask shaken. Dark orange-red crystals immediately precipitated from solution. Unfortunately, the crystals that precipitated from solution were not of X-ray quality.

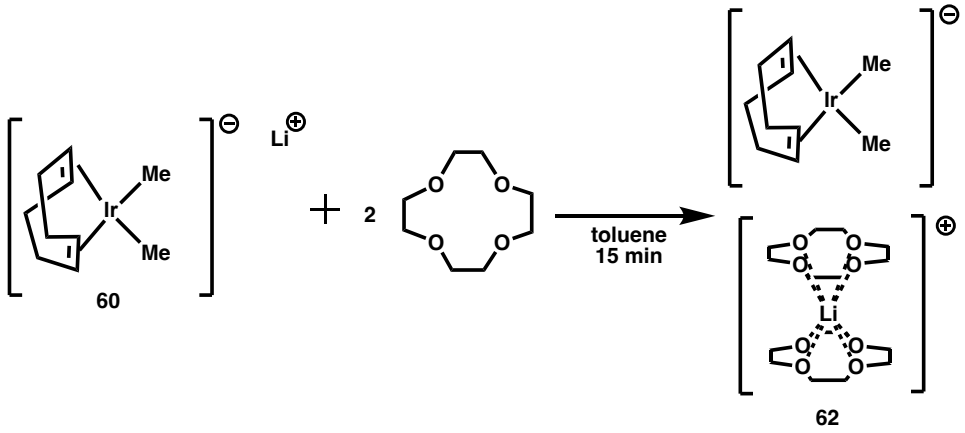

*Scheme 33 Synthesis of [(12-crown-4)$_2$Li]$^+$[(COD)Ir(Me)$_2$]$^-$ (**62**)*

The ^{1}H NMR spectrum of [(12-crown-4)$_2$Li]$^+$[(COD)Ir(Me)$_2$]$^-$ (**62**) displayed a singlet at δ 3.74 integrating to 32H, providing evidence for two 12-crown-4 molecules per lithium cation. The methyl resonance shifted substantially upfield from δ 0.77 to 0.25. The COD signals were also shifted upfield when compared to **60** (**60**: δ 3.06, 2.06, 1.52; **62**: δ 2.80, 1.87, and 1.32). The ^{7}Li{^{1}H} NMR signal changed from δ 0.2 to –1.6. It should be noted that due to differences in solubility, NMR spectra of **60** were acquired in benzene-d_6, but

the NMR data of **62** was recorded in THF-d_8; hence, differences do not necessarily indicate anything. The crystals were isolated as complex **62** in a 47% yield.

Complex **62** was reacted with one equivalent of $H^{Mes}L$ in THF-d_8 at ambient temperature (Scheme 34). The solution bubbled vigorously when THF-d_8 was added to the two solids and turned brown from bright orange. The $^{31}P\{^1H\}$ NMR spectrum exhibited one singlet at δ 17.1, as well as approximately 15% $H^{Mes}L$. Methane was observed at δ 0.19 but no COD or methyl ligand resonances were detected. Despite sequestering the lithium cation, it appears that when $H^{Mes}L$ and **62** are combined, $Li^{Mes}L$ is still the major product. The reason for this was hypothesized to be that the product, $[Li]^+[^{Mes}LIr(Me)]^-$ is not thermodynamically stable. The solution bubbling, and the resonance at δ 0.19, suggests that methane is lost, and therefore N–H oxidative addition must occur at iridium as this is the only source of hydrogen. With the loss of methane this would produce the desired product, and rapid decomposition likely occurs proceeding this, in which one decomposition product is $Li^{Mes}L$. An experiment at reduced temperature may prevent decomposition, and $[Li]^+[^{Mes}LIr(Me)]^-$ may be isolated.

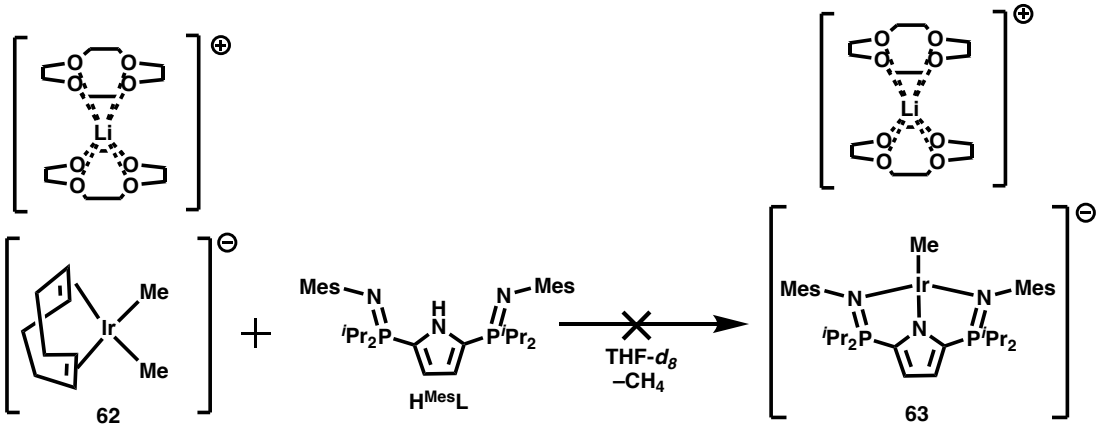

*Scheme 34 Attempted synthesis of $[(12\text{-crown-4})_2Li]^+[^{Mes}LIr(Me)]^-$ (**63**)*

3.4.4.2.2 Reaction of $[Li]^+[(COD)Ir(Me)_2]^-$ with an Imidazolinium Chloride Salt

Since attempts to use **60** and **62** as a starting material for monoanionic ligands was unsuccessful, an imidazolinium chloride salt ($[C_3H_5(NMes)_2]^+[Cl]^-$), was prepared to synthesize the *N*-heterocyclic carbene (NHC) complex (COD)Ir(Me)($C_3H_4(NMes)_2$) (**64**, Scheme 35). Reaction of **60** with ($[C_3H_5(NMes)_2]^+[Cl]^-$ in THF-d_8 at ambient temperature immediately resulted in the solution bubbling and a colour change to bright red. The ^1H NMR spectrum obtained after 10 minutes revealed a resonance at δ 0.15 integrating to 3H assigned as the methyl ligand. The resonance at δ 9.29 of the imidazolinium chloride salt, attributed to the acidic hydrogen, was no longer present. In the $^{13}C\{^1H\}$ NMR spectrum, a signal at δ 216.1 appeared, assigned to the carbene. The presence of COD was confirmed by two signals in the ^1H NMR spectrum at δ 3.28 and 2.99, attributed to the alkene resonances of coordinated COD (*c.f.* δ 5.58 for free COD). Two signals (δ 74.8 and 62.9) in the $^{13}C\{^1H\}$ NMR spectrum also substantiated the idea that COD remained. The substantial difference between the chemical shifts of the two resonances can be explained

by which groups are *trans* to the double bond; the more upfield shifted double bond resonance is likely *trans* to the carbene ligand as it is a stronger σ-donor than the methyl group.

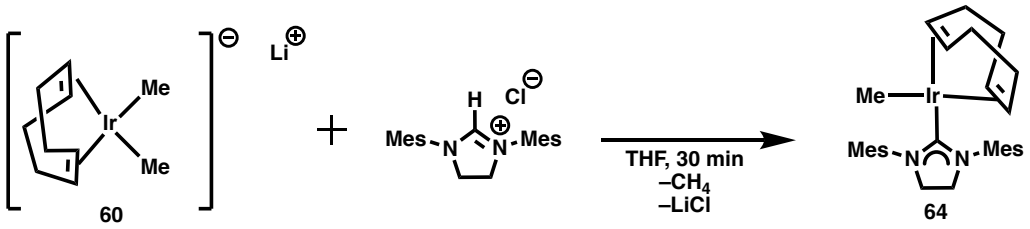

*Scheme 35 Synthesis of (COD)Ir(Me)(C_3H_4(Nmes)$_2$) (**64**)*

X-ray quality crystals of **64** were grown from a pentane solution stored at –30 °C for two days (Figure 24). Iridium exhibits square planar geometry ($\tau^4 = 0.087$). The Ir–Me distance is the same within error as that observed in **60** (2.113(10) Å), at 2.114(4) Å. The Ir–carbene distance is 2.039(4) Å, which is similar to the average from 74 other neutral, monodentate iridium imidazolinium NHC complexes found in the Cambridge Structural Database (2.038 Å).[100] Notably, none of the structures used for comparison contained an Ir–Me functionality. To the best of my knowledge, there are no other imidazolinium NHC methyl iridium crystal structures.

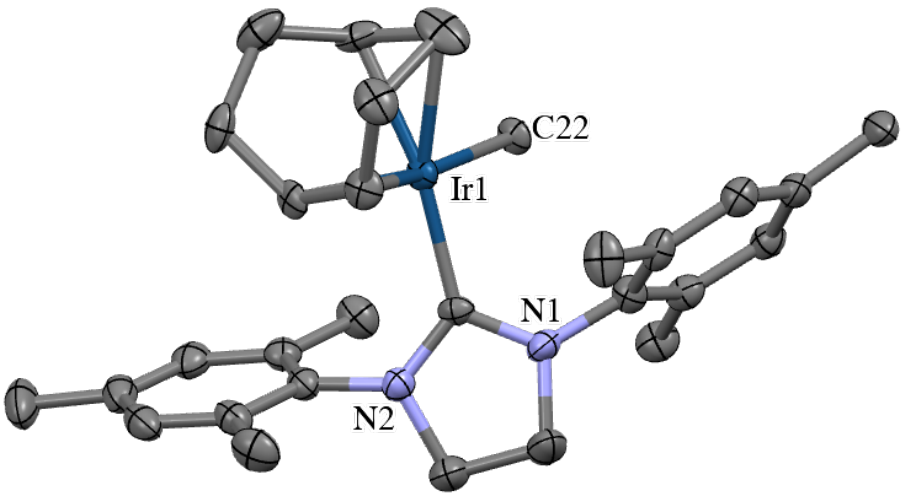

*Figure 24 Displacement ellipsoid plot (50% probability) of complex **64**. Hydrogen atoms were removed for clarity. Space group: $P2_1/c$. R_1 = 3.58%. Selected bond distances (Å) and angles (°): Ir1–C1: 2.039(4); Ir1–C22: 2.114(4); C1–Ir1–C22: 91.24(16)*

3.5 Summary and Concluding Remarks

The cyclooctene complex, ^{Pipp}LIr(COE) (**52**) was synthesized. This complex cannot be isolated as an analytically pure solid because it is not stable under reduced pressure. Synthesizing the complex *in situ* allowed for further study of its reaction chemistry, namely with silanes and dihydrogen.

Reaction of complex **52** with dihydrogen at ambient temperature yielded rapid decomposition of the putative product ^{Pipp}LIr(H)$_2$. The square pyramidal complex ^{Pipp}LIr(H)$_2$ can be isolated at –30 °C, but it is not stable above this temperature for prolonged periods. While complex **53** is formed at –30 °C, free COE is rapidly

hydrogenated. Complex **52** was also able to undergo oxidative addition of Si–H bonds, which allowed for the synthesis of the three iridium silyl hydride complexes ^{Pipp}LIr(H)(SiR$_3$) (R$_3$ = H$_2$Ph, HPh$_2$, Et$_3$).

Although complex **52** is reactive towards dihydrogen and silanes, in terms of catalytic applications another alternative to **52** is required. Specifically, to prevent competing processes caused by free COE in solution, a vacuum stable complex was sought. Reaction with CO produced ^{Pipp}LIr(CO)$_2$, but a comproportionation reaction with complex **52** failed to yield ^{Pipp}LIr(CO). In addition, reaction with triphenylphosphine led to a mixture of products. Furthermore, reaction of (PPh$_3$)$_3$IrCl with Na^{Pipp}L did not afford ^{Pipp}LIr(PPh$_3$); rather, IrCl(PPh$_3$)$_3$ *ortho*-cyclometallated at 40 °C.

An anionic iridium starting material, [Li]$^+$[(COD)Ir(Me)$_2$]$^-$ (**60**) which had been previously reported, but not thoroughly characterized, was synthesized. The first X-ray crystal structure of this complex has now been acquired. Reaction of this material with H^{Mes}L led only to lithiated ligand. Attempts to sequester the lithium ion with 12-crown-4 did not lead to a change in reactivity. On the contrary, reaction of **60** with [C$_3$H$_5$(NMes)$_2$]$^+$[Cl]$^-$ led to the generation of the iridium *N*-heterocyclic carbene complex, (COD)Ir(Me)(C$_3$H$_4$(NMes)$_2$), which was comprehensively characterized in both the solid and solution states.

As complex **52** was able to activate the small molecules dihydrogen and HSiR$_3$, the next step was to test the complexes in catalytic applications. Chapter 4 will discuss the capability

^{Pipp}LIr(H)$_2$ to catalyze alkene hydrogenation and alkane dehydrogenation, and the complexes ^{Pipp}LIr(H)(SiR$_3$) (R$_3$ = H$_2$Ph, HPh$_2$, Et$_3$) to catalyze hydrosilylation.

CHAPTER 4 – PRELIMINARY REACTION CHEMISTRY OF IRIDIUM SILYL HYDRIDE AND DIHYDRIDE COMPLEXES

Chapter 3 described the synthesis, characterization, and reactivity of ^{Pipp}LIr(COE). The complexes ^{Pipp}LIr(H)$_2$ and ^{Pipp}LIr(H)(SiR$_3$) (R$_3$ = Et$_3$, Ph$_2$H, PhH$_2$) were synthesized and characterized. The efficacy of ^{Pipp}LIr(H)$_2$ to catalyze hydrogenation and dehydrogenation was explored; hence, reaction with cyclooctene and cyclohexane was investigated. In addition, the ability of ^{Pipp}LIr(H)(SiR$_3$) to promote hydrosilylation of benzophenone was attempted. These reactions will be discussed in detail in this chapter.

4.1 Preface

The goal of the reactions performed were to investigate the reactivity of ^{Pipp}LIr(H)$_2$ and ^{Pipp}LIr(H)(SiR$_3$). For this reason, the temperature of the hydrogenation of COE and the hydrosilylation of benzophenone with HSiEt$_3$ was changed over the course of the reaction and an internal standard was not used. Accordingly, the kinetic analysis presented in this chapter should not be considered quantitative. Due to time constraints, a full kinetic analysis was not conducted.

4.2 Hydrogenation of Cyclooctene at –30 °C

4.2.1 Conditions and NMR Spectra for the Hydrogenation of Cyclooctene

In Chapter 3, the synthesis of $^{Pipp}LIr(H)_2$ (**53**) was described. During the synthesis of **53**, hydrogenation of free cyclooctene (COE) to cyclooctane (COA) was observed at –30 °C. To synthesize **53**, six separate additions of dihydrogen was required, as there was hypothesized to be a dynamic equilibrium between $^{Pipp}LIr(H)_2$ and $^{Pipp}LIr + H_2$. Upon completion of the final addition of dihydrogen, all $^{Pipp}LIr(COE)$ (**52**) had been converted to **53**. Furthermore, all of the free COE that was liberated during synthesis of **52** was hydrogenated to COA. This stoichiometric hydrogenation of COE prompted the question as to whether or not unsaturated substrates could be catalytically hydrogenated by complex **53**.

Complex **53** was prepared *in situ* because it is unstable at low pressure and temperatures above –30 °C. Specifically, one atmosphere of dihydrogen was introduced into a J. Young NMR tube charged with one equivalent (10 mol%) of **52** and 10 equivalents of COE at –30 °C in 0.5 mL of toluene-d_8 (Scheme 36). The tube was kept at this temperature until carefully inserted into a pre-cooled NMR probe set to –30 °C.

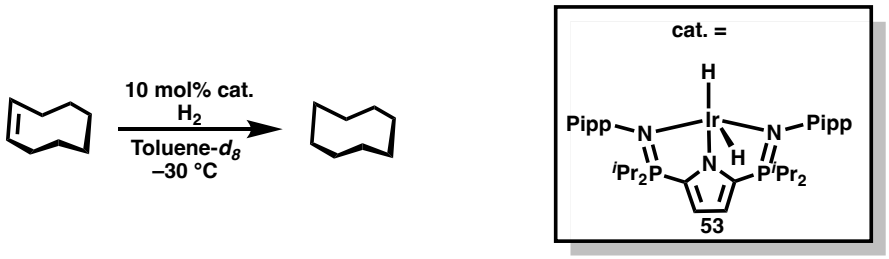

Scheme 36 Hydrogenation of COE catalyzed by ^{Pipp}LIr(H)$_2$

The progress of the reaction was monitored by ^{1}H and ^{31}P{^{1}H} NMR spectroscopy. The first 19 hours of the reaction were monitored at a constant temperature of –30 °C. For the first 3.5 hours, ^{1}H and ^{31}P{^{1}H} NMR spectra were collected every 30 minutes. During this period, the concentration of **52** increased from zero until it comprised approximately 10% of the ligated species (relative ratio in ^{31}P{^{1}H} NMR spectrum: 9:1 **53**:**52**). After 19 hours, the temperature of the probe was increased to –25 °C for one hour, followed by one hour at –20 °C. These temperature changes were made in an effort to test the stability of the catalyst. During both temperature increases, more of complex **52** was observed in the ^{31}P{^{1}H} NMR spectrum (–25 °C: 4:1; –20 °C: 7:3, **53**:**52**). For this reason, the temperature was again reduced to –30 °C. After another 19 hours at –30 °C, for a total of 40 hours of reaction time, no free COE remained.

4.2.2 Comparison of the Hydrogenation Activity of ^{Pipp}LIr(H)$_2$ to Literature Complexes

When compared to other catalysts in the literature, this reaction was conducted at a lower temperature, albeit, the time to completion was longer. For context, two examples of catalytic COE hydrogenation are briefly discussed (Table 6). The first example,

PNP-Ir(COD) (**65**), gave low conversion to product (11%) after 24 hours at ambient temperature.[107] The second example, *NSi*-Ir(H)(Me)(COE) (**66**), proceeded to completion within 10 minutes at ambient temperature.[108]

*Table 6 Conditions and conversion of literature complexes and **53** in catalytic COE hydrogenation*

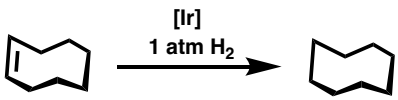

[Ir]	Solvent	Catalyst Loading	Temperature	Time, Conversion
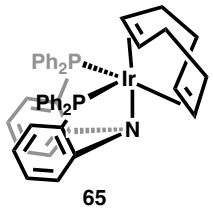 65	Benzene	0.5%	Ambient	24 h, 11%
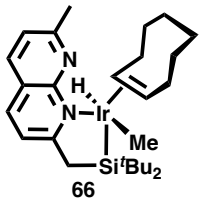 66	Benzene-d_6	1%	Ambient	<10 min, ~100%
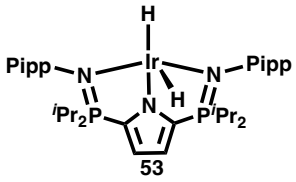 53	Toluene-d_8	10%	–30 °C	40 h, ~100%

4.2.3 Kinetic Analysis and Mechanism

Figure 25 shows a semiquantitative kinetic analysis of the hydrogenation of COE catalyzed by **53**. As noted above, the temperature was changed to –25 °C and –20 °C to test the stability of the catalyst, and these points have been excluded from analysis. The reaction is first order in COE with a $k = 0.10\ h^{-1}$.

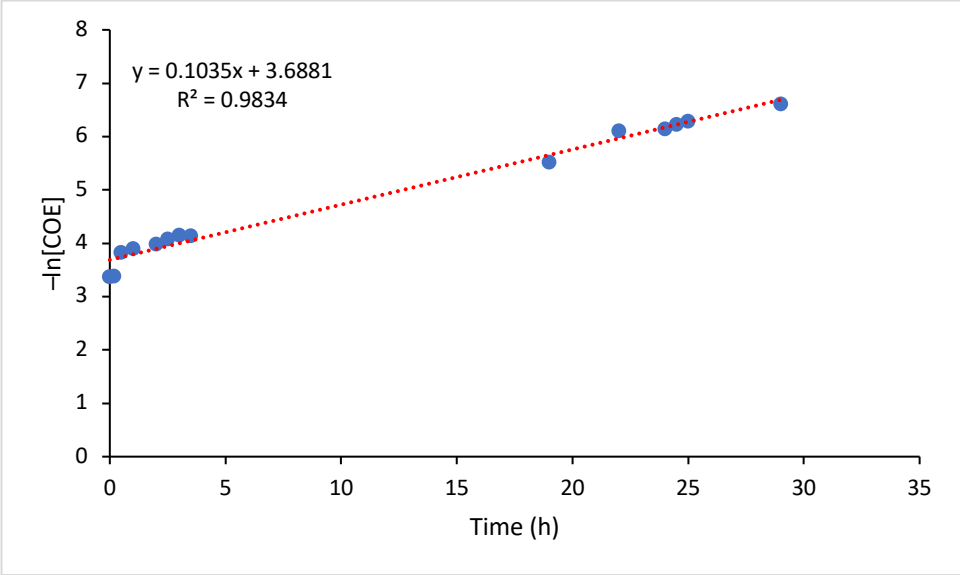

Figure 25 Plot of –ln[COE] versus time (h). A linear trendline is included in red. Data acquired at –25 °C and –20 °C were excluded

Over the course of the catalytic reaction, the proportion of ^{Pipp}LIr(COE) (**52**) increased. The typical hydrogenation pathway[109] is presumably operating: coordination of COE to iridium, alkene insertion into Ir–H, and finally, COA is reductively eliminated (and regeneration of complex **53** by oxidative addition of dihydrogen, Scheme 37). However, the formation of

complex **52** suggests a competing equilibrium between **53** and COE, and **52** and dihydrogen exists.

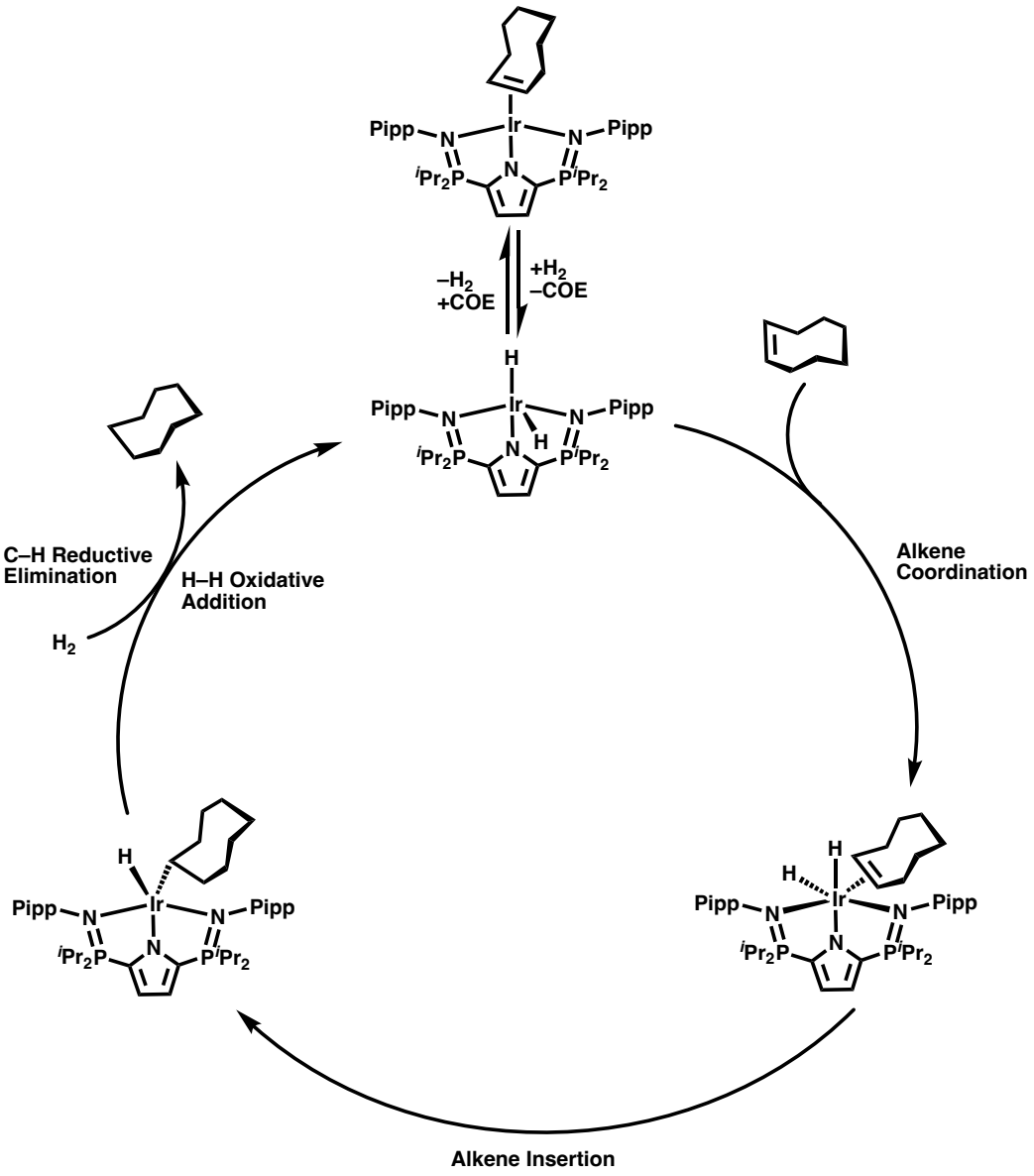

Scheme 37 Proposed catalytic cycle for catalytic COE hydrogenation by ^{Pipp}*LIr(H)*$_2$

4.3 Preliminary Attempt at Catalytic Alkane Dehydrogenation

In Chapter 3, it was discussed that after complete hydrogenation of COE, an increase in temperature (up to 15 °C) resulted in the disappearance of the resonances attributed to the hydride, which was explained by a dynamic equilibrium between ^{Pipp}LIr(H)$_2$ and ^{Pipp}LIr + H_2. In addition, generation of ^{Pipp}LIr(COE) (**52**) was observed after all of the free COE in solution had been hydrogenated to COA. Hence, it was postulated that dehydrogenation of COA may be occurring.

Cyclohexane was chosen as a dehydrogenation substrate because early examples utilized cyclohexane allowing for direct comparison.[110] As discussed previously, the complex ^{Pipp}LIr(H)$_2$ (**53**) was generated *in situ*. Complex **53** and 10 equivalents of cyclohexane were dissolved in 0.5 mL of toluene-d_8 in a J. Young NMR tube and placed under one atmosphere of dihydrogen at –30 °C (Scheme 38). Tetramethylsilane (TMS) in toluene-d_8 was used as an internal standard in a sealed glass capillary. The reaction mixture was injected into a pre-cooled NMR probe at –30 °C. The temperature of the NMR probe was increased incrementally every 30–90 minutes (5–10 °C per temperature increase), and changes were monitored by ^{1}H and ^{31}P{^{1}H} NMR spectroscopy.

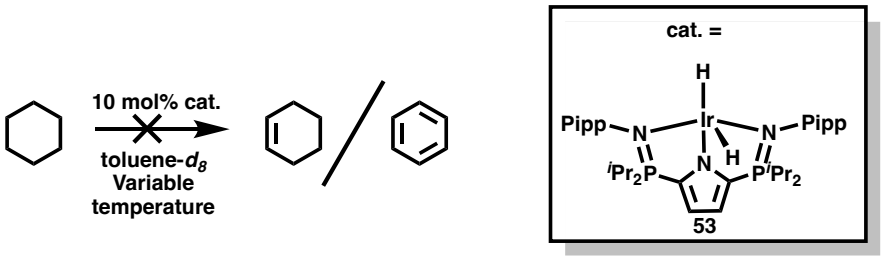

Scheme 38 Attempted catalytic dehydrogenation of cyclohexane

Free cyclohexane appeared as a broad resonance at δ 1.39 in the ^{1}H NMR spectrum at –30 °C. COA overlapped with this signal. After 1 hour at –30 °C, only 18% of the free COE generated from the synthesis of ^{Pipp}LIr(COE) (**52**) was hydrogenated. In an attempt to promote dehydrogenation, the temperature was increased to –20 °C for 30 minutes. The cyclohexane resonance became sharper (whh: 36.6 Hz at –30 °C *c.f.* 14.2 Hz at –20 °C), but there was no evidence of cyclohexene formation. Next, the temperature was changed again to –10 °C for one hour, and no formation of cyclohexene was observed. Instead, there was substantial production of complex **52**, as indicated by the ^{31}P{^{1}H} NMR spectrum (relative integrations of 2:1 for **53**:**52**). After an additional two hours and 45 minutes at 0 °C, there was still no evidence for cyclohexene formation. Even after 16 hours, no dehydrogenation had occurred. At this point, there was only a single observable ^{31}P{^{1}H} resonance at δ 63.3. The low concentration of the phosphorus-containing product compared to cyclohexane (<10:1) prevented characterization of the species by ^{1}H NMR spectroscopy.

4.4 Catalytic Hydrosilylation of Benzophenone

4.4.1 Triethylsilane

In Chapter 3, the synthesis and characterization of ^{Pipp}LIr(H)(SiEt$_3$) (**57**) was described. Oxidative addition of an Si–H bond to form a silyl hydride is the first step in the Chalk-Harrod mechanism of hydrosilylation[58] (see Chapters 1 and 3 for the catalytic cycle). As such, the isolation of **57** prompted investigation into the catalytic hydrosilylation of benzophenone.

A 10 mol% catalyst loading of complex **57** (compared to benzophenone and HSiEt$_3$) was used in 0.5 mL of benzene-d_6 (Scheme 39). No changes were observed after 3.5 hours at ambient temperature. As such, the temperature was increased to 50 °C, but no reaction was observed. Next, the temperature was incrementally increased by 10 °C, until 100 °C, in which the reaction proceeded at an appreciable rate (*vide infra*).

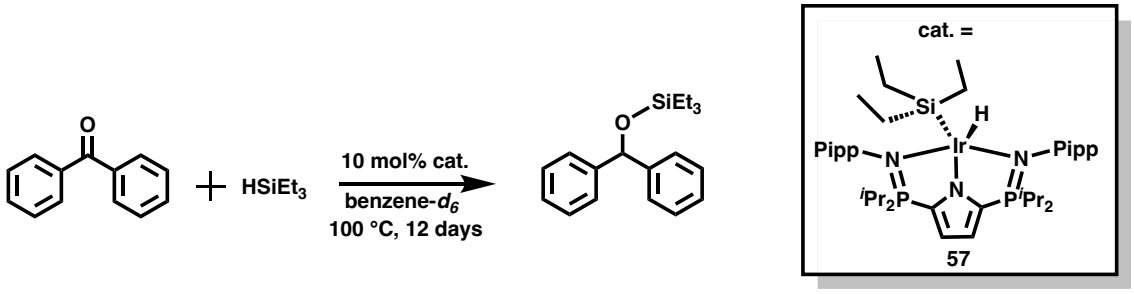

*Scheme 39 Hydrosilylation of benzophenone using ^{Pipp}LIr(H)(SiEt$_3$) (**57**) as a catalyst*

Figure 26 shows a semiquantitative kinetic analysis of the catalytic hydrosilylation of benzophenone by **57**. Any data collected below 100 °C was not included in the analysis. The reaction is first order in $HSiEt_3$ with $k = 0.0059\ h^{-1}$. No starting material was observed in the ^1H NMR spectrum after 12 days at 100 °C.

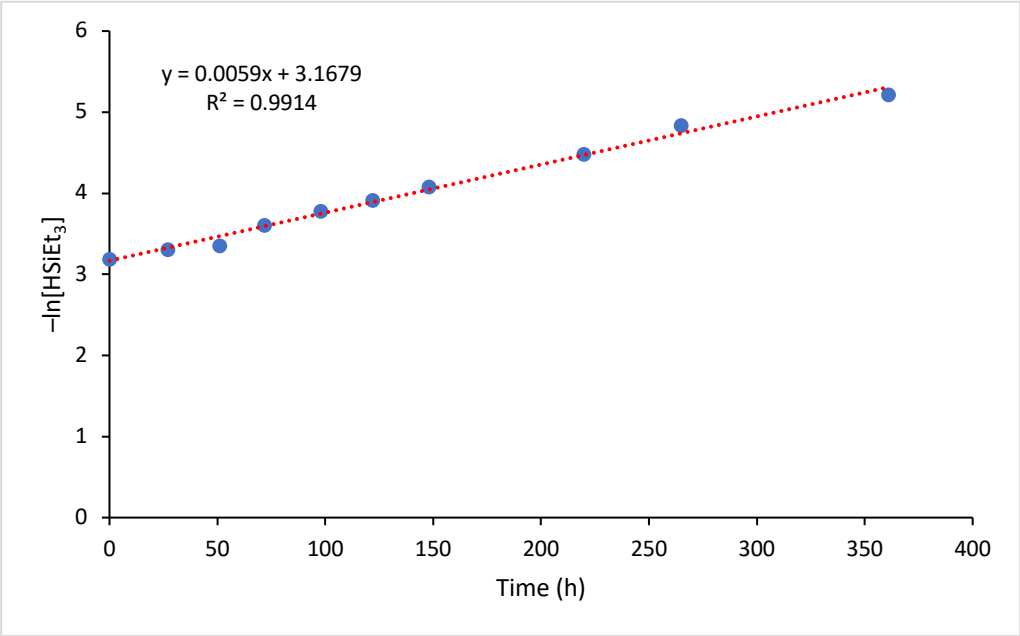

Figure 26 Plot of –ln[HsiEt₃] versus time (h). A linear trendline is provided in red. Only data acquired at 100 °C was included in analysis

Although the iridium silyl hydride **57** was first observed at δ 60.0 in the $^{31}P\{^1H\}$ NMR spectrum at ambient temperature, after 27 hours at 80 °C that resonance started to decrease in intensity and a new resonance at δ 47.8 appeared (Figure 27). After 21 hours at 90 °C, followed by 26 hours at 100 °C, complex **57** was no longer detected. In addition, the resonance in the ^1H NMR spectrum attributed to the hydride of **57** (δ –16.79) was not found.

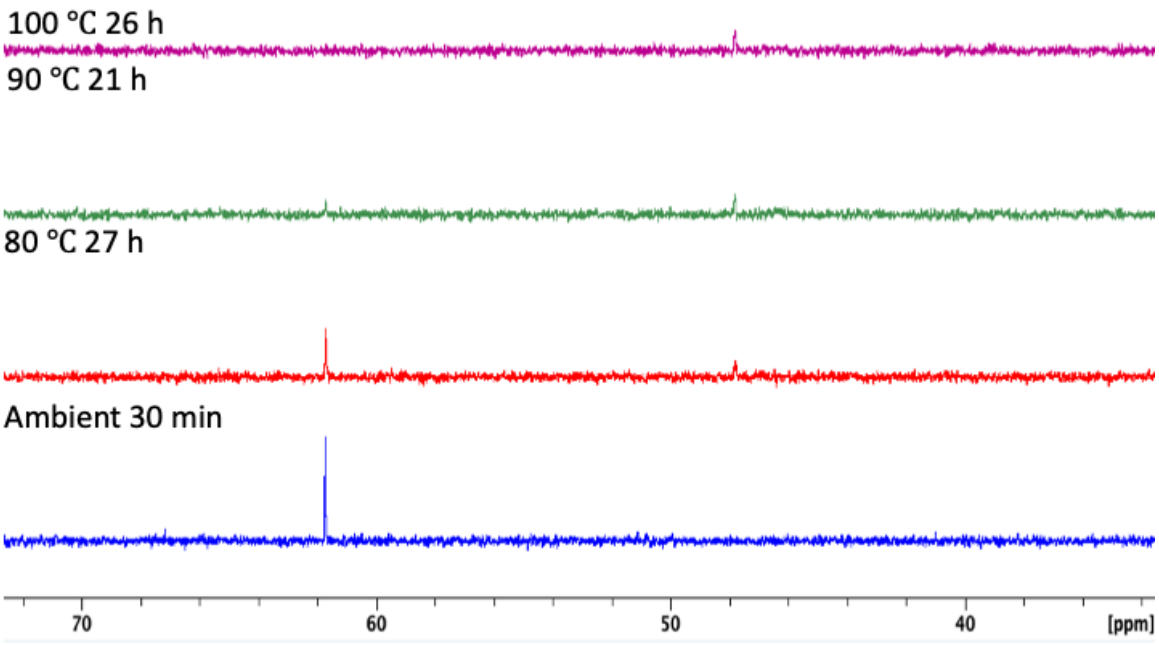

Figure 27 $^{31}P\{^{1}H\}$ NMR spectra (283.419 MHz) of the hydrosilylation of benzophenone in benzene-d_6 by ^{Pipp}LIr(H)($SiEt_3$) over 74 hours at temperatures between ambient and 100 °C

Although the ^{1}H NMR spectrum was saturated with peaks attributed to $HSiEt_3$ and benzophenone, some of the resonances corresponding to the catalytically active species were detectable. The observed resonances display asymmetry; two singlets at δ 6.59 and 6.44, which are the resonances of the pyrrole, were observed. Additionally, there are two septets at δ 2.80 and 2.67 in the ^{1}H NMR spectrum attributed to Pipp-C*H*$(CH_3)_2$. It is peculiar that a second resonance in the $^{31}P\{^{1}H\}$ NMR spectrum was not observed; a stoichiometric experiment would need to be conducted in order to acquire detailed spectroscopic data of the active catalyst. Performing the reaction stoichiometrically would increase the concentration of the active species and therefore allow for clear observation of all resonances attributed to the active catalyst. This would, in turn, provide a better understanding of the mechanism.

The complex, *NN*-Rh(Cl)(COD) (**67**, Scheme 40), was reported by Buchmeiser *et al*. to catalyze the hydrosilylation of benzophenone with $HsiEt_3$.[111] The hydrosilylation of benzophenone with their reported catalyst used 0.002 mol% catalyst loading at 70 °C over 1.5 hours in THF to achieve a 97% yield. Sodium *tert*-butoxide was required as an activator to remove the chloride ligand. When comparing **67** to **57**, the catalyst loading (**67**: 0.002 mol%, **57**: 10 mol%**)**, the temperature required (**67**: 70 °C, **57**: 100 °C), and the time to fully hydrosilylate (**67**: 1.5 hours, **57**: 12 days) benzophenone were lower.

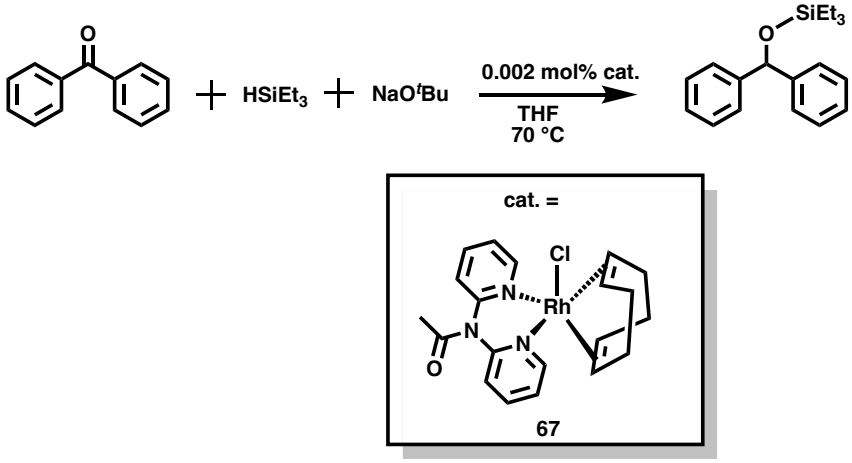

Scheme 40 Rhodium catalyzed hydrosilylation of benzophenone reported by Buchmeiser and colleagues[111]

4.4.2 Diphenylsilane

In Chapter 3 ^{Pipp}LIr(H)($SiHPh_2$) (**56**) was reported, which was synthesized by the addition of H_2SiPh_2 to ^{Pipp}LIr(COE) (**52**, Scheme 41). As explored in section 4.4.1, the hydrosilylation of benzophenone was used as a model reaction, with 10 mol% catalyst

loading compared to benzophenone and H_2SiPh_2 in 0.5 mL of benzene-d_6 at ambient temperature (Scheme 41).

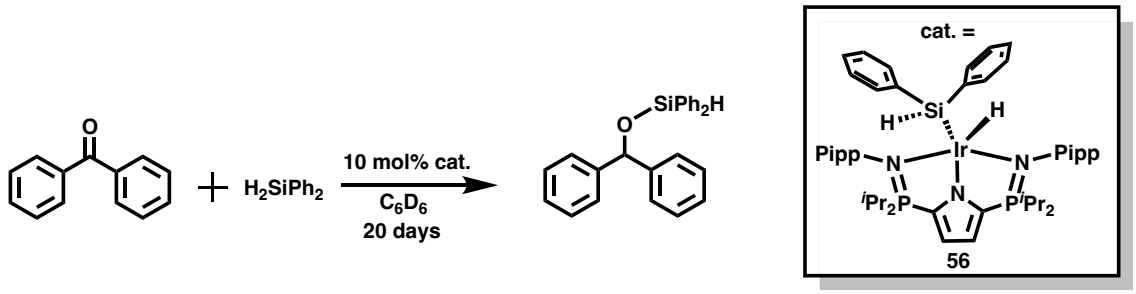

*Scheme 41 Hydrosilylation of benzophenone using ^{Pipp}LIr(H)(SiHPh$_2$) (**56**) as a catalyst*

Figure 28 shows a semiquantitative kinetic analysis of the catalytic hydrosilylation of benzophenone by **56**. The reaction is first order in H_2SiPh_2 with $k = 0.0075$ h^{-1}. No starting material was observed in the ^{1}H NMR spectrum after 488 hours (~20 days) at ambient temperature. There is a change in rate at approximately 276 hours (0–276 hours $k = 0.0059$ h^{-1}; 276–488 hours $k = 0.0097$ h^{-1}); however, because only one run was performed more work would be required to confirm this observation.

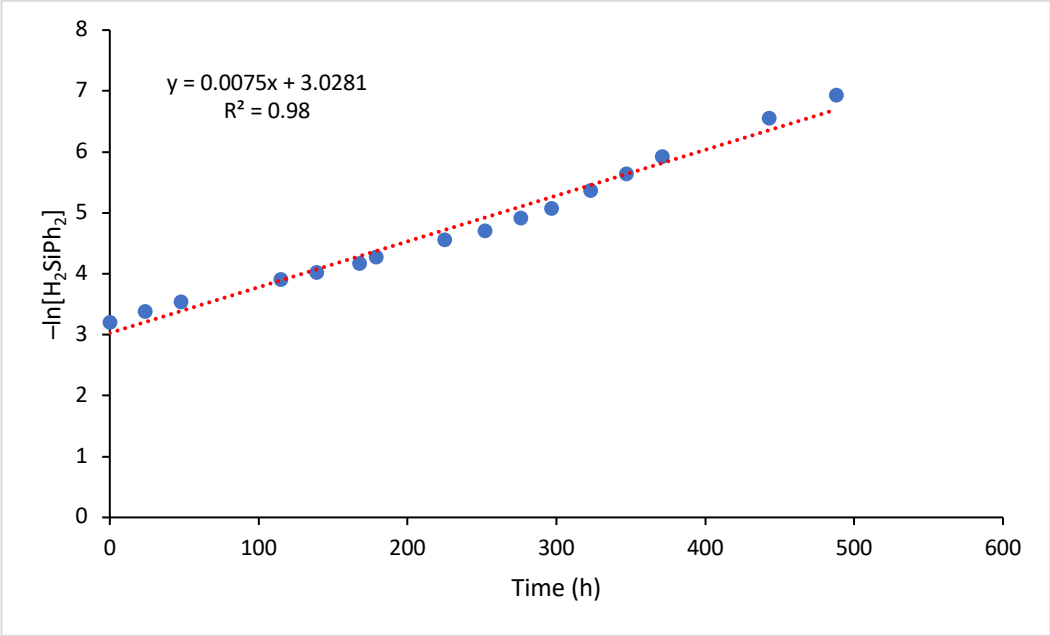

Figure 28 Plot of –ln[H_2SiPh_2] versus time (h). A linear trendline in red is provided.

Over the course of the reaction, the signal due to **56** in the $^{31}P\{^1H\}$ NMR spectrum slowly decreased until it was no longer observed (after 15 days). This would seem to suggest that **56** is not required for catalysis to proceed; however, a control reaction of benzophenone with H_2SiPh_2 at ambient temperature in the absence of a catalyst showed no reaction after one week in benzene-d_6. It is more likely that over 15 days complex **56** converts into a new complex that was not detected by $^{31}P\{^1H\}$ NMR spectroscopy because of its low concentration (10 mol%). A stoichiometric study would be required to test whether there is a new complex.

When comparing **56** to the iridium silylene complex, [*PNP*-Ir(H)($SiPh_2$)]$^+$[$B(C_6F_5)_4$]$^-$ (**68**), reported by Tilley *et al.*, complex **56** was a substantially less active catalyst based on time and catalyst loading (Scheme 42).[112] Complex **68** was able to catalyze the hydrosilylation

of benzophenone with H_2SiPh_2 in 4.5 hours at an 88% yield and 1 mol% catalyst loading. The mechanism for catalytic hydrosilylation by silylene complexes is substantially different than through the Chalk Harrod mechanism, however. When SiRR' = SiHAr, the multiple bond is thought to be inserted at the Si–H, rather than the M–H with many ruthenium complexes, such as $(P^iPr_3)Ru(H)_2(Cp^*)(SiRH)$ (Cp* = pentamethylcyclopentadiene).[113] In Tilley's report where SiRR' = $SiPh_2$, they were unable to confirm what mechanism was operative, but the two pathways either started with coordination of benzophenone to the metal centre or to silicon.

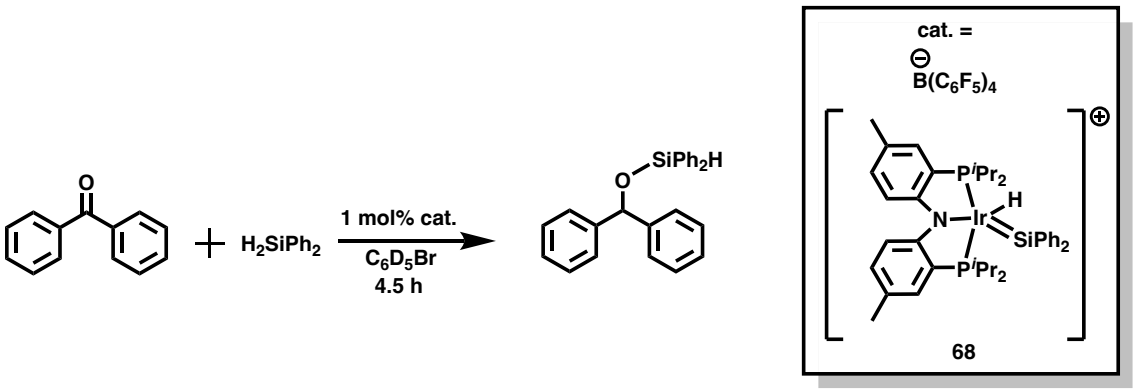

Scheme 42 Iridium silylene catalyzed hydrosilylation of benzophenone reported by Tilley and colleagues[112]

4.4.3 Phenylsilane

In Chapter 3 $^{Pipp}LIr(H)(SiH_2Ph)$ (**55**) was reported, which was synthesized by the addition of H_3SiPh to $^{Pipp}LIr(COE)$ (Scheme 43). As with **57** and **56**, benzophenone was used as a model substrate for hydrosilylation at 10 mol% catalyst loading in 0.5 mL of benzene-d_6 at

ambient temperature. The ^{1}H NMR spectrum obtained 10 minutes after the start of the reaction showed changes to **55**. Specifically, the SiH_2 (δ 4.96) and hydride (δ –16.16) resonances vanished, and there was evidence of free dihydrogen at δ 4.46.

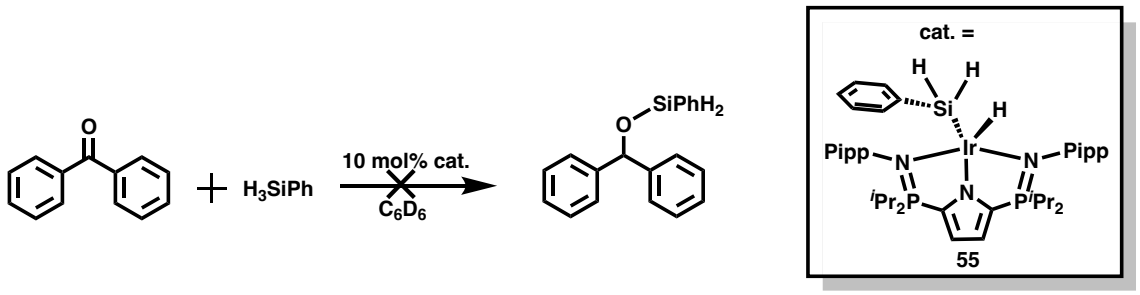

*Scheme 43 Attempted hydrosilylation of benzophenone catalyzed by ^{Pipp}LIr(H)(SiH_2Ph) (**55**)*

It was unclear whether complex **55** had decomposed from releasing the silyl ether, or if a reaction with excess H_3SiPh had occurred. A control reaction between **55** and 10 equivalents of H_3SiPh (Scheme 44) displayed the same initial changes as during the hydrosilylation attempt (disappearance of the SiH_2 and hydride signals, Figure 29, red). After 16 hours, the starting material had completely converted into a new complex that gave rise to a ^{31}P{^{1}H} NMR resonance at δ 64.3 (from δ 62.6, Figure 30, green). A singlet at δ 3.87 with ^{29}Si satellites ($^{1}J_{H\text{-}Si}$ = 179.1 Hz), integrating to approximately 4H, arose in the ^{1}H NMR spectrum arose during this period. The ^{29}Si signal was observed as a singlet at δ –26.3 in the ^{29}Si{^{1}H} NMR spectrum, a substantial downfield shift compared to **55** (δ –42.9). No signals were observed between δ 0 and –60 in the ^{1}H NMR spectrum. Removal of volatiles from the reaction mixture yielded an orange oil in 90% yield. The product was hypothesized to be the ^{Pipp}LIr(SiH_2Ph)$_2$ (**69**).

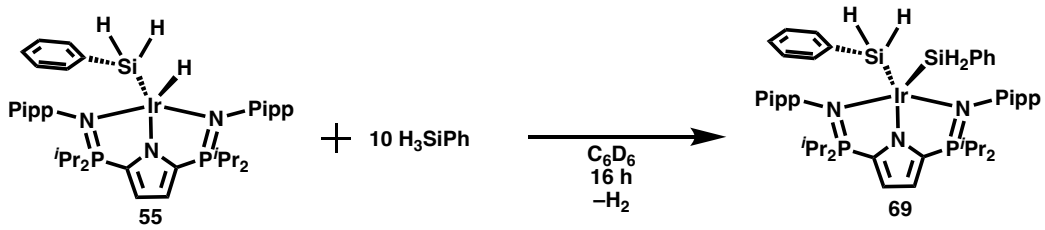

*Scheme 44 Reaction of **55** with H_3SiPh to produce $^{Pipp}LIr(SiH_2Ph)_2$ (**69**)*

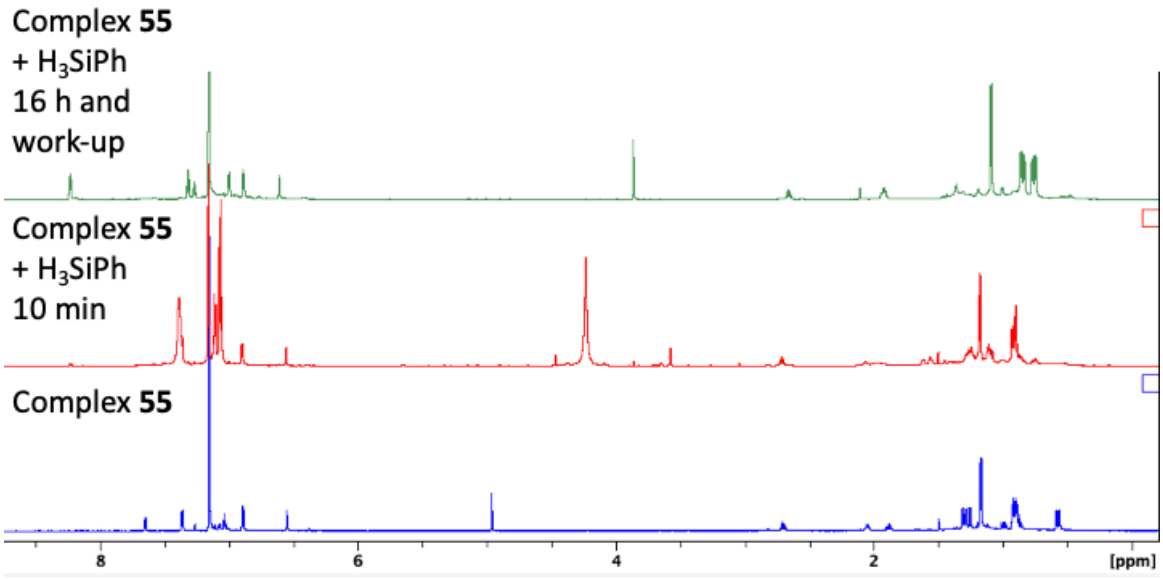

*Figure 29 ^1H NMR spectra (700.13 MHz) in benzene-d_6 of complex **55** and reaction of **55** with H_3SiPh at ambient temperature*

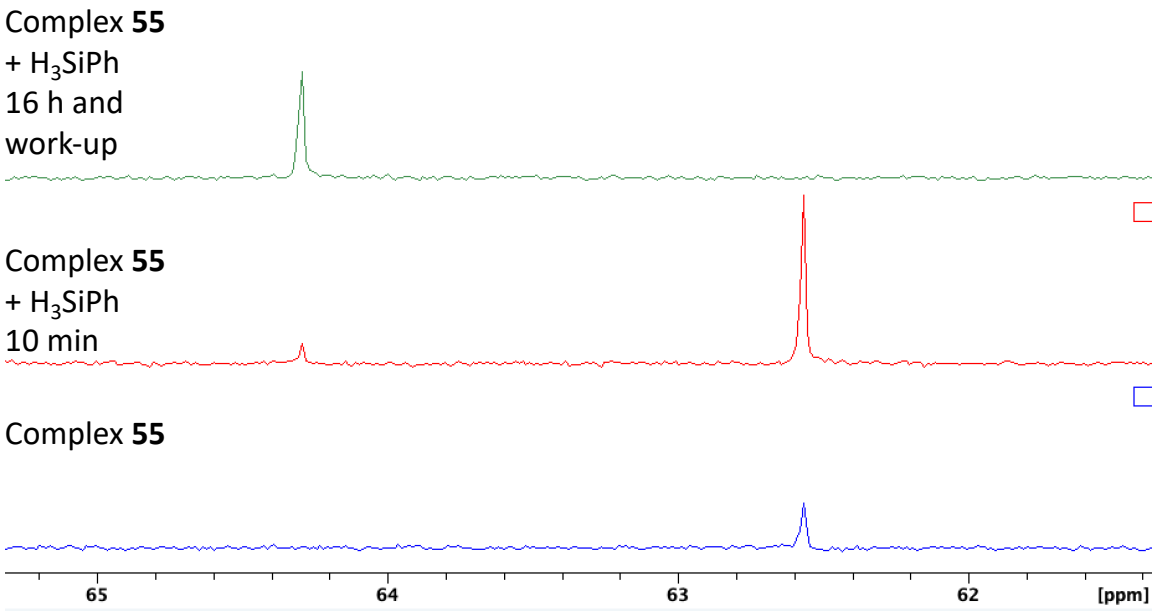

*Figure 30 $^{31}P\{^{1}H\}$ NMR spectra (283.419 MHz) of complex **55** and reaction of **55** with H_3SiPh in benzene-d_6 at ambient temperature*

There are other bis(silyl)dihydride complexes reported in the literature, some of which reductively eliminate dihydrogen to form disilyl complexes,[113] and others that do not and are stable Ir(V) complexes.[98, 99] Figure 31 depicts *PNP*-Ir(H)(SiH_2Trip) (**70**, Trip = 2,4,6-triisopropylphenyl) and *PNP*-Ir($SiH_2Ph)_2$ (**71**) and their $^{31}P\{^{1}H\}$ and ^{29}Si NMR chemical shifts for comparison to complex **69**. Unfortunately, they did not synthesize *PNP*-Ir(H)(SiH_2Ph) so an ideal comparison could not be made. Nonetheless, as was seen with the reaction between **55** and H_3SiPh, changing from LIr(H)(SiR_3) to LIr($SiR_3)_2$, a substantial downfield shift in the ^{29}Si NMR spectrum was observed (δ –74.1 to δ –37.5). Their $^{31}P\{^{1}H\}$ NMR chemical shift moved more upfield from complex **70** to **71**. With complex **69**, the $^{31}P\{^{1}H\}$ NMR resonance shifted downfield. Comparing the phosphine to

phosphinimine donors, however, the effect on the chemical shift may be different because of their different donor abilities.

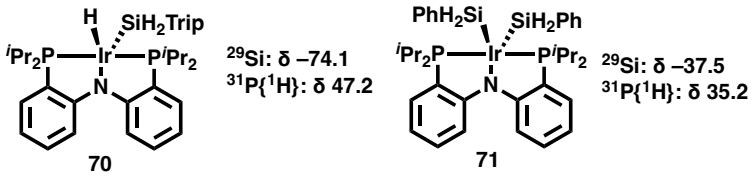

Figure 31 Tilley et al. silyl hydride and disilyl complexes

4.5 Summary and Concluding Remarks

The catalytic hydrogenation of cyclooctene at 10 mol% catalyst loading of $^{Pipp}LIr(H)_2$ has been reported. The process occurred at –30 °C and was complete after 40 hours at this temperature. There appears to be an equilibrium between $^{Pipp}LIr(H)_2$ + COE and $^{Pipp}LIr(COE)$ + H_2. Dehydrogenation of cyclohexane was attempted, but complex decomposition was observed at 0 °C, with no evidence for dehydrogenation.

Hydrosilylation of benzophenone with $^{Pipp}LIr(H)(SiR_3)$ (R_3 = Et_3, HPh_2) as a catalyst proceeded to completion. When $HSiEt_3$ was used the reaction mixture had to be heated to 100 °C for a reaction to be observed, but with H_2SiPh_2 the reaction progressed at ambient temperature. When attempting hydrosilylation with $^{Pipp}LIr(H)(SiH_2Ph)$ as a potential catalyst, however, the complex underwent a reaction with excess H_3SiPh to produce $^{Pipp}LIr(SiH_2Ph)_2$.

CHAPTER 5 – FUTURE WORK

5.1 Thesis Summary

This thesis has described the synthesis, characterization, and reactivity of 1,5-cyclooctadiene (COD) and cyclooctene (COE) complexes of iridium supported by a monoanionic *NNN*-pincer ligand. The complexes ^{Pipp}LIr(H)(SiR$_3$) (L = 2,5-(^{i}Pr$_2$P=NPipp)$_2$C$_4$H$_2$N, Pipp = *para*-isopropylphenyl, R$_3$ = Et$_3$, Ph$_2$H, PhH$_2$) and ^{Pipp}LIr(H)$_2$ were synthesized, characterized, and their chemical reactivity probed. The iridium dihydride complex ^{Pipp}LIr(H)$_2$ was capable of catalytic hydrogenation of COE at reduced temperature, but attempts at alkane dehydrogenation with cyclohexane showed complex decomposition. Two of the three iridium silyl hydride complexes, ^{Pipp}LIr(H)(SiEt$_3$) and ^{Pipp}LIr(H)(SiHPh$_2$), were capable of mediating the catalytic hydrosilylation of benzophenone, although the process was slow compared to literature catalysts. Efforts to hydrosilylate benzophenone using ^{Pipp}LIr(H)(SiH$_2$Ph) as a catalyst underwent a reaction with excess silane to produce the iridium disilyl complex, ^{Pipp}LIr(SiH$_2$Ph)$_2$.

Alternatives for ^{Pipp}LIr(COE) were investigated to avoid competing reactivity of free COE in solution. Since ^{Pipp}LIr(COE) and ^{Pipp}LIr(H)$_2$ cannot be isolated as analytically pure solids, and ^{Pipp}LIr(H)$_2$ is not stable above –30 °C and hydrogenates free COE to cyclooctane (COA) at this temperature, free COE/COA would compete with other substrates during chemical transformations. Accordingly, two iridium dicarbonyl complexes, ^{Pipp}LIr(CO)$_2$ and ^{Mes}LIr(CO)$_2$, were synthesized. Investigating analogous reactivity to rhodium chemistry previously undertaken in the Hayes group, a comproportionation reaction with

^{Pipp}LIr(CO)$_2$ and ^{Pipp}LIr(COE) was conducted in an effort to generate ^{Pipp}LIr(CO). Attempts to synthesize ^{Pipp}LIr(PPh$_3$) and ^{Mes}LIr(PPh$_3$) were unsuccessful. Two iridate species, [Li]$^+$[(COD)Ir(Me)$_2$]$^-$ and [(12-crown-4)$_2$Li]$^+$[(COD)Ir(Me)$_2$]$^-$, were synthesized, but tridentate monoanionic ligand coordination was unsuccessful. Using the imidazolinium chloride salt, [C$_3$H$_5$(NMes)$_2$]$^+$[Cl]$^-$, with [Li]$^+$[(COD)Ir(Me)$_2$]$^-$ yielded the *N*-heterocyclic carbene complex (COD)Ir(Me)(C$_3$H$_4$(NMes)$_2$).

5.2 Future Work: Synthetic Targets

5.2.1 Iridium Monocarbonyl Complexes

Accessing ^{Pipp}LIr(CO) (**58**), similar to the method reported by Hayes *et al*. for ^{Pipp}LRh(CO), would open multiple opportunities into new species and chemical transformations (Scheme 45). First, it may be possible to cause dissociation of one phosphinimine donor to allow oxidative addition of dihydrogen (**72**, Scheme 45, top). CO is much less labile than COE; therefore, the phosphinimine donor would be much more likely to dissociate in **58** than it would in ^{Pipp}LIr(COE). This may lead to a complex that is stable at or above ambient temperature that could catalyze alkane dehydrogenation. This could occur by using either *tert*-butylethylene (TBE) to remove H$_2$, and/or light, which could remove the CO ligand, presumably forming a highly reactive species that could mediate alkane dehydrogenation.

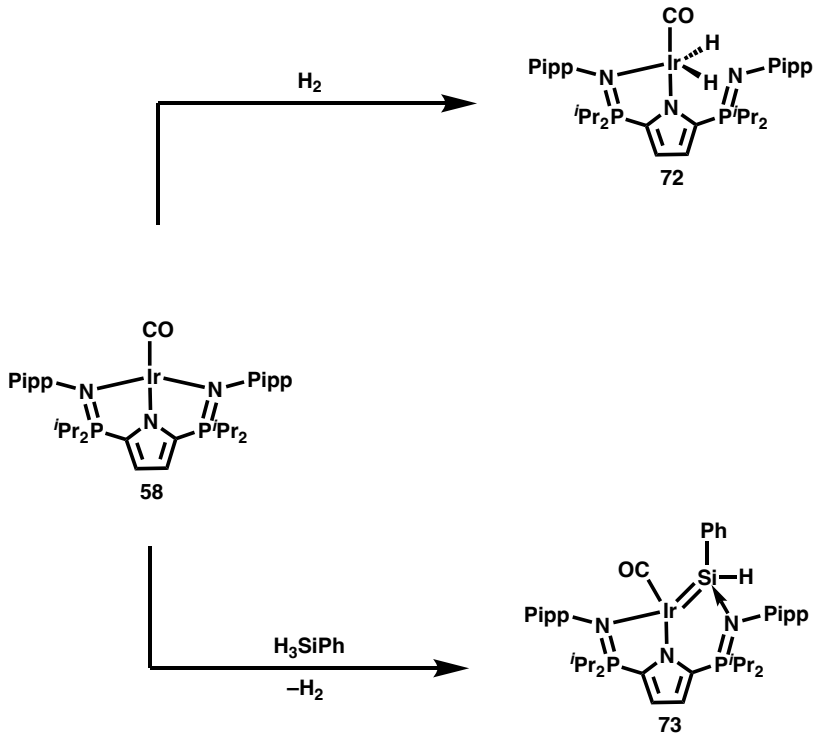

Scheme 45 Proposed reaction chemistry of ^{Pipp}*LIr(CO)*

Second, reaction with phenyl silane may undergo similar reactivity to that reported by Hayes *et al*. (silane dehydrogenation), in which dihydrogen could be lost to produce a base-stabilized silylene (**73**, Scheme 45, bottom).[78] The resultant complex, ^{Pipp}LIr(CO)(SiHPh), may be capable of hydrosilylation, hopefully at a faster rate than the silyl hydrides, ^{Pipp}LIr(H)(SiR_3) (R_3 = Et_3, Ph_2H), reported in this thesis. In addition, the structure, bonding, and reactivity of silylene complexes is of great fundamental interest.[78]

The original preparation of ^{Pipp}LRh(CO) utilized by the Hayes group may be an effective methodology to access the iridium analogue **58**. Specifically, elevated temperature and periodic evacuation of the headspace of the vessel was used to remove one carbonyl ligand from the metal.[77] In addition, trying the comproportionation with ^{Pipp}LIr(COD) (**42**) could

be another possible avenue to ^{Pipp}LIr(CO) (Scheme 46). Complex **42** is more thermally stable than ^{Pipp}LIr(COE), thus, the comproportionation reaction could be performed at a higher temperature than attempts using ^{Pipp}LIr(COE) (60–70 °C).

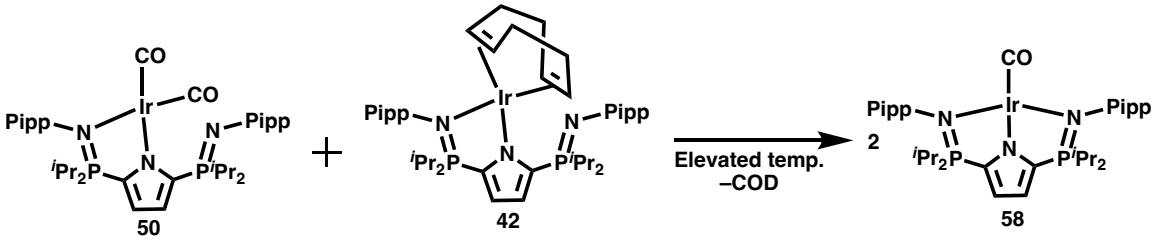

Scheme 46 Proposed synthesis of ^{Pipp}LIr(CO)

Fine-tuning the *NNN*-pincer ligand may influence the reaction chemistry of ^{Ar}LIr(CO)$_2$ and the thermodynamic stability of ^{Ar}LIr(CO). Figure 32 shows two possible modifications of the pincer ligand scaffold. Altering the aryl group on nitrogen (blue) to Dipp (2,6-diisopropylphenyl) or Mes (2,4,6-trimethylphenyl) would exert greater steric influence about the metal centre. If **50** is more thermodynamically stable than ^{Ar}LIr(CO), increasing the steric bulk may promote elimination of a CO ligand due to steric crowding. In addition, changing the functionalities on phosphorus from isopropyl to phenyl, or other electron withdrawing groups, may benefit attempts at the synthesis of ^{Pipp}LIr(CO). The electron withdrawing nature from the phosphorus of the phosphinimine donor would decrease the donation from iridium to CO. This would make the CO ligands easier to remove. All of the proposed ligand substituent changes have been synthesized and is done by either changing the chlorophosphine or aryl azide.

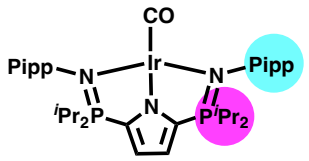

Figure 32 Possible modification of NNN-pincer ligand to promote comproportionation

5.2.2 Iridium Phosphine Complexes

Attempts at replacing COD and COE with triphenylphosphine were unsuccessful. Reaction of ^{Mes}LIr(COD) and ^{Pipp}LIr(COE) with triphenylphosphine did not lead to a reaction and led to a mixture of products, respectively. In addition, reacting $(PPh_3)_3IrCl$ with Na^{Pipp}L led to cyclometallation of $(PPh_3)_3IrCl$ at 40 °C. It is possible that triphenylphosphine is too sterically demanding to access the iridium centre if the mechanism is associative. Using a phosphine with a smaller cone angle, such as trimethylphosphine (triphenylphosphine: 152.0°, trimethylphosphine: 122.1° for $IrCl_3(CO)_2$(phosphine))[114] could alleviate this issue. Trimethylphosphine is also more electron donating. If reaction of triphenylphosphine and ^{Pipp}LIr(COE) affords a mixture of products because insufficient electronic donation from triphenylphosphine (*i.e.* equilibrium between ^{Pipp}LIr(PPh_3) and ^{Pipp}LIr + PPh_3), a more donating phosphine may assist in stabilization of the resulting complex.

5.2.3 $[Li]^+[(COD)Ir(Me)_2]^-$

When $[Li]^+[(COD)Ir(Me)_2]^-$ or $[(12\text{-crown-4})_2Li]^+[(COD)Ir(Me)_2]^-$ were reacted with H^{Mes}L at ambient temperature in THF-d_8, lithiated ligand was the product of the both reactions. Lithiated ligand is hypothesized to be a rapid decomposition product of

$[Li]^+[^{Mes}LIr(Me)]^-$, as the product is presumably not thermodynamically stable. An anionic bidentate ligand, such as a *β*-diketiminate (nacnac) ligand, may prevent the formation of lithiated ligand, as COD would likely remain coordinated to iridium. If COD remains coordinated, the resulting complex (**74**) would be 18-electrons and could be more thermodynamically stable. Oxidative addition across the C–H bond rather than the N–H bond may be a problem that could arise, but bulky R' groups such as Mes or Ad may prevent this (Scheme 47).

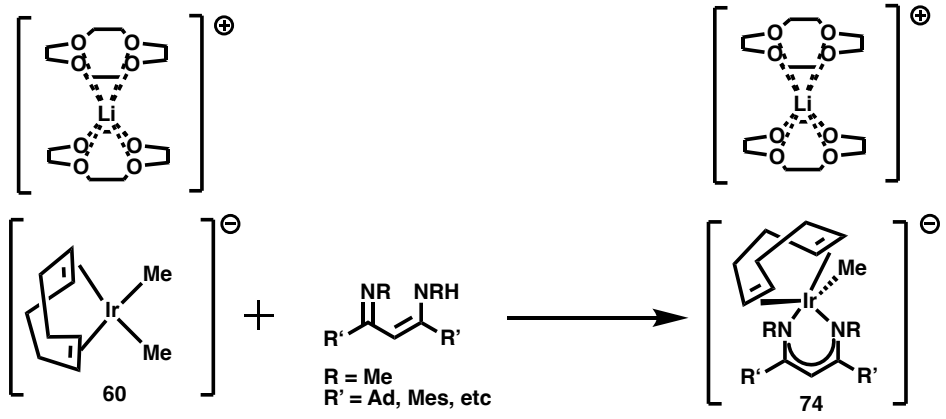

Scheme 47 Proposed synthesis of $[(12\text{-crown-4})_2]^+[(COD)Ir(Me)(nacnac)]^-$

Reaction of $[Li]^+[(COD)Ir(Me)_2]^-$ with the *N*-heterocyclic carbene precursor $[C_3H_5(NMes)_2]^+[Cl]^-$ yielded $(COD)Ir(Me)(C_3H_4(NMes)_2)$ (**64**) in high purity and yield. Reaction of **64** with dihydrogen could lead to the loss of methane and production of the monohydride complex, $(COD)Ir(H)(C_3H_4(NMes)_2)$ (**75**, Scheme 48). Similar reaction chemistry could be discovered with silanes, that through the loss of methane an iridium silyl complex, $(COD)Ir(SiR_3)(C_3H_4(NMes)_2)$ (**76**), could be synthesized. Lastly, replacing the COD ligand with CO is one route to an alternative ligand to COD (complex **77**).

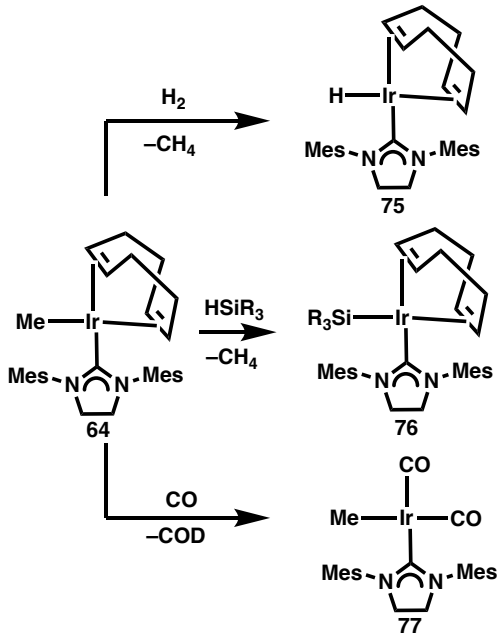

*Scheme 48 Proposed small molecule activation by (COD)Ir(Me)(C_3H_4(NMes)$_2$) (**64**)*

With the goal of alkane dehydrogenation considered, a 3-coordinate, 14-electron complex is desirable. In the literature, some have used tris(pentafluorophenyl)borane to abstract a methide from iridium.[115] With complex **64**, abstraction of the methide ligand from iridium may produce a 3-coordinate, 14-electron species, (COD)Ir(C_3H_4(NMes)$_2$) (**78**), which would presumably activate the C(sp^3)–H bonds of alkanes. The resultant β-hydride elimination could lead to the iridium dihydride, (COD)Ir(H)$_2$(C_3H_4(NMes)$_2$) (**79**), that in the presence of *tert*-butylethylene could regenerate the 3-coordinate complex **78**. There appears to only be one example of alkane dehydrogenation with an NHC ligand (**80**, Scheme 49),[116] but the conversion was poor (0.48% converted after 10 hours at 200 °C).

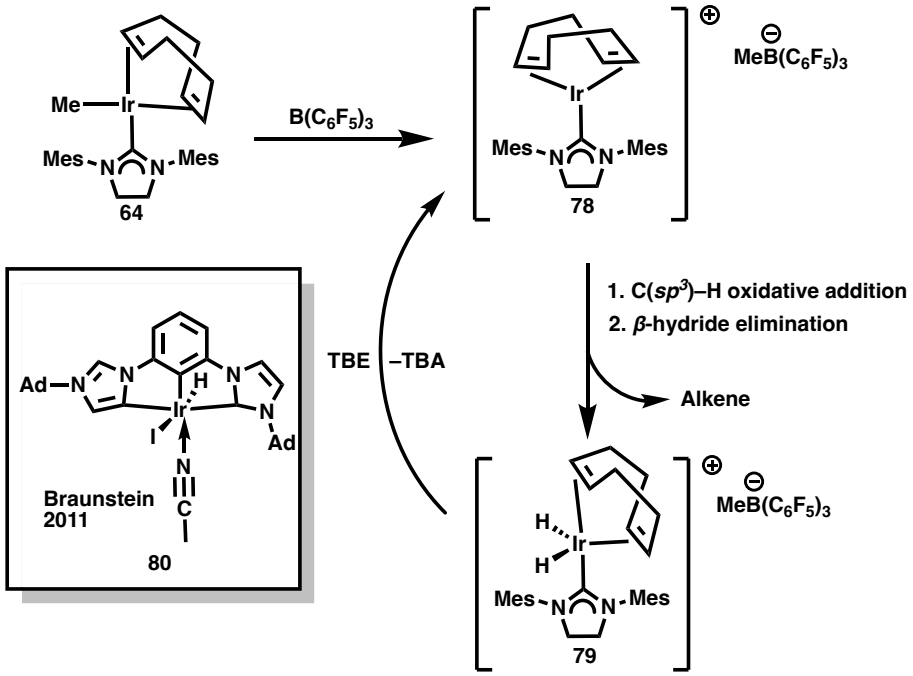

Scheme 49 Proposed synthesis of (COD)Ir(C_3H_4(NMes)$_2$) and (COD)Ir(H)$_2$(C_3H_4(NMes)$_2$)

5.2.4 Disilyl Complexes of Iridium

When considering ^{Pipp}LIr(SiH_2Ph)$_2$, discovered during attempts at hydrosilylation in which ^{Pipp}LIr(H)(SiH_2Ph) reacted with excess H_3SiPh, there are many opportunities for further exploration. First, reaction of ^{Pipp}LIr(H)(SiH_2Ph) (**55**) with a different silane, such as H_2SiPh_2, could lead to the mixed disilyl complex ^{Pipp}LIr(SiH_2Ph)($SiHPh_2$) (**81**) (Scheme 50).

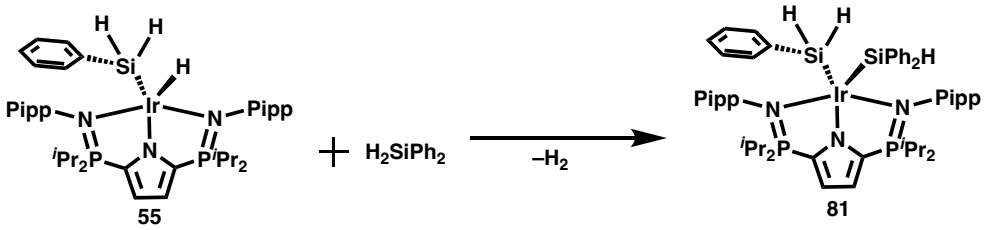

Scheme 50 Proposed synthesis of ^{Pipp}LIr(SiH$_2$Ph)(SiHPh$_2$)

Interest in organosilicon compounds by synthetic organic and materials scientists has grown substantially since the late 1990's.[117] Much of the work on introducing two silicon units using transition metals has focused on the activation of Si–Si bonds. There are very few examples of Si–Si bond activation by iridium, but one example is provided in Scheme 51.[118]

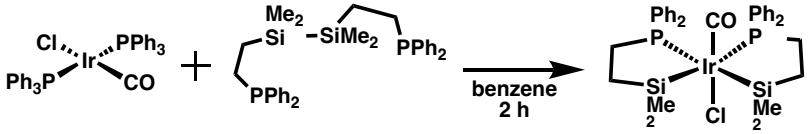

Scheme 51 Si–Si bond activation by iridium

Although ^{Pipp}LIr(SiH$_2$Ph)$_2$ did not show silylation activity, it is postulated that reaction of **81** with a stoichiometric quantity of alkyne would afford a mixed disilane. Selectivity and complex decomposition would impose challenges in the proposed reaction. In particular, there may be a challenge to achieve *trans* selectivity as 1,2-insertion must occur *cis*. In addition, if the reaction is stoichiometric, once both silicon units are transferred to the alkyne a 3-coordinate, 14-electron species that would presumably decompose rapidly would be formed. Under these conditions, it is unlikely the reaction could be done

catalytically as regeneration of **81** would be slow since there is an unknown intermediate before $^{Pipp}LIr(SiH_2Ph)_2$ is formed.

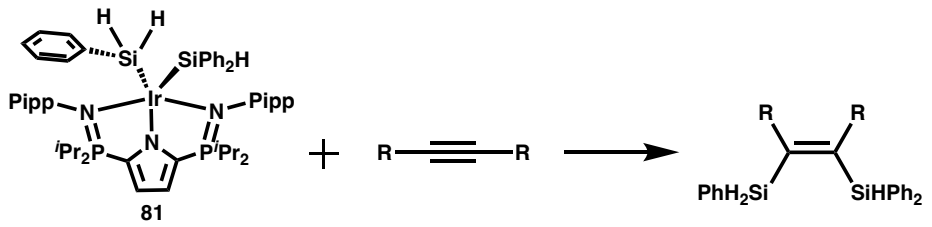

Scheme 52 Proposed transfer of two silicon units to an alkyne

Si–Si oxidative addition is another target reaction. Using $Me_3Si–SiMe_3$ with $^{Pipp}LIr(COE)$ it is proposed that oxidative addition could occur to produce $^{Pipp}LIr(SiMe_3)_2$ (**82**) (Scheme 53). Observing Si–Si oxidative addition could alleviate the issues discussed with **81**. The addition to alkynes could be done catalytically, as has been seen with some palladium complexes.[119] Most examples have provided symmetric silanes, as has been proposed here. However, if Si–Si oxidative addition does occur, it could be possible to use an unsymmetrical disilane and achieve unsymmetric (bis)silylation.

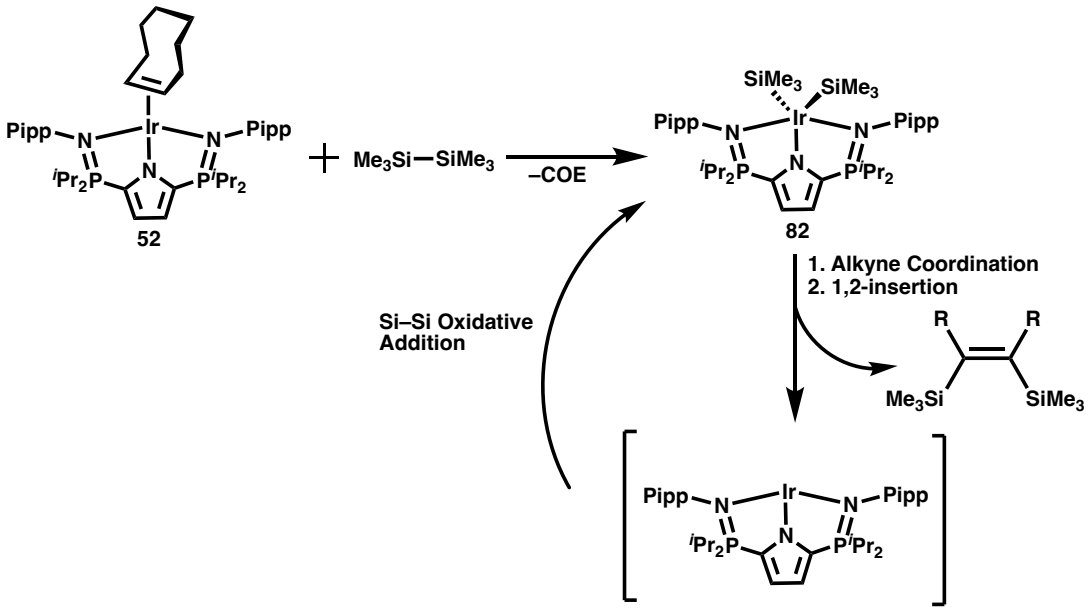

Scheme 53 Proposed synthesis of ^{Pipp}LIr(SiMe$_3$)$_2$ through Si–Si oxidative addition

5.3 Future Work: Catalytic Reactions with ^{Pipp}LIr(H)$_2$ and ^{Pipp}LIr(H)(SiR$_3$)

5.3.1 Alkane Dehydrogenation

Preliminary attempts at catalytic (10 mol%) alkane dehydrogenation using ^{Pipp}LIr(H)$_2$, starting at–30 °C and slowly increasing the temperature, led to complex decomposition. Others have found that with a *PCP*-ligand scaffold, adamantyl (Ad) groups on phosphorus provided higher thermal stability than its analogous *tert*-butyl (^{t}Bu) substituents.[41] They suggested that although the steric and electronic differences between Ad and ^{t}Bu are minor, that the cage-like structure could prevent the hypothesized decomposition pathways (catalyst-catalyst intermolecular interactions, cyclometallation, etc). In the case of ^{Pipp}LIr(H)$_2$, changing from a Pipp functionality on nitrogen to Ad substituents would have

a profound steric and electronic influence. Changing from an aromatic substituent to an alkyl one would increase electron donation possibly increasing the efficacy of ^{Ad}LIr to oxidatively add C(sp^3)–H bonds. In addition, Ad functionalities are larger than phenyl, and Pipp groups do not have steric bulk directed towards the metal centre. This could prevent catalyst-catalyst intermolecular interactions or other unwanted decomposition pathways. Ad groups also are commonly known to be more robust than other alkyl substituents, and if ^{Ad}LIr(H)$_2$ could be synthesized, higher thermal stability may be observed. This could prevent the necessity of using reduced temperature and the observed complex decomposition.

Another possible improvement would include using TBE as an H_2 acceptor at –30 °C. The T-shaped, 14-electron species would still be accessed but the reduced temperature may assist in kinetic stabilization.

5.3.2 Scoping Experimental Conditions for Catalytic Hydrosilylation

Benzophenone hydrosilylation reactions with $HSiEt_3$ and H_2SiPh_2 and 10 mol% ^{Pipp}LIr(H)(SiR_3) (R_3 = Et_3, HPh_2) as a catalyst underwent the desired hydrosilylation reactivity. Compared to other literature catalysts, the reaction proceeds more slowly (*e.g.* 1.5 hours and 4.5 hours versus >300 hours, respectively). Scoping of the conditions and ligand fine-tuning may improve the reaction speed. In particular, with ^{Pipp}LIr(H)($SiHPh_2$), an increase in the temperature would improve the rate of hydrosilylation.

Discovering the active catalyst would provide information into how to improve the rate of hydrosilylation. This could be done by performing stoichiometric reactions between ^{Pipp}LIr(H)(SiR_3), benzophenone, and the corresponding silane in an attempt to isolate the resting state of the catalyst.

Tuning the steric and electronic properties at phosphorus and nitrogen on the ligand may also improve the rate. Although the steric properties at nitrogen cannot be decreased with the available aryl azides (Ph, Dipp, Pipp, Mes), electronics could be changed by altering the group in the *para* position, such as to an electronic withdrawing group (e.g. $–NO_2$). This would make the iridium centre less electron rich and may be more reactive towards insertion of benzophenone. This has been seen with rhodium, in that insertion of an alkene into oxygen was more rapid with electron poor ligands.[120] If the substituents on phosphorus were changed to phenyl, a similar effect could be observed.

One other avenue would be to pursue the iridium silylene complex, ^{Pipp}LIr(CO)(SiPhH) discussed in 5.2.1. Iridium silylene complexes sometimes undergo a different mechanism for hydrosilylation (insertion of the multiple bond into Si–H, rather than Ir–H), and this pathway may improve the rate.

5.4 Conclusions

This thesis has described the synthesis, characterization, and reaction chemistry of a variety of new iridium complexes supported by a monoanionic *NNN*-pincer ligand. Up to 2016, a book chapter that reviewed monoanionic *NNN*-pincer ligands only revealed one example

of an iridium complex supported by such ligands, and I am not aware of any others.[121, 122] The most commonly used pincer ligands with iridium are *PCP*-based, and the synthesis of these new iridium complexes with nitrogen donors shows potential for different reactivity. An example from this thesis includes ^{Pipp}LIr(H)$_2$. Most iridium dihydride complexes supported by *PCP*-pincer ligands are trigonal bipyramidal and thermally robust, compared to ^{Pipp}LIr(H)$_2$ which displays square pyramidal geometry in solution and is not stable above –30 °C.

Much of the hydrosilylation literature does not focus on characterizing intermediates. This thesis has some of the few examples of fully characterized iridium silyl hydride complexes supported by pincer ligands. Although hydrosilylation proceeds slowly with ^{Pipp}LIr(H)(SiR$_3$) (R$_3$ = Et$_3$, Ph$_2$H; >300 hours to completion), fully characterized silyl hydride complexes provide new fundamental information about iridium complexes supported by monoanionic *NNN*-pincer ligands.

This chapter has outlined some of the avenues in which future work could expand on what has been accomplished in this thesis. We hope that the new iridium complexes supported by monoanionic *NNN*-pincer ligands, and their chemistry reported here will motivate others to explore such avenues.

CHAPTER 6 – EXPERIMENTAL METHODS

6.1 Generation Considerations

6.1.1 Equipment

All reactions were carried out using a double-manifold vacuum line under a positive pressure of argon or in an argon-filled MBraun Labmaster 130 glove box, unless otherwise specified. Glove box antechambers and vacuum lines utilized an Edwards RV12 vacuum pump. All glassware used was stored in an oven set at 115 °C for a minimum of 12 hours. The glassware was attached to the line or placed in the antechamber and evacuated while hot. Speciality glassware used in this work included a swivel frit apparatus and Teflon-sealed, thick-walled glass bombs, referred to as bombs in subsequent sections.

6.1.2 Solvents

All solvents used were purchased from Millipore Sigma, Cambridge Isotopes, or retrieved from a Solvent Purification System (SPS). All solvents for air- and moisture-sensitive chemistry were dried as follows. Non-halogenated solvents (benzene, pentane, toluene, tetrahydrofuran, and diethylether) were dried over activated 3 Å molecular sieves, degassed by three freeze-pump-thaw cycles, and distilled directly into 500 mL bombs containing Na/benzophenone (for use on a double-manifold vacuum line) or activated 3 Å molecular sieves (for use in the glove box). Chloroform was dried over CaH_2, degassed by three freeze-pump-thaw cycles, then distilled into a new bomb for storage. Solvents used on a

double-manifold vacuum line were transferred from the bomb containing the solvent over Na/benzophenone to the reaction vessel under reduced temperature and pressure. Deuterated solvents (benzene-d_6, toluene-d_8, tetrahydrofuran-d_8, and chloroform-*d*) were dried and stored in the same manner as non-deuterated solvents.

6.1.3 Use and Purification of Chemicals

The materials ^{n}BuLi (2.5 M in hexanes) and MeLi (1.6 M in diethylether) were purchased from Millipore Sigma and used without further purification. The reagent $IrCl_3 \bullet xH_2O$ was purchased from Pressure Chemicals and used without further purification. The azides $PippN_3$ (Pipp = *para*-isopropylphenyl),[123] $DippN_3$ (Dipp = 2,6-diisopropylphenyl),[124] and $MesN_3$ (Mes = 2,4,6-trimethylphenyl)[124] were synthesized *via* literature procedures. The starting materials $[IrCl(COD)]_2$[125], $IrCl(PPh_3)_3$[105], and the imidazolinium chloride salt ($[C_3H_5(NMes)_2]^+[Cl]^-$)[126] were synthesized *via* literature procedures. The reagent $[IrCl(COE)_2]_2$ was purchased from Strem Chemicals and used without further purification. Triphenylphosphine was purchased from Sigma Aldrich and recrystallized from diethylether before use. All gases (H_2, CO, and Ar) were purchased from Linde Canada and used in isolated systems, but without purification. Sodium hydride was purchased from Alfa Aesar and used without further purification. The *NNN*-pincer ligand (2,5-(^{i}Pr$_2$P=NAr)$_2$C$_4$H$_2$N, Ar = Pipp, Dipp, Mes) was synthesized by methods reported by previous group members.[71, 77, 82]

6.1.4 NMR Spectroscopy

All NMR spectra (^{1}H, ^{7}Li{^{1}H}, ^{13}C{^{1}H}, ^{29}Si, ^{29}Si{^{1}H}, ^{31}P{^{1}H}, APT, DEPT-90, DEPT-135, ^{1}H-^{1}H COSY, ^{1}H-^{13}C HSQC, ^{1}H-^{13}C HMBC), were acquired on a Bruker Avance II 300 MHz spectrometer (^{1}H 300.13 MHz, ^{13}C 75.47 MHz, ^{29}Si 59.63 MHz, ^{31}P 121.49 MHz) or on a Bruker Avance III HD 700 MHz spectrometer (^{1}H 700.13 MHz, ^{7}Li 272.097 MHz, ^{13}C 176.048 MHz, ^{31}P 283.42 MHz). All experiments were acquired at 22 °C, except for variable temperature experiments in which the temperature is specified. ^{1}H and ^{13}C{^{1}H} spectra were referenced to tetramethylsilane with internal solvent resonances, respectively: benzene-d_6 (δ 7.16 and δ 128.39), toluene-d_8 (δ 2.09, 6.98, 7.02, 7.09, and δ 20.4, 125.2, 128.0, 128.9, 137.5), tetrahydrofuran-d_8 (δ 1.73, 3.58 and δ 25.3, 67.4), and chloroform-*d* (δ 7.27 and δ 77.36). NMR spectral references used in catalytic experiments are specified in the corresponding sections. All chemical shifts are provided in ppm, and are reported as follows: chemical shift (ppm), multiplicity (s = singlet, d = doublet, t = triplet, dd = doublet of doublets, ddd = doublet of doublet of doublets, tt = triplet of triplets, sp = septet, m = multiplet, br = broad, ov = overlapping signals), integration, *J*-coupling (Hz), assignment.

6.1.5 Elemental Analysis

Elementar Americas Vario Microcube instrument was used for CHNS elemental analyses. All elemental analyses of iridium containing compounds used vanadium oxide as a combustion agent.

6.1.6 X-ray Crystallography

X-ray crystallographic data was acquired on a Rigaku SuperNova diffractometer containing a 130 Dectis Pilatus 200K-A detector, Oxford Cryostream cooling system, and molybdenum ($\lambda = 0.71073$ Å) and copper ($\lambda = 1.5406$ Å) radiation sources. Data collection was performed under a stream of N_2 at 100 K to prevent decomposition and decrease thermal motion. Crystals were coated with Paratone oil and placed on a glass slide then observed under a standard microscope or polarizing light microscope. Once a suitable crystal was chosen, the crystal was mounted on a MiTeGen Dual Thickness Micromount attached to a goniometer head and centered on the diffractometer for data collection. CrysAlisPro[127] was used for data reduction and to determine the unit cell parameters. SHELXL[128] was used for structure solution and SHELXT[129] was used for structure refinement in Olex2 1.5-alpha.[130] Mercury 2022.1.0[131] was used for structure visualization.

6.2 Methods for Catalytic Experiments

6.2.1 Cyclooctene Hydrogenation

In a J. Young NMR tube, 3.4 mg (1 equiv, 0.0058 mmol) of $Na^{Pipp}L$ and 2.6 mg (0.5 equiv, 0.0029 mmol) of $[IrCl(COE)_2]_2$ were added and dissolved in 0.5 mL of toluene-d_8. The reaction mixture was left to react in a glove box for 48 hours or until ^1H and $^{31}P\{^1H\}$ NMR spectra indicated complete consumption of starting materials. Once the reaction had reached completion, 3.9 μL (10 equiv, 0.030 mmol) of cyclooctene was added and the mixture degassed by three freeze-pump-thaw cycles. An atmosphere of H_2 was added at

–30 °C, and the J. Young NMR tube injected into a pre-cooled NMR spectrometer at –30 °C. The mixture was transported in a Dewar filled with cooled acetone (approximately –50 °C) to ensure the mixture did not warm above this temperature. Hydrogenation was monitored by ^{1}H NMR spectroscopy, observing the disappearance of the resonance attributed to the alkene hydrogen atoms.

6.2.2 General Procedure for Hydrosilylation

In a J. Young NMR tube, the catalyst (^{Pipp}LIr(H)(SiR_3), R_3 = Et_3, Ph_2H, PhH_2) was added and dissolved in 0.5 mL of benzene-d_6. Excess (10 equiv) of the corresponding silane was added *via* microsyringe to the orange solution, and the tube shaken. The contents of the J. Young NMR tube were transferred to a 2 mL vial containing benzophenone (10 equiv), then back to the J. Young NMR tube. The vial was rinsed with benzene-d_6 for quantitative transfer. The progress of the reaction was monitored by NMR spectroscopy, and temperature increased if no reaction was observed. The progress was monitored by integrating the resonances attributed to the *ortho*-C*H* of the starting material (benzophenone) and product. As the reaction progressed, the solution became pale yellow (~24 – 48 hours). The ^{1}H NMR spectrum was referenced to tetramethylsilane by internal solvent resonances (δ 7.16).

6.2.3 Cyclohexane Dehydrogenation

In a J. Young NMR tube, 1.9 mg (1 equiv, 0.0032 mmol) of Na^{Pipp}L and 1.6 mg (0.5 equiv, 0.0018 mmol) of $[IrCl(COE)_2]_2$ were added and dissolved in 0.5 mL of toluene-d_8. The

reaction mixture was left for 48 hours in the glove box and checked for completion by ^{1}H and $^{31}P\{^{1}H\}$ NMR spectra. Once all starting materials were consumed, 1.9 µL (10 equiv, 0.018 mmol) of cyclohexane was added in one portion *via* microsyringe. A sealed glass capillary containing tetramethylsilane in toluene-d_8 was also added to the J. Young NMR tube. The reaction mixture was degassed by three freeze-pump-thaw cycles and the J. Young NMR tube was exposed to an atmosphere of H_2 at –30 °C. The solution turned from reddish-brown to yellowish-brown in colour. The J. Young NMR tube was then injected into a pre-cooled NMR spectrometer at –30 °C. The mixture was transported in a Dewar filled with cooled acetone (approximately –50 °C) to ensure the mixture did not warm above this temperature. The temperature was increased incrementally (5–10 °C per temperature increase), and dehydrogenation was monitored by the appearance of the alkene resonance of cyclohexene (δ 5.66).

6.3 Synthesis of New Compounds and Characterization

6.3.1 Compounds from Chapter 2

6.3.1.1 ^{Pipp}LIr(COD) (L = 2,5-(^{i}Pr$_2$P=NPipp)$_2$C$_4$H$_2$N) ***(42)***

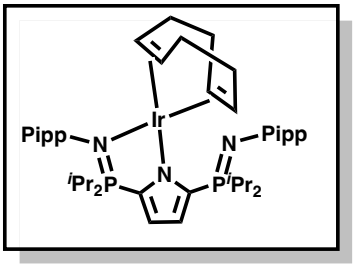

In an argon-filled glove box, 23.2 mg of Na^{Pipp}L (1 equiv, 0.039 mmol) and 13.5 mg of [IrCl(COD)]$_2$ (0.5 equiv, 0.020 mmol) were combined in a 20 mL scintillation vial and dissolved in ~4 mL of toluene. The reaction mixture was left for 16 hours with constant stirring. The bright yellow solution was filtered through Celite,

and volatiles removed under vacuum. Pentane (~5 mL) was added to the yellow oily solid, yielding a yellow powder when the pentane was removed *in vacuo*. Yield: 15.1 mg (83.9%). ^{1}H NMR (700.13 MHz, benzene-d_6): δ 7.25 (d, 2H, $^{3}J_{H\text{-}H}$ = 8.0 Hz, Pipp-C*H*), 7.22 (d, 2H, $^{3}J_{H\text{-}H}$ = 8.0 Hz, Pipp-C*H*), 7.11 (d, 2H, $^{3}J_{H\text{-}H}$ = 8.2 Hz, Pipp-C*H*), 7.08 (d, 2H, $^{3}J_{H\text{-}H}$ = 8.1 Hz, Pipp-C*H*), 6.81 (m, 1H, C$_4$*H*$_2$N), 6.46 (m, 1H, C$_4$*H*$_2$N), 4.94 (m, 2H, *H*C=C*H*), 3.23 (m, 2H, *H*C=C*H*), 2.99 (sp, 1H, $^{3}J_{H\text{-}H}$ = 6.9 Hz, Pipp-C*H*(CH$_3$)$_2$), 2.72 (sp, 1H, $^{3}J_{H\text{-}H}$ = 6.9 Hz, Pipp-C*H*(CH$_3$)$_2$), 2.52 (m, 2H, PC*H*(CH$_3$)$_2$), 2.20 (m, 4H, COD-C*H*$_2$), 2.03 (sp, 2H, $^{3}J_{H\text{-}H}$ = 7.1 Hz, PC*H*(CH$_3$)$_2$), 1.91 (m, 4H, COD-C*H*$_2$), 1.49 (m, 4H, COD-C*H*$_2$), 1.42 (d, 6H, $^{3}J_{H\text{-}H}$ = 6.9 Hz, Pipp-CH(C*H*$_3$)$_2$), 1.37 (dd, 6H, $^{3}J_{H\text{-}H}$ = 7.1 Hz, $^{3}J_{H\text{-}P}$ = 15.3 Hz, PCH(C*H*$_3$)$_2$), 1.22 (dd, 6H $^{3}J_{H\text{-}H}$ = 7.8 Hz, PCH(C*H*$_3$)$_2$), 1.14 (d, 6H, $^{3}J_{H\text{-}H}$ = 6.9 Hz, Pipp-CH(C*H*$_3$)$_2$), 0.99 (dd, 6H, $^{3}J_{H\text{-}H}$ = 7.1 Hz, $^{3}J_{H\text{-}P}$ = 15.4 Hz, PCH(C*H*$_3$)$_2$), 0.92 (dd, 6H, $^{3}J_{H\text{-}H}$ = 7.0 Hz, $^{3}J_{H\text{-}P}$ = 16.2 Hz, PCH(C*H*$_3$)$_2$). ^{13}C{^{1}H} NMR (176.05 MHz, benzene-d_6): δ 152.21 (d, $^{2}J_{C\text{-}P}$ = 1.8 Hz, Pipp-*ipso*), 144.76 (s, Pipp-*ipso*), 144.74 (d, $^{2}J_{C\text{-}P}$ = 13.5 Hz, Pipp-*ipso*), 137.14 (br, pyrrole-*C*P), 135.68 (s, Pipp-*ipso*), 129.35 (d, $^{4}J_{C\text{-}P}$ = 6.4 Hz, Pipp-*C*H), 129.01 (ov, pyrrole-*C*P), 126.80 (s, Pipp-*C*H), 126.62 (s, Pipp-*C*H), 125.28 (d, $^{3}J_{C\text{-}P}$ = 16.9 Hz, Pipp-*C*H), 123.29 (br, pyrrole-*C*H), 116.28 (br, pyrrole-*C*H), 61.89 (s, H*C*=*C*H), 59.58 (s, H*C*=*C*H), 34.45 (s, Pipp-*C*H(CH$_3$)$_2$), 34.07 (s, Pipp-*C*H(CH$_3$)$_2$), 33.28 (s, COD-*C*H$_2$), 30.96 (s, COD-*C*H$_2$), 30.56 (s, P*C*H(CH$_3$)$_2$), 30.52 (s, P*C*H(CH$_3$)$_2$), 28.10 (s, P*C*H(CH$_3$)$_2$), 27.81 (s, P*C*H(CH$_3$)$_2$), 25.42 (Pipp-CH(*C*H$_3$)$_2$), 24.59 (s, Pipp-CH(*C*H$_3$)$_2$), 18.74 (d, $^{2}J_{C\text{-}P}$ = 3.2 Hz, PCH(*C*H$_3$)$_2$), 17.34 (s, PCH(*C*H$_3$)$_2$), 16.60 (d, $^{2}J_{C\text{-}P}$ = 3.0 Hz, PCH(*C*H$_3$)$_2$), 16.22 (s, PCH(*C*H$_3$)$_2$). ^{31}P{^{1}H} NMR (283.42 MHz, benzene-d_6): 58.7 (s, chelated), 13.34 (s, free). Anal. Cald. (%) for C$_{42}$H$_{64}$IrN$_3$P$_2$: C, 58.31; H, 7.46; N, 4.86. Found: C, 58.10; H, 7.47; N, 4.72.

6.3.1.2 ^{Dipp}LIr(COD) (L = 2,5-(^{i}Pr$_2$P=NDipp)$_2$C$_4$H$_2$N) ***(43)***

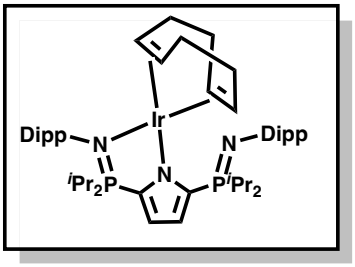

Method 1

In a J. Young NMR tube, 24.1 mg (1 equiv, 0.036 mmol) of Na^{Dipp}L and 14.0 mg (0.5 equiv, 0.021 mmol) [IrCl(COD)]$_2$ were dissolved in 0.5 mL of benzene-*d*$_6$ yielding an orange-brown solution. After 16 hours the ^{1}H and ^{31}P{^{1}H} NMR spectra indicated complete consumption of the starting materials. At this point the solution was yellow-brown in colour. In benzene-*d*$_6$, ^{1}H, ^{13}C{^{1}H}, and 2-dimensional NMR spectra were acquired; however, the ^{1}H NMR spectrum was broad and a low temperature ^{1}H NMR spectrum was required. The solution was filtered into a 20 mL scintillation vial and volatiles were removed under vacuum. The resultant yellow powder was redissolved in toluene-*d*$_8$ for subsequent NMR characterization at –20 °C. Yield: 16.3 mg (92.6%). ^{1}H NMR (300.13 MHz, 22 °C, benzene-*d*$_6$): δ 7.23 (d, 2H, Dipp-*m*-C*H*), 7.00 (ov, 6H, Dipp-C*H*, C$_4$*H*$_2$N), 6.31 (br, 1H, C$_4$*H*$_2$N), 5.20 (br, *H*C=C*H*), 3.89 (br sp, 2H, $^{3}J_{H\text{-}H}$ = 6.6 Hz, Dipp-C*H*(CH$_3$)$_2$), 2.79 (br), 1.99 (br), 1.39 (br ov m, PCH(C*H*$_3$)$_2$), 1.23 (d, 12H, $^{3}J_{H\text{-}H}$ = 6.6 Hz, Dipp-CH(C*H*$_3$)$_2$), 0.80 (br ov m, PCH(C*H*$_3$)$_2$). *Four of the resonances corresponding to the Dipp groups (both aromatic and alkyl) and some of the P^{i}Pr resonances were too broad to be observed, nor could all observed resonances be assigned. See next for characterization at reduced temperature.* ^{1}H NMR (300.13 MHz, –20 °C, toluene-*d*$_8$): δ 7.22 (d, 2H, $^{3}J_{H\text{-}H}$ = 7.5 Hz, Dipp-*m*-C*H*), 7.03 (ov, Dipp-*m*-C*H*), 7.02 – 6.91 (ov, 5H, Dipp-*p*-C*H*, C$_4$*H*$_2$N), 6.27 (br, 1H, C$_4$*H*$_2$N), 5.22 (br, 2H, *H*C=C*H*), 4.17 (br, 2H, *H*C=C*H*), 3.80 (ov, 2H, PC*H*(CH$_3$)$_2$), 3.50 (ov, 2H, Dipp-C*H*(CH$_3$)$_2$), 3.31 (br, 2H, Dipp-C*H*(CH$_3$)$_2$), 2.74 (m, 4H, COD-C*H*$_2$), 2.31 (ov, 2H, PC*H*(CH$_3$)$_2$), 1.92 (ov d, 12H, $^{3}J_{H\text{-}H}$ =

6.5 Hz, Dipp-CH(CH_3)$_2$), 1.73 (ov m, 6H, PCH(CH_3)$_2$), 1.30 (ov m, 22H, COD-CH_2, PCH(CH_3)$_2$, Dipp-CH(CH_3)$_2$), 0.90 (m, 6H, PCH(CH_3)$_2$), 0.56 (m, 6H, PCH(CH_3)$_2$). ^{13}C{^{1}H} NMR (75.47 MHz, 22 °C, benzene-d_6): δ 145.93 (s, Dipp-*ipso*), 142.60 (s, Dipp-*ipso*), 1421.57 (s, Dipp-*ipso*), 141.93 (ov dd, $J_{C\text{-}P}$ = 89.8 Hz, $^4J_{C\text{-}P}$ = 12.1 Hz, pyrrole-*C*P), 140.90 (d, $^3J_{C\text{-}P}$ = 7.5 Hz, Dipp-*ipso*), 130.41 (ov dd, $^4J_{C\text{-}P}$ = 12.8 Hz, pyrrole-*C*P), 125.62 (d, $^4J_{C\text{-}P}$ = 2.3 Hz, Dipp-*C*H), 124.81 (br s, Dipp-*C*H), 123.58 (s, Dipp-*C*H), 121.37 (dd, $^2J_{C\text{-}P}$ = 18.1 Hz, $^3J_{C\text{-}P}$ = 11.3 Hz, pyrrole-*C*H), 117.88 (s, Dipp-*C*H), 115.28 (dd, $^2J_{C\text{-}P}$ = 24.2 Hz, $^3J_{C\text{-}P}$ = 9.8 Hz, pyrrole-*C*H), 67.48 (s, H*C*=*C*H), 61.70 (s, H*C*=*C*H), 32.27 (s, P*C*H(CH$_3$)$_2$), 29.16 (s, P*C*H(CH$_3$)$_2$), 28.77 (br s, COD-*C*H$_2$) 28.59 (br s, Dipp-*C*H(CH$_3$)$_2$), 28.05 (br s, COD-*C*H$_2$), 27.21 (s, Dipp-*C*H(CH$_3$)$_2$), 26.16 (s, Dipp-CH(*C*H$_3$)$_2$), 25.00 (s, Dipp-CH(*C*H$_3$)$_2$), 18.15 (s, PCH(*C*H$_3$)$_2$), 17.50 (s, PCH(*C*H$_3$)$_2$). ^{31}P{^{1}H} NMR (121.50 MHz, benzene-d_6): δ 50.0 (s, chelated), –2.92 (s, free).

Method 2

In an argon-filled glove box, 12.9 mg (1 equiv, 0.020 mmol) of H^{Dipp}L and 6.6 mg (0.5 equiv, 0.0099 mmol) of [IrCl(COD)]$_2$ were combined in a 20 mL scintillation vial, followed by ~2 mL of toluene. The bright orange solution was stirred for 16 hours. Once the toluene was removed under vacuum, a bright yellow powder was acquired. Yield: 8.2 mg (82.8%). Anal. Cald. (%) for $C_{48}H_{76}IrN_3P_2$: C, 60.73; H, 8.07; N, 4.43. Found: C, 60.97; H, 8.32; N, 3.73.

6.3.1.3 ^{Mes}LIr(COD) (L = 2,5-(^{i}Pr$_2$P=NMes)$_2$C$_4$H$_2$N) ***(44)***

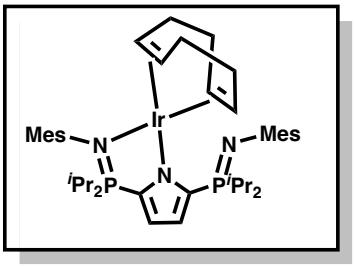

Method 1

In an argon-filled glove box, 15.2 mg (1 equiv, 0.026 mmol) of Na^{Mes}L and 9.0 mg (0.5 equiv, 0.013 mmol) of [IrCl(COD)]$_2$ were added to a 20 mL scintillation vial. Toluene (~2 mL) was added to the vial, yielding a brownish-yellow solution. The reaction mixture was left for 16 hours after which it was filtered through Celite, and toluene removed under vacuum. A yellow-brown powder was isolated. Yield: 10.7 mg (93.9%).

Method 2

In an argon-filled glove box, 17.6 mg (1 equiv, 0.031 mmol) of H^{Mes}L and 11.4 mg (0.5 equiv, 0.017 mmol) of [IrCl(COD)]$_2$ were added to a 20 mL scintillation vial. Toluene (~2 mL) was added resulting in a bright yellow solution, which turned into a yellow suspension within 30 minutes of stirring. The toluene was removed *in vacuo* affording a yellow powder. Yield: 12.5 mg (92.5%). ^{1}H NMR (300.13 MHz, benzene-d_6): δ 6.94 (ov, 3H, MesC*H* and C$_4$*H*$_2$N), 6.78 (s, 2H, MesC*H*), 6.24 (s, 1H, C$_4$*H*$_2$N), 5.15 (br s, 2H, *H*C=C*H*), 4.37 (br sp, 1H, PC*H*(CH$_3$)$_2$), 3.44 (br sp, 1H, PC*H*(CH$_3$)$_2$), 3.10 (br s, 2H, *H*C=C*H*), 2.51 (s, 6H, *o*-MesC*H*$_3$), 2.44 (s, 6H, *o*-MesC*H*$_3$), 2.29 (s, 3H, *p*-MesC*H*$_3$), 2.14 (ov, 12H, *p*-MesC*H*$_3$, COD-C*H*$_2$, PC*H*(CH$_3$)$_2$), 1.57 (dd, $^{3}J_{H\text{-}H}$ = 7.2 Hz, $^{3}J_{H\text{-}P}$ = 14.9 Hz, PCH(C*H*$_3$)$_2$), 1.33 (m, 4H, COD-C*H*$_2$), 1.161 (ov dd, 12H, PCH(C*H*$_3$)$_2$), 0.72 (dd, 6H, $^{3}J_{H\text{-}H}$ = 6.8 Hz, $^{3}J_{H\text{-}P}$ = 16.3 Hz, PCH(C*H*$_3$)$_2$). ^{13}C{^{1}H} NMR (75.47 MHz, benzene-d_6): δ 146.88 (s, Mes-

ipso), 143.39 (m, pyrrole-*C*P), 142.20 (m, pyrrole-*C*P), 136.04 (d, $^{2}J_{C\text{-}P}$ = 5.3 Hz, Mes-*ipso*), 133.07 (d, $^{3}J_{C\text{-}P}$ = 2.3 Hz, Mes-*ipso*), 130.46 (s, Mes-*ipso*), 130.25 (s, Mes-*ipso*), 130.03 (d, $^{4}J_{C\text{-}P}$ = 1.5 Hz, Mes-*C*H), 128.90 (s, Mes-*C*H), 125.23 (s, Mes-*ipso*), 120.48 (m, pyrrole-*C*H), 155.56 (m, pyrrole-*C*H), 62.26 (s, H*C*=*C*H), 60.32 (s, H*C*=*C*H), 32.92 (s, P*C*H(CH$_3$)$_2$), 31.26 (s, P*C*H(CH$_3$)$_2$), 31.18 (s, P*C*H(CH$_3$)$_2$), 30.16 (s, P*C*H(CH$_3$)$_2$), 27.51 (s, COD-*C*H$_2$), 26.79 (s, COD-*C*H$_2$), 22.84 (s, *o*-Mes*C*H$_3$), 22.50 (*o*-Mes*C*H$_3$), 21.76 (s, *p*-Mes*C*H$_3$), 21.26 (s, *p*-Mes*C*H$_3$), 18.32 (d, $^{3}J_{C\text{-}P}$ = 3.8 Hz, PCH(*C*H$_3$)$_2$), 18.03 (s, PCH(*C*H$_3$)$_2$), 16.71 (d, $^{3}J_{C\text{-}P}$, PCH(*C*H$_3$)$_2$), 16.61 (s, PCH(*C*H$_3$)$_2$). $^{31}P\{^{1}H\}$ NMR (121.50 MHz, benzene-d_6): δ 52.0 (s, chelated), –0.9 (s, free). Anal. Cald. (%) for $C_{42}H_{64}IrN_3P_2$: C, 58.31; H, 7.46; N, 4.86. Found: C, 59.19; H, 7.04; N, 5.23.

6.3.1.4 ^{Pipp}LIr(CO)$_2$ (L = 2,5-(^{i}Pr$_2$P=NPipp)$_2$C$_4$H$_2$N) ***(50)***

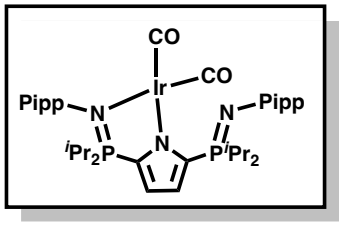

In a J. Young NMR tube, 14.2 mg (1 equiv, 0.024 mmol) of Na^{Pipp}L and 10.8 mg (0.5 equiv, 0.012 mmol) of [IrCl(COE)$_2$]$_2$ were added and dissolved in 0.5 mL of benzene-d_6. The reaction mixture was left for 48 hours, or until ^{1}H and $^{31}P\{^{1}H\}$ NMR spectra indicated completion. The solution was degassed by three freeze-pump-thaw cycles. An atmosphere of CO was added at ambient temperature, and the reaction monitored by ^{1}H and $^{31}P\{^{1}H\}$ NMR spectroscopy. Within 20 minutes the reaction was complete. Excess CO was removed *in vacuo*. The J. Young NMR tube was brought back into a glove box, filtered through Celite, and then added to a 20 mL scintillation vial. The J. Young NMR tube was rinsed once with 2 mL of toluene to ensure quantitative transfer.

Volatiles were removed under vacuum. Pentane (2 mL) was added and removed under vacuum twice to assist in the removal of free COE. A light brown powder was obtained. Yield: 9.5 mg (97.9%). IR: νCO (cm^{-1}) 2048 (s), 1963 (s). ^{1}H NMR (700.13 MHz, benzene-*d*$_6$): δ 7.23 (d, 2H, $^{3}J_{H-H}$ = 8.3 Hz, Pipp-C*H*), 7.17 (ov, 2H, Pipp-C*H*), 7.12 (d, 2H, $^{3}J_{H-H}$ = 7.1 Hz, Pipp-C*H*), 7.04 (d, 2H, $^{3}J_{H-H}$ = 8.3 Hz, Pipp-C*H*), 6.70 (m, 1H, C_4H_2N), 6.41 (dd, 1H, $^{3}J_{H-H}$ = 1.4 Hz, $^{4}J_{H-P}$ = 5.8 Hz, C_4H_2N), 2.92 (sp, 1H, $^{3}J_{H-H}$ = 6.9 Hz, Pipp-C*H*$(CH_3)_2$), 2.71 (sp, 1H, $^{3}J_{H-H}$ = 6.9 Hz, Pipp-C*H*$(CH_3)_2$), 2.57 (m, 2H, PC*H*$(CH_3)_2$), 1.90 (m, 2H, PC*H*$(CH_3)_2$), 1.40 (dd, 6H, $^{3}J_{H-H}$ = 7.2 Hz, $^{3}J_{H-P}$ = 15.3 Hz, PCH(C*H*$_3)_2$), 1.34 (d, 6H, $^{3}J_{H-H}$ = 6.9 Hz, Pipp-CH(C*H*$_3)_2$), 1.16 (dd, 6H, $^{3}J_{H-H}$ = 7.1 Hz, $^{3}J_{H-P}$ = 16.2 Hz, PCH(C*H*$_3)_2$), 1.13 (d, 6H, $^{3}J_{H-H}$ = 6.9 Hz, Pipp-CH(C*H*$_3)_2$), 0.80 (dd, 6H, $^{3}J_{H-H}$ = 7.1 Hz, $^{3}J_{H-P}$ = 16.4 Hz, PCH(C*H*$_3)_2$). ^{13}C{^{1}H} NMR (176.05 MHz, benzene-*d*$_6$): δ 174.26 (s, Ir*C*O), 172.68 (s, Ir*C*O), 152.04 (d, $^{2}J_{C-P}$ = 3.7 Hz, Pipp-*ipso*), 148.57 (s, Pipp-*ipso*), 145.42 (d, $^{2}J_{C-P}$ = 1.6 Hz, Pipp-*ipso*), 137.35 (dd, J_{C-P} = 82.7 Hz, $^{4}J_{C-P}$ = 11.4 Hz, pyrrole-*C*P), 136.31 (s, Pipp-*ipso*), 129.92 (dd, J_{C-P} = 122.8 Hz, $^{4}J_{C-P}$ = 10.9 Hz, pyrrole-*C*P), 127.74 (d, $^{3}J_{C-P}$ = 5.7 Hz, Pipp-*C*H), 127.30 (s, Pipp-*C*H), 126.73 (s, Pipp-*C*H), 125.30 (d, $^{3}J_{C-P}$ = 16.0 Hz, Pipp-*C*H), 120.92 (m, pyrrole-*C*H), 117.28 (dd, $^{2}J_{C-P}$ = 22.9 Hz, $^{3}J_{C-P}$ = 8.3 Hz, pyrrole-*C*H), 34.30 (s, Pipp-*C*H$(CH_3)_2$), 34.06 (s, Pipp-*C*H$(CH_3)_2$), 29.70 (d, J_{C-P} = 74.2 Hz, P*C*H$(CH_3)_2$), 26.72 (d, J_{C-P} = 53.7 Hz, P*C*H$(CH_3)_2$), 25.23 (s, Pipp-CH(*C*H$_3)_2$), 24.56 (s, Pipp-CH(*C*H$_3)_2$), 18.52 (d, $^{2}J_{C-P}$ = 3.5 Hz, PCH(*C*H$_3)_2$), 17.02 (s, PCH(*C*H$_3)_2$), 16.15 (d, $^{2}J_{C-P}$ = 3.0 Hz, PCH(*C*H$_3)_2$), 15.86 (d, $^{2}J_{C-P}$ = 1.7 Hz, PCH(*C*H$_3)_2$). ^{31}P{^{1}H} NMR (283.42 MHz, benzene-*d*$_6$): δ 58.3 (s, chelated), 10.2 (s, free). Anal. Cald. (%) for $C_{38}H_{52}IrN_3O_2P_2$: C, 53.19; H, 6.85; N, 5.17. Found: C, 52.93; H, 6.42; N, 5.19.

6.3.1.5 ^{Mes}LIr(CO)$_2$ (L = 2,5-(^{i}Pr$_2$P=NMes)$_2$C$_4$H$_2$N) ***(51)***

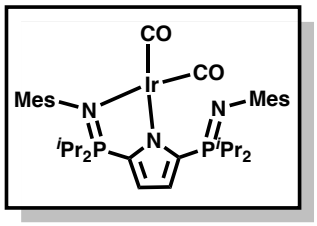

In a J. Young NMR tube, 10.7 mg (0.012 mmol) of ^{Mes}LIr(COD) was weighed and dissolved in 0.5 mL of benzene-*d*$_6$. The solution was degassed three times by freeze-pump-thaw cycles before an atmosphere CO was added at ambient temperature. There were no observable changes. The reaction was monitored *via* ^{1}H and ^{31}P{^{1}H} NMR spectroscopy. After 24 hours, the reaction mixture had become pale yellow in colour and the ^{1}H and ^{31}P{^{1}H} NMR spectra indicated completion. The J. Young NMR tube was briefly evacuated to remove excess CO then brought back into a glove box whereby the product was transferred to a 20 mL scintillation vial. The J. Young NMR tube was rinsed with 2 mL of toluene for quantitative transfer and volatiles removed under vacuum. Pentane (4 mL) was added to the vial and removed under vacuum. This process was repeated three times to assist in the removal of free COD, leaving an off-white powder. Yield: 9.8 mg (97.0%). IR: νCO (cm^{-1}) 2030 (s), 1950 (s). ^{1}H NMR (700.13 MHz, benzene-*d*$_6$): δ 7.04 (s, 2H, Mes-C*H*), 6.79 (s, 2H, Mes-C*H*), 6.63 (m, 1H, C$_4$*H*$_2$N), 6.28 (s, 1H, C$_4$*H*$_2$N), 2.79 (sp, 2H, 7.0 Hz, PC*H*(CH$_3$)$_2$), 2.55 (s, 6H, *o*-Mes-C*H*$_3$), 2.47 (s, 6H, *o*-Mes-C*H*$_3$), 2.35 (s, 3H, *p*-Mes-C*H*$_3$), 2.14 (s, 3H, *p*-Mes-C*H*$_3$), 1.99 (m, 2H, PC*H*(CH$_3$)$_2$), 1.31 (dd, 6H, $^3J_{H\text{-}H}$ = 7.2 Hz, $^3J_{H\text{-}P}$ = 15.7 Hz, PCH(C*H*$_3$)$_2$), 1.22 (dd, 6H, $^3J_{H\text{-}H}$ = 7.1 Hz, $^3J_{H\text{-}P}$ = 16.1 Hz, PCH(C*H*$_3$)$_2$), 0.94 (dd, 6H, $^3J_{H\text{-}H}$ = 7.1 Hz, $^3J_{H\text{-}P}$ = 15.8 Hz, PCH(C*H*$_3$)$_2$), 0.64 (dd, 6H, $^3J_{H\text{-}H}$ = 7.0 Hz, $^3J_{H\text{-}P}$ = 16.9 Hz, PCH(C*H*$_3$)$_2$). ^{13}C{^{1}H} NMR (176.05 MHz, benzene-*d*$_6$): δ 173.86 (s, Ir*C*O), 170.93 (s, Ir*C*O), 146.84 (s, Mes-*ipso*), 144.87 (d, $^3J_{C\text{-}P}$ = 2.0 Hz, Mes-*ipso*), 139.46 (dd, $J_{C\text{-}P}$ = 97.0 Hz, $^4J_{C\text{-}P}$ = 11.0 Hz, pyrrole-*C*P), 135.78 (d, $^2J_{C\text{-}P}$ = 4.1 Hz, Mes-*ipso*), 134.35 (d, $^3J_{C\text{-}P}$ = 2.5 Hz, Mes-*ipso*), 131.85 (d, $^2J_{C\text{-}P}$ = 7.0 Hz, Mes-*ipso*),

130.12 (d, $^{4}J_{C\text{-}P}$ = 1.8 Hz, Mes-*C*H), 129.50 (s, Mes-*C*H), 127.87 (ov dd, $J_{C\text{-}P}$ = 55.2 Hz, $^{4}J_{C\text{-}P}$ = 11.5 Hz, pyrrole-*C*P), 126.17 (d, $^{3}J_{C\text{-}P}$ = 1.9 Hz, Mes-*ipso*), 118.81 (dd, $^{2}J_{C\text{-}P}$ = 17.9 Hz, $^{3}J_{C\text{-}P}$ = 11.4 Hz, pyrrole-*C*H), 115.81 (dd, $^{2}J_{C\text{-}P}$ = 22.1 Hz, $^{3}J_{C\text{-}P}$ = 9.2 Hz, pyrrole-*C*H), 29.67 (d, $J_{C\text{-}P}$ = 70.0 Hz, P*C*H(CH$_3$)$_2$), 26.58 (d, $J_{C\text{-}P}$ = 55.0 Hz, P*C*H(CH$_3$)$_2$), 22.54 (s, Mes-*o*-*C*H$_3$), 21.83 (s, Mes-*o*-*C*H$_3$), 21.39 (s, Mes-*p*-*C*H$_3$), 21.11 (s, Mes-*p*-*C*H$_3$), 17.77 (d, $^{2}J_{C\text{-}P}$ = 2.4 Hz, PCH(*C*H$_3$)$_2$), 17.36 (s, PCH(*C*H$_3$)$_2$), 16.56 (d, $^{2}J_{C\text{-}P}$ = 3.0 Hz, PCH(*C*H$_3$)$_2$), 16.32 (d, $^{2}J_{C\text{-}P}$ = 1.6 Hz, PCH(*C*H$_3$)$_2$). ^{31}P{^{1}H} NMR (283.42 MHz, benzene-d_6): δ 53.7 (s, chelated), –2.0 (s, free). *Despite exhaustive efforts, all attempts at elemental analysis provided low carbon percentages. The best values are provided here*. Anal. Cald. (%) for $C_{36}H_{52}IrN_3O_2P_2$: C, 53.19; H, 6.95; N, 5.17. Found: C, 51.50; H, 6.35; N, 5.38.

6.3.2 Compounds from Chapter 3

6.3.2.1 ^{Pipp}LIr(COE) (L = 2,5-(^{i}Pr$_2$P=NPipp)$_2$C$_4$H$_2$N) ***(52)***

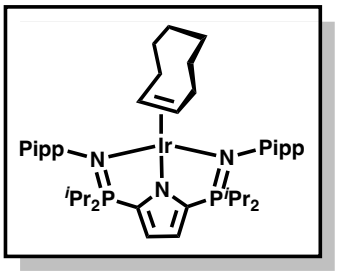

In a 20 mL scintillation vial, 56.9 mg of Na^{Pipp}L (1 equiv, 0.097 mmol) and 43.4 mg of [IrCl(COE)$_2$] (0.5 equiv, 0.048 mmol) were combined, then dissolved in 5 mL of toluene. Upon stirring, the initial yellow-orange solution turned reddish-brown in five minutes. The reaction mixture was allowed to stir for 48 hours at ambient temperature. Toluene was removed *in vacuo* and 5 mL of pentane was added to the reddish-brown oil then removed under vacuum. The addition and removal of pentane was repeated an additional four times to assist in the removal of free COE. A reddish-brown

powder was isolated. This material was only ~65-70% the desired complex. The product is not vacuum stable. The NMR data provided only include the major product. Further reaction chemistry required the complex to be made *in situ*, yielding ~85 – 90% purity. *Because the complex is not vacuum stable, an isolated yield nor elemental analysis data could not be acquired.* ^{1}H NMR (700.13 MHz, benzene-d_6): δ 7.33 (d, 4H, $^{3}J_{H\text{-}H}$ = 7.7 Hz, Pipp-C*H*), 6.98 (d, 4H, $^{3}J_{H\text{-}H}$ = 7.7 Hz, Pipp-C*H*), 6.65 (s, 2H, C_4H_2N), 3.16 (m, 2H, *H*C=C*H*), 2.70 (sp, 2H, $^{3}J_{H\text{-}H}$ = 6.8 Hz, Pipp-C*H*$(CH_3)_2$), 2.24 (m, 2H, COE-CH_2), 2.11 (m, 4H, PC*H*$(CH_3)_2$), 1.68 (ov m, COE-CH_2), 1.30 (ov m, COE-CH_2), 1.15 (d, 2H, $^{3}J_{H\text{-}H}$ = 6.9 Hz, Pipp-CH(C$H_3)_2$), 1.00 (ov dd, 24H, PCH(C$H_3)_2$). ^{13}C{^{1}H} NMR (176.05 MHz, benzene-d_6): δ 148.40 (s, Pipp-*ipso*), 143.35 (s, Pipp-*ipso*), 133.11 (dd, $J_{C\text{-}P}$ = 140.8 Hz, $^{4}J_{C\text{-}P}$ = 10.6 Hz, pyrrole-*C*P), 131.39 (m, *o*-*C*H Pipp), 126.00 (s, *m*-*C*H Pipp), 115.15 (m, pyrrole-*C*H), 45.69 (s, H*C*=*C*H), 34.28 (s, Pipp-*C*H$(CH_3)_2$), 31.85 (s, COE-*C*H_2), 30.42 (s, COE-*C*H_2), 27.75 (s, COE-*C*H_2), 27.43 (s, P*C*H$(CH_3)_2$) 24.65 (s, Pipp-CH(*C*$H_3)_2$), 16.81 (s, PCH(*C*$H_3)_2$), 16.4 (s, PCH(*C*$H_3)_2$). ^{31}P{^{1}H} NMR (283.42 MHz, benzene-d_6): δ 56.1 (s).

6.3.2.2 ^{Pipp}LIr(H)$_2$ (L = 2,5-(^{i}Pr$_2$P=NPipp)$_2$C$_4$H$_2$N) ***(53)***

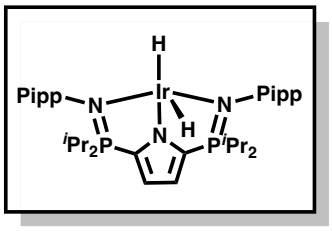

In a J. Young NMR tube, 18.3 mg (1 equiv, 0.031 mmol) of Na^{Pipp}L and 13.9 mg (0.5 equiv, 0.016 mmol) of [IrCl(COE)$_2$]$_2$ were added and dissolved in 0.5 mL of toluene-d_8. The mixture was allowed to react for 48 hours at ambient temperature, or until ^{1}H and ^{31}P{^{1}H} NMR spectra indicated complete consumption of the starting

materials. Once the reaction was complete, the solution was degassed by three freeze-pump-thaw cycles. An atmosphere of H_2 was added at –52.5 °C and immediately injected into a pre-cooled NMR spectrometer set to –30 °C. The mixture was transported in a Dewar filled with cooled acetone (approximately –50 °C) to ensure the mixture did not warm above this temperature. The relative integrations in the $^{31}P\{^1H\}$ NMR spectrum indicated only 62% of the mixture had converted to the desired compound, but no free H_2 was observed at δ 4.46 in the ^1H NMR spectrum. Another 5 additions of H_2 were required to convert all of the starting material to the desired compound. The compound is not stable above –30 °C and hydrogenates free cyclooctene in solution at this temperature. *Because the complex cannot be isolated as a solid, an isolated yield nor elemental analysis could not be acquired.* ^1H NMR (300.13 MHz, –30 °C, toluene-d_8): δ 7.60 (d, 4H, $^3J_{H\text{-}H}$ = 7.1 Hz, Pipp-C*H*), 6.96 (d, 4H, $^3J_{H\text{-}H}$ = 8.1 Hz, Pipp-C*H*), 6.77 (m, 2H, C_4H_2N), 4.10 (br, 2H, H_2), 2.85 (ov m, 4H, PC*H*$(CH_3)_2$), 2.71 (ov sp, 2H, $^3J_{H\text{-}H}$ = 6.8 Hz, Pipp-C*H*$(CH_3)_2$), 1.55 (s, 16H, COA), 1.31 (ov m, PCH(C*H*$)_3)_2$, 1.19 (d, 12H, $^3J_{H\text{-}H}$ = 6.8 Hz, Pipp-CH(C*H*$_3)_2$), 0.96 (br m, PCH(C*H*$_3)_2$), 0.59 (br m, PCH(C*H*$_3)_2$), –6.90 (br s, 1H, Ir*H*), –14.62 (br s, 1H, Ir*H*). $^{13}C\{^1H\}$ NMR (75.47 MHz, –30 °C, toluene-d_8): δ 151.42 (s, Pipp-*ipso*), 141.50 (s, Pipp-*ipso*), 128.30 (ov, Pipp-*C*H), 125.18 (ov, Pipp-C*H*), 118.31 (m, pyrrole-C*H*), 33.60 (s, Pipp-*C*H$(CH_3)_2$), 32.05 (br s, P*C*H$(CH_3)_2$), 26.70 (s, COA), 24.35 (s, Pipp-CH(*C*H$_3)_2$), 16.78 (br s, PCH(*C*H$_3)_2$), 16.42 (br s, PCH(*C*H$_3)_2$). *The ipso carbon atoms of pyrrole were not observed.* $^{31}P\{^1H\}$ NMR (121.50 MHz, –30 °C, toluene-d_8): δ 60.2 (s)

6.3.2.3 ^{Pipp}LIr(H)SiPhH$_2$ (L = 2,5-(^{i}Pr$_2$P=NPipp)$_2$C$_4$H$_2$N) ***(55)***

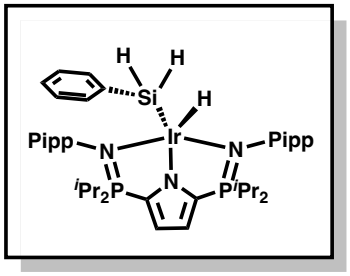

In a J. Young NMR tube, 20.5 mg (1 equiv, 0.035 mmol) of Na^{Pipp}L and 16.4 mg (0.5 equiv, 0.018 mmol) of [IrCl(COE)$_2$]$_2$ were combined and dissolved in 0.5 mL of benzene-d_6. The reaction mixture was left to react for 48 hours, and until ^{1}H and ^{31}P{^{1}H} NMR spectra indicated all starting materials had been consumed. Once the reaction was complete, 2.1 µL (1 equiv relative to ^{Pipp}LIr(COE), 0.017 mmol) of phenylsilane was added to the dark reddish-brown solution. The red colour intensified. After ^{1}H and ^{31}P{^{1}H} NMR spectroscopy indicated complete consumption of starting materials (one hour), the J. Young NMR tube was brought into a glove box. The mixture was filtered through Celite into a 20 mL scintillation vial, and volatiles removed under vacuum. Pentane (4 mL) was added to the red residue and removed *in vacuo*. The addition and removal of pentane was repeated an additional two times to assist in the removal of free COE. A red powder was obtained. Yield: 14.9 mg (98.7%). ^{1}H NMR (700.13 MHz, benzene-d_6): δ 7.65 (d, 2H, $^3J_{H\text{-}H}$ = 6.72 Hz, *o*-SiPh), 7.37 (d, 4H, $^3J_{H\text{-}H}$ = 7.8 Hz, Pipp-C*H*), 7.07 (d, 2H, $^3J_{H\text{-}H}$ = 7.1 Hz, *m*-SiPh), 7.04 (t, 1H, $^3J_{H\text{-}H}$ = 7.1 Hz, *p*-SiPh), 6.90 (d, 4H, $^3J_{H\text{-}H}$ = 8.1 Hz, Pipp-C*H*), 6.56 (br dd, 2H, C$_4$*H*$_2$N), 4.96 (s, 2H, Si*H*), 2.71 (sp, 2H, $^3J_{H\text{-}H}$ = 6.9 Hz, Pipp-C*H*(CH$_3$)$_2$), 2.06 (m, 2H, PC*H*(CH$_3$)$_2$), 1.89 (m, 2H, PC*H*(CH$_3$)$_2$), 1.31 (dd, 6H, $^3J_{H\text{-}H}$ = 7.1 Hz, $^3J_{H\text{-}P}$ = 16.0 Hz, PCH(C*H*$_3$)), 1.18 (d, 6H, $^3J_{H\text{-}H}$ = 3.78 Hz, Pipp-CH(C*H*$_3$)$_2$), 1.17 (d, 6H, $^3J_{H\text{-}H}$ = 3.78 Hz, Pipp-CH(C*H*$_3$)$_2$), 0.92 (m, 12H, PCH(C*H*$_3$)$_2$), 0.58 (dd, $^3J_{H\text{-}H}$ = 7.2 Hz, $^3J_{H\text{-}P}$ = 15.4 Hz, PCH(C*H*$_3$)), –16.16 (br t, 1H, $^3J_{H\text{-}H}$ = 2.8 Hz, Ir*H*). ^{13}C{^{1}H} NMR (176.05 MHz, benzene-d_6): δ 151.39 (s, Pipp-*ipso*), 143.59 (d, $J_{C\text{-}Si}$ = 3.52, SiPh-*ipso*), 142.87 (s, Pipp-*ipso*), 135.76 (s, SiPh-*o*-*C*H), 133.18 (dd, $J_{C\text{-}P}$

= 140.8 Hz, $^{4}J_{C\text{-}P}$ = 10.6 Hz, pyrrole-*C*P), 128.68 (s, *o*-*C*H Pipp), 127.04 (s, SiPh-*p*-*C*H), 126.92 (s, SiPh-*m*-*C*H), 126.14 (s, Pipp-*C*H), 116.71 (m, pyrrole-*C*H), 34.09 (s, Pipp-*C*H(CH_3)$_2$), 29.83 (d, $J_{C\text{-}P}$ = 52.8 Hz, P*C*H(CH_3)$_2$), 26.72 (d, $J_{C\text{-}P}$ = 54.6 Hz, P*C*H(CH_3)$_2$), 24.78 (ov s, Pipp-CH(*C*H_3)$_2$), 16.97 (s, PCH(*C*H_3)$_2$), 16.38 (s, PCH(*C*H_3)$_2$), 16.19 (s, PCH(*C*H_3)$_2$). ^{29}Si NMR (59.63 MHz, benzene-d_6): δ –42.9 (tt, $J_{Si\text{-}H}$ = 175.9 Hz, $^{3}J_{Si\text{-}H}$ = 6.0 Hz, *Si*PhH_2). ^{31}P{^{1}H} NMR (283.42 MHz, benzene-d_6): δ 62.6 (s). *Despite exhaustive efforts, all attempts at elemental analysis provided low carbon percentages. The best values are provided here*. Anal. Cald. (%) for $C_{40}H_{60}IrN_3P_2Si$: C, 55.58; H, 6.99; N, 4.86. Found: C, 53.68; H, 6.69; N, 4.52.

6.3.2.4 ^{Pipp}LIr(H)SiPh$_2$H (L = 2,5-(^{i}Pr$_2$P=NPipp)$_2$C$_4$H$_2$N) ***(56)***

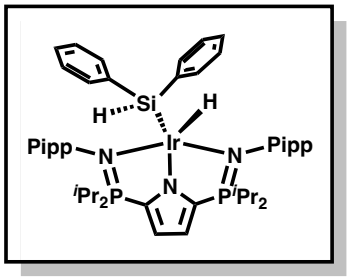

In a J. Young NMR tube, 12.2 mg (1 equiv, 0.021 mmol) of Na^{Pipp}L and 10.2 mg (0.5 equiv, 0.012 mmol) of [IrCl(COE)$_2$]$_2$ were added. The reagents were dissolved in 0.5 mL of benzene-d_6 and left to react for 48 hours, or until ^{1}H and ^{31}P{^{1}H} NMR spectra indicated all starting materials had been consumed. Once the reaction was complete, 1.9 µL (1 equiv relative to ^{Pipp}LIr(COE), 0.010 mmol) of diphenylsilane was added to the dark reddish-brown solution. The red colour intensified. After ^{1}H and ^{31}P{^{1}H} NMR spectroscopy indicated complete consumption of starting materials (one hour), the J. NMR Young tube was brought into a glove box. The mixture was filtered through Celite into a 20 mL scintillation vial, and volatiles removed under vacuum. Pentane (4 mL) was added to the red residue and removed *in vacuo*. The addition

and removal of pentane was repeated an additional two times to assist in the removal of free COE. A pale red powder was acquired. Yield: 9.8 mg (91.6%). ^{1}H NMR (700.13 MHz, benzene-d_6): δ 7.72 (d, 4H, $^{3}J_{H\text{-}H}$ = 6.7 Hz, *o*-SiPh), 7.18 (d, 4H, $^{3}J_{H\text{-}H}$ = 7.8 Hz, Pipp-C*H*), 7.01 (m, 2H, *p*-SiPh), 6.98 (t, 4H, $^{3}J_{H\text{-}H}$ = 6.9 Hz, *m*-SiPh), 6.78 (d, 4H, $^{3}J_{H\text{-}H}$ = 8.3 Hz, Pipp-C*H*), 6.56 (br, 2H, C_4H_2N), 5.16 (d, 1H, $^{4}J_{H\text{-}H}$ = 2.6 Hz, Si*H*), 2.73, (sp, 2H, $^{3}J_{H\text{-}H}$ = 6.9 Hz, Pipp-C*H*$(CH_3)_2$), 1.90 (m, 4H, PC*H*$(CH_3)_2$), 1.23 (d, 12H, $^{3}J_{H\text{-}H}$ = 6.9 Hz, Pipp-CH(C*H*$_3)_2$), 1.20 (ov dd, 6H, PCH(C*H*$_3)_2$), 0.95 (dd, 6H, $^{3}J_{H\text{-}H}$ = 6.9 Hz, $^{3}J_{H\text{-}P}$ = 17.3 Hz, PCH(C*H*$_3)_2$), 0.85 (dd, 6H, $^{3}J_{H\text{-}H}$ = 7.0 Hz, $^{3}J_{H\text{-}P}$ = 16.0 Hz, PCH(C*H*$_3)_2$), 0.52 (dd, 6H, $^{3}J_{H\text{-}H}$ = 7.1 Hz, $^{3}J_{H\text{-}P}$ = 12.3 Hz, PCH(C*H*$_3)_2$), –15.37 (br, 1H, Ir*H*). ^{13}C{^{1}H} NMR (176.05 MHz, benzene-d_6): δ 151.21 (s, Pipp-*ipso*), 145.85 (s, SiPh-*ipso*), 142.56 (s, Pipp-*ipso*), 135.40 (s, SiPh-*o*-*C*H), 133.25 (dd, $J_{C\text{-}P}$ = 139.1 Hz, $^{4}J_{C\text{-}P}$ = 10.6 Hz, pyrrole-*C*P), 128.68 (s, Pipp-*C*H), 127.07 (s, SiPh *m*-*C*H), 126.67 (s, SiPh *p*-*C*H), 125.89 (s, Pipp-*C*H), 116.85 (m, pyrrole *C*H), 34.14 (s, Pipp-*C*H$(CH_3)_2$), 30.02 (d, $J_{C\text{-}P}$ = 52.8 Hz, P*C*H$(CH_3)_2$), 26.73 (d, $J_{C\text{-}P}$ = 54.6 Hz, P*C*H$(CH_3)_2$), 24.93 (s, Pipp-CH(*C*H$_3)_2$), 24.88 (s, Pipp-CH(*C*H$_3)_2$), 16.96 (s, PCH(*C*H$_3)_2$), 16.57 (s, PCH(*C*H$_3)_2$), 16.39 (s, PCH(*C*H$_3)_2$), 16.06 (s, PCH(*C*H$_3)_2$). ^{29}Si NMR (59.63 MHz, benzene-d_6): δ –10.3 (d, $J_{Si\text{-}H}$ = 176.9 Hz, *Si*Ph_2H). ^{31}P{^{1}H} NMR (283.42 MHz, benzene-d_6): δ 63.1 (s). *Despite exhaustive efforts, all attempts at elemental analysis provided low carbon percentages. The best values are provided here*. Anal. Cald. (%) for $C_{46}H_{64}IrN_3P_2Si$: C, 58.70; H, 6.85; N, 4.46. Found: C, 53.68; H, 6.13; N, 4.39.

6.3.2.5 ^{Pipp}LIr(H)SiEt$_3$ (L = 2,5-(^{i}Pr$_2$P=NPipp)$_2$C$_4$H$_2$N) ***(57)***

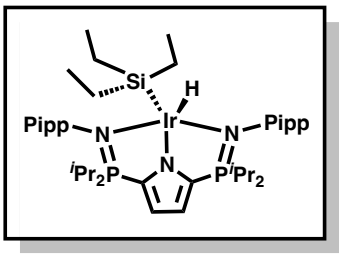

To a 20 mL scintillation vial, 15.1 mg (1 equiv, 0.026 mmol) of Na^{Pipp}L and 11.5 mg (0.5 equiv, 0.013 mmol) of [IrCl(COE)$_2$]$_2$ were added. The reagents were dissolved in ~4 mL of toluene and left to react for 48 hours with stirring. After 48 hours, 2.1 µL (1 equiv relative to ^{Pipp}LIr(COE), 0.012 mmol) of triethylsilane was added to the dark reddish-brown solution. The red colour had intensified after 16 hours of stirring with triethylsilane. Volatiles were removed under vacuum. The product was reconstituted in pentane and stored at –30 °C. Large, bright red block crystals precipitated from solution within two days. Yield: 6.4 mg (57.7%). ^{1}H NMR (700.13 MHz, benzene-d_6): δ 7.67 (d, 4H, $^3J_{H\text{-}H}$ = 7.0 Hz, Pipp-C*H*), 7.00 (d, 4H, $^3J_{H\text{-}H}$ = 7.7 Hz, Pipp-C*H*), 6.57 (br, 2H, C$_4$*H*$_2$N), 2.74 (sp, 2H, $^3J_{H\text{-}H}$ = 7.0 Hz, Pipp-C*H*(CH$_3$)$_2$), 2.23 (m, 2H, PC*H*(CH$_3$)$_2$), 1.83 (m, 2H, PC*H*(CH$_3$)$_2$), 1.35 (dd, 6H, $^3J_{H\text{-}H}$ = 7.0 Hz, $^3J_{H\text{-}P}$ = 14.0 Hz, PCH(C*H*$_3$)$_2$), 1.19 (m, 12H, Pipp-CH(C*H*$_3$)$_2$), 1.15 (t, 9H, $^3J_{H\text{-}H}$ = 7.7 Hz, SiCH$_2$C*H*$_3$), 0.95 (ov dd, 12H, PCH(C*H*$_3$)$_2$), 0.80 (q, 6H, $^3J_{H\text{-}H}$ = 7.7 Hz, SiC*H*$_2$CH$_3$), 0.54 (dd, 6H, $^3J_{H\text{-}H}$ = 7.7 Hz, 15.4 Hz, PCH(C*H*$_3$)$_2$), –16.79 (s, Ir*H*). ^{13}C{^{1}H} NMR (176.05 MHz, benzene-d_6): δ 152.95 (s, Pipp-*ipso*), 143.14 (s, Pipp-*ipso*), 133.90 (dd, $J_{C\text{-}P}$ = 35.2 Hz, $^4J_{C\text{-}P}$ = 0.6 Hz, pyrrole-*C*P), 128.68 (s, Pipp-*C*H), 125.99 (s, Pipp-*C*H), 117.43 (m, pyrrole-*C*H), 34.14 (s, Pipp-*C*H(CH$_3$)$_2$), 29.05 (d, $J_{C\text{-}P}$ = 17.61 Hz, P*C*H(CH$_3$)$_2$), 28.75 (d, $J_{C\text{-}P}$ = 15.8 Hz, P*C*H(CH$_3$)$_2$), 24.83 (s, Pipp-CH(*C*H$_3$)$_2$), 24.73 (s, Pipp-CH(*C*H$_3$)$_2$), 17.14 (s, PCH(*C*H$_3$)$_2$), 16.51 (s, PCH(*C*H$_3$)$_2$), 16.32 (s, PCH(*C*H$_3$)$_2$), 15.84 (s, PCH(*C*H$_3$)$_2$), 10.03 (s, Si*C*H$_2$*C*H$_3$). ^{29}Si NMR (59.63 MHz, benzene-d_6): δ 9.0 (s). ^{31}P{^{1}H} NMR (283.42 MHz, benzene-d_6): δ 60.0 (s). Anal. Cald. (%) for C$_{40}$H$_{68}$IrN$_3$P$_2$: C, 55.02; H, 7.85; N, 4.81. Found: C, 54.63; H, 8.04; N, 4.89.

6.3.2.6 $[Li]^+[(COD)Ir(Me)_2]^-$ ***(60)***

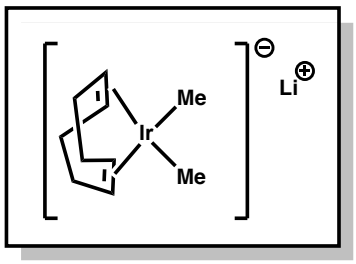

In a glove box, 93.6 mg of $[IrCl(COD)]_2$ (1 equiv, 0.14 mmol) was added to a 2-neck RBF then attached to a double-manifold vacuum line. Diethylether (50 mL) was vacuum transferred to the vessel containing $[IrCl(COD)]_2$ at –94 °C. The solution was warmed to ambient temperature to ensure all of $[IrCl(COD)]_2$ was dissolved. The solution was then cooled to –94 °C, and methyllithium (4 equiv, 0.56 mmol, 0.35 mL of 1.6 M in diethylether) was added dropwise over 30 seconds, causing the solution to change from dark orange to deep red. The reaction mixture was allowed to stir at –94 °C for one hour by which time the colour had changed to bright orange. While cold (best results are achieved around –50 °C), diethylether was removed *in vacuo*, affording a bright orange residue which was brought into a glove box. The residue was dissolved in ~10 mL of toluene, filtered through Celite, and stored at –30 °C. Bright orange crystals precipitated from solution within 16 hours. Yield: A total of 20.2 mg was obtained from two successive recrystallizations (43.9%). ^{1}H NMR (700.13 MHz, benzene-d_6): δ 3.06 (br, 4H, *H*C=C*H*), 2.06 (m, 4H, COD-CH_2), 1.52 (m, 4H, COD-CH_2), 0.77 (s, 6H, Ir-CH_3). ^{7}Li{^{1}H} (272.097 MHz, benzene-d_6): δ 0.1 (s). ^{13}C{^{1}H} NMR (176.05 MHz, benzene-d_6): δ 68.15 (br s, H*C*=*C*H), 32.12 (s, COD-*C*H_2), 11.51 (s, Ir-*C*H_3). Anal. Cald. (%) for $C_{20}H_{36}Li_2Ir_2$: C, 35.60; H, 5.38. Found: C, 36.05; H, 5.39.

6.3.2.7 [(12-crown-4)$_2$Li]$^+$[(COD)Ir(Me)$_2$]$^-$ ***(62)***

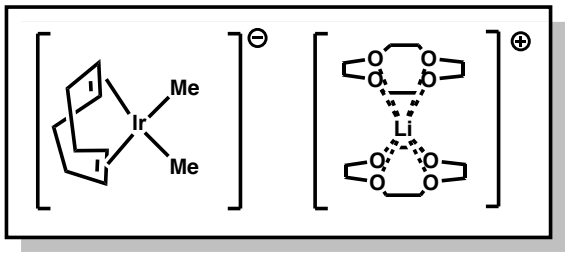

In a 20 mL scintillation vial, 10.1 mg (1 equiv, 0.030 mmol) of [Li]$^+$[(COD)Ir(Me)$_2$]$^-$ was added and dissolved in ~2 mL of toluene. *Via* microsyringe, 4.8 µL (1 equiv, 0.030 mmol) of 12-crown-4 was added to the solution. The vial was shaken, causing immediate precipitation of orange-red crystals. The remaining solution was orange-brown in colour. The mixture was left to stand for 15 minutes. The solution was then decanted from the crystals and residual solvent removed under vacuum. Although one equivalent of 12-crown-4 was used, the ^{1}H NMR spectrum indicated that there were two 12-crown-4 molecules per lithium. Yield: 9.6 mg (46.6%). ^{1}H NMR (300.13 MHz, *d*$_8$-THF): δ 3.74 (s, 32H, crown ether), 2.80 (m, 4H, *H*C=C*H*), 1.87 (m, 4H, COD-C*H*$_2$), 1.32 (m, 4H, COD-C*H*$_2$), 0.25 (s, 6H, Ir–C*H*$_3$). ^{7}Li{^{1}H} (272.097 MHz, benzene-*d*$_6$): δ –1.6 (br s). ^{13}C{^{1}H} NMR (176.05 MHz, benzene-*d*$_6$): δ 69.92 (s, crown ether), 58.42 (s, H*C*=*C*H), 33.85 (s, COD-*C*H$_2$), 13.92 (s, Ir–*C*H$_3$).

6.3.2.8 (COD)Ir(Me)(C$_3$H$_4$(NMes)$_2$) ***(64)***

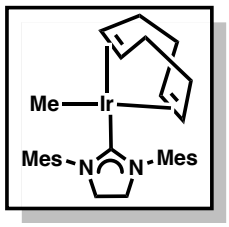

In a 4 mL vial, 14.9 mg (1 equiv, 0.044 mmol) of [Li]$^+$[(COD)Ir(Me)$_2$]$^-$ and 15.0 mg (1 equiv, 0.044 mmol) of [C$_3$H$_5$(NMes)$_2$]$^+$[Cl]$^-$ were weighed and ~2 mL of THF was added. The solution bubbled vigorously and immediately turned bright red in colour. The solution

was allowed to stand for 30 minutes before the THF was removed under vacuum. The solid was then dissolved in ~2 mL of toluene, filtered through Celite, and the toluene removed *in vacuo* leaving an oily red solid. The solid was triturated once with pentane and volatiles removed under vacuum, yielding a dark red powder. X-ray quality crystals grew from the pentane solution at –30 °C after 3 days. Yield of red powder: 24.1 mg (88.0%). ^{1}H NMR (700.13 MHz, d_8-THF): δ 6.89 (s, 2H, Mes-C*H*), 6.87 (s, 2H, Mes-C*H*), 3.87 (m, 4H, NHC-CH_2), 3.28 (m, 2H, *H*C=C*H*), 2.99 (m, 2H, *H*C=C*H*), 2.38 (s, 6H, *ortho*-MesCH_3), 2.36 (s, 6H, *ortho*-MesCH_3), 2.26 (s, 6H, *para*-MesCH_3), 1.51 (m, 4H, COD-CH_2), 1.29 (m, 4H, COD-CH_2), 0.15 (s, 3H, Ir-CH_3).). ^{13}C{^{1}H} NMR (176.05 MHz, THF-d_8): δ 216.06 (s, carbene), 138.76 (s, Mes-*ipso*), 137.79 (s, Mes-*ipso*), 137.69 (s, Mes-*ipso*), 136.88 (s, Mes-*ipso*), 129.93 (s, Mes-*C*H), 129.37 (s, Mes-*C*H), 74.83 (s, H*C*=*C*H), 62.90 (s, H*C*=*C*H), 52.79 (s, NHC-*C*H$_2$), 33.19 (s, COD-*C*H$_2$), 31.39 (s, COD-*C*H$_2$), 21.24 (s, *para*-Mes*C*H$_3$), 19.78 (s, *ortho*-Mes*C*H$_3$), 19.12 (s, *ortho*-Mes*C*H$_3$), 8.53 (s, Ir–*C*H$_3$). Anal. Cald. (%) for $C_{30}H_{41}IrN_2$: C, 57.94; H, 6.65; N, 4.50. Found: C, 58.49; H, 6.94; N, 4.65.

6.3.3 Compounds from Chapter 4

6.3.3.1 ^{Pipp}LIr(SiH$_2$Ph)$_2$ (L = 2,5-(^{i}Pr$_2$P=NPipp)$_2$C$_4$H$_2$N) ***(69)***

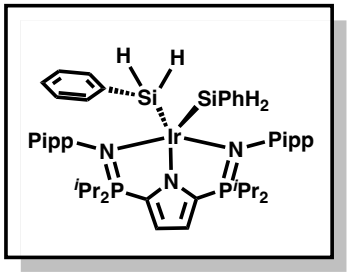

^{Pipp}LIr(H)(SiH$_2$Ph) (3.5 mg, 1 equiv, 0.0041 mmol) was dissolved in 0.5 mL of benzene-d_6 in an NMR tube, giving an orange solution. With a microsyringe, 5.0 µL (10 equiv, 0.041 mmol) of phenylsilane was added with no observable

changes. The reaction was monitored by ^{1}H and ^{31}P{^{1}H} NMR spectroscopy. After 16 h, the NMR spectra indicated complete consumption of the starting materials. The reaction was transferred into a 20 mL scintillation vial. The volatiles were then removed *in vacuo*, leaving an orange oil. Yield: 3.5 mg (89.7%). ^{1}H NMR (700.13 MHz, benzene-d_6): δ 8.23 (d, 4H, $^{3}J_{H\text{-}H}$ = 6.8 Hz, Si-*o*-Ph), 7.36 (m, 4H, Si-*m*-Ph), 7.27 (t, 2H, $^{3}J_{H\text{-}H}$ = 7.2 Hz, Si-*p*-Ph), 7.00 (d, 4H, $^{3}J_{H\text{-}H}$ = 7.4 Hz, Pipp-C*H*), 6.89 (d, 4H, $^{3}J_{H\text{-}H}$ = 8.1 Hz, Pipp-C*H*), 6.61 (s, 2H, C_4H_2N), 3.87 (s, 4H, SiH_2), 2.66 (sp, 2H, $^{3}J_{H\text{-}H}$ = 6.7 Hz, Pipp-C*H*$(CH_3)_2$), 1.93 (m, 4H, PC*H*$(CH_3)_2$), 1.09 (d, 12H, $^{3}J_{H\text{-}H}$ = 6.9 Hz, PippCH(C*H*$_3)_2$), 0.85 (dd, 6H, $^{3}J_{H\text{-}H}$ = 7.0 Hz, $^{3}J_{H\text{-}P}$ = 16.6 Hz, PCH(C*H*$_3)_2$), 0.76 (dd, 6H, $^{3}J_{H\text{-}H}$ = 7.1 Hz, $^{3}J_{H\text{-}P}$ = 15.8 Hz, PCH(C*H*$_3)_2$). ^{13}C{^{1}H} NMR (176.05 MHz, benzene-d_6): δ 146.01 (s, Pipp-*ipso*), 144.13 (s, Pipp-*ipso*), 142.60 (s, SiPh-*ipso*), 137.93 (s, SiPh-*ortho*), 131.52 (dd, $^{4}J_{C\text{-}P}$ = 11.1 Hz, $J_{C\text{-}P}$ = 137.0 Hz, pyrrole-*C*P), 130.59 (m, Pipp-*C*H), 127.45 (s, SiPh-*para*), 127.33 (s, SiPh-*meta*), 126.08 (s, Pipp-*C*H), 116.80 (m, pyrrole-*C*H), 34.09 (s, Pipp-*C*H$(CH_3)_2$), 26.73 (d, $J_{C\text{-}P}$ = 54.6 Hz, P*C*H$(CH_3)_2$), 24.56 (s, Pipp-CH(*C*H$_3)_2$), 16.43 (s, PCH(*C*H$_3)_2$), 16.08 (s, PCH(*C*H$_3)_2$). ^{29}Si{^{1}H} NMR (59.63 MHz, benzene-d_6): δ –26.3 (s). ^{31}P{^{1}H} NMR (283.42 MHz, benzene-d_6): δ 64.3 (s).

6.4 X-Ray Crystallography Data Tables

Table 7 Summary of X-ray crystallographic data collection and structure refinement ^{Pipp}LIr(COD), ^{Dipp}LIr(COD), and ^{Mes}LIr(COD)

	^{Pipp}LIr(COD)[80]	**^{Dipp}LIr(COD)**	**^{Mes}LIr(COD)**
Empirical formula	$C_{42}H_{64}IrN_3P_2$	$C_{48}H_{76}IrN_3P_2$	$C_{42}H_{64}IrN_3P_2$
Formula weight	865.10	949.25	865.10
Crystal Colour	Yellow	Yellow	Yellow
Temperature/K	100.0(3)	99.99(10)	100.02(10)
Crystal system	monoclinic	monoclinic	monoclinic
Space group	Pn	$P2_1/n$	$P2_1/n$
a/Å	11.34430(10)	20.4688(5)	12.0627(4)
b/Å	12.64700(10)	10.4236(2)	25.3267(9)
c/Å	15.20090(10)	23.1356(5)	14.9335(5)
α/°	90	90	90
β/°	111.3820(10)	104.776(2)	91.731(3)
γ/°	90	90	90
Volume/Å^3	2030.78(3)	4772.94(19)	4560.2(3)
Z	2	4	4
ρ_{calc}g/cm^3	1.415	1.321	1.260
μ/mm^{-1}	7.337	2.898	3.026
F(000)	888.0	1968.0	1776.0
Crystal size/mm^3	—	0.14 × 0.12 × 0.07	0.13 × 0.07 × 0.05
Radiation	Cu Kα (λ = 1.54184)	Mo Kα (λ = 0.71073)	Mo Kα (λ = 0.71073)
2Θ range for data collection/°	6.99 to 159.84	4.116 to 76.804	4.218 to 67.484

Index ranges	$-14 \leq h \leq 14$, $-15 \leq k \leq 14$, $-19 \leq l \leq 18$	$-34 \leq h \leq 34$, $-17 \leq k \leq 17$, $-39 \leq l \leq 39$	$-18 \leq h \leq 18$, $-38 \leq k \leq 34$, $-22 \leq l \leq 20$
Reflections collected	32367	126737	75730
Independent reflections	8427 [R_{int} = 0.0420, R_{sigma} = 0.0376]	24664 [R_{int} = 0.0570, R_{sigma} = 0.0505]	15775 [R_{int} = 0.0800, R_{sigma} = 0.0757]
Data/restraints/parameters	8427/2/441	24664/0/503	15775/1/458
Goodness-of-fit on F^2	1.059	1.016	1.027
Final R indexes [I>=2σ (I)]	R_1 = 0.0308, wR_2 = 0.0835	R_1 = 0.0334, wR_2 = 0.0640	R_1 = 0.0557, wR_2 = 0.1318
Final R indexes [all data]	R_1 = 0.0318, wR_2 = 0.0843	R_1 = 0.0508, wR_2 = 0.0678	R_1 = 0.0800, wR_2 = 0.1406
Largest diff. peak/hole / e $Å^{-3}$	1.24/-0.87	2.09/-0.62	6.00/-1.40
Flack Parameter	-0.027(6)	—	—

Table 8 Summary of X-ray crystallographic data collection and structure refinement ^{Pipp}LIr(H)($SiPh_2H$), ^{Pipp}LIr(H)($SiEt_3$), and ^{Pipp}LIr(CO)$_2$

	^{Pipp}LIr(H)($SiPh_2H$)	**^{Pipp}LIr(H)($SiEt_3$)**	**^{Pipp}LIr(CO)$_2$**
Empirical formula	$C_{46}H_{62}IrN_3P_2Si$	$C_{42.5}H_{74}IrN_3P_2Si$	$C_{36}H_{52}IrN_3O_2P_2$
Formula weight	939.21	909.27	812.94
Crystal Colour	Red	Red	Colourless
Temperature/K	99.98(18)	100.00(11)	100.01(10)
Crystal system	monoclinic	monoclinic	triclinic

Space group	P2/c	$P2_1/c$	P-1
a/Å	16.2864(4)	28.1401(2)	8.1033(2)
b/Å	13.3716(3)	16.65370(10)	10.0910(4)
c/Å	20.6221(4)	20.3001(2)	23.1297(6)
α/°	90	90	80.268(3)
β/°	91.581(2)	106.0490(10)	85.027(2)
γ/°	90	90	75.387(3)
Volume/Å^3	4489.27(17)	9142.59(13)	1801.88(10)
Z	4	8	2
ρ_{calc}g/cm^3	1.390	1.321	1.498
μ/mm^{-1}	3.106	6.783	3.828
F(000)	1920.0	3768.0	824.0
Crystal size/mm^3	0.18 × 0.09 × 0.08	0.19 × 0.13 × 0.11	0.13 × 0.1 × 0.05
Radiation	Mo Kα (λ = 0.71073)	Cu Kα (λ = 1.54184)	Mo Kα (λ = 0.71073)
2Θ range for data collection/°	3.942 to 76.588	6.232 to 149.964	4.83 to 67.676
Index ranges	$-27 \le h \le 27$, $-23 \le k \le 22$, $-35 \le l \le 34$	$-31 \le h \le 35$, $-20 \le k \le 19$, $-22 \le l \le 25$	$12 \le h \le 12$, $-15 \le k \le 15$, $-34 \le l \le 34$
Reflections collected	117597	90240	56015
Independent reflections	23029 [R_{int} = 0.0496, R_{sigma} = 0.0461]	18505 [R_{int} = 0.0402, R_{sigma} = 0.0293]	12577 [R_{int} = 0.0485, R_{sigma} = 0.0512]
Data/restraints/parameters	23029/1/511	18505/0/932	12577/2/419

Goodness-of-fit on F^2	1.018	1.041	1.008
Final R indexes [I>=2σ (I)]	R_1 = 0.0331, wR_2 = 0.0630	R_1 = 0.0261, wR_2 = 0.0581	R_1 = 0.0342, wR_2 = 0.0675
Final R indexes [all data]	R_1 = 0.0554, wR_2 = 0.0678	R_1 = 0.0302, wR_2 = 0.0595	R_1 = 0.0462, wR_2 = 0.0705
Largest diff. peak/hole / e $Å^{-3}$	1.88/-0.63	0.72/-0.96	1.46/-1.01

Table 9 Summary of X-ray crystallographic data collection and structure refinement $[Li]^+[(COD)Ir(Me)_2]^-$ and $(COD)Ir(Me)(C_3H_4(NMes)_2)$

	$[Li]^+[(COD)Ir(Me)_2]^-$	**$(COD)Ir(Me)(C_3H_4(NMes)_2)$**
Empirical formula	$C_{20}H_{36}Ir_2Li_2$	$C_{30}H_{41}IrN_2$
Formula weight	674.77	621.85
Crystal Colour	Orange	Red
Temperature/K	100.00(10)	100.00(10)
Crystal system	triclinic	monoclinic
Space group	P-1	$P2_1/c$
a/Å	8.2618(4)	15.2343(2)
b/Å	14.2802(5)	11.8913(2)
c/Å	18.0673(7)	14.9553(2)
α/°	72.522(3)	90
β/°	83.810(4)	105.900(2)
γ/°	76.625(4)	90
Volume/$Å^3$	1976.34(15)	2605.58(7)

Z	4	4
ρ_{calc}g/cm^3	2.268	1.585
μ/mm^{-1}	25.630	10.051
F(000)	1264.0	1248.0
Crystal size/mm^3	0.169 × 0.066 × 0.043	0.09 × 0.06 × 0.03
Radiation	Cu Kα (λ = 1.54184)	Cu Kα (λ = 1.54184)
2Θ range for data collection/°	6.638 to 150.018	6.032 to 160.572
Index ranges	-10 ≤ h ≤ 10, -17 ≤ k ≤ 17, -22 ≤ l ≤ 22	-19 ≤ h ≤ 19, -15 ≤ k ≤ 15, -16 ≤ l ≤ 19
Reflections collected	32072	26094
Independent reflections	7872 [R_{int} = 0.0626, R_{sigma} = 0.0490]	5682 [R_{int} = 0.0481, R_{sigma} = 0.0384]
Data/restraints/parameters	7872/642/441	5682/0/305
Goodness-of-fit on F^2	1.100	1.074
Final R indexes [I>=2σ (I)]	R_1 = 0.0494, wR_2 = 0.1356	R_1 = 0.0358, wR_2 = 0.0947
Final R indexes [all data]	R_1 = 0.0628, wR_2 = 0.1430	R_1 = 0.0403, wR_2 = 0.0977
Largest diff. peak/hole / e Å^{-3}	2.72/-3.18	1.36/-1.87

REFERENCES

1. 26 - Cobalt, Rhodium and Iridium. In *Chemistry of the Elements (Second Edition)*, Greenwood, N. N.; Earnshaw, A., Eds. Butterworth-Heinemann: Oxford, 1997; pp 1113-1143.

2. Vaska, L.; DiLuzio, J. W. *J. Am. Chem. Soc.* **1961**, *83*, 2784-2785.

3. Vaska, L.; DiLuzio, J. W. *J. Am. Chem. Soc.* **1962**, *84*, 679-680.

4. Polukeev, A. V.; Wendt, O. F. *J. Organomet. Chem.* **2018**, *867*, 33-50.

5. Bézier, D.; Brookhart, M., Transfer Dehydrogenations of Alkanes and Related Reactions Using Iridium Pincer Complexes. In *C-H Bond Activation and Catalytic Functionalization II*, Dixneuf, P. H.; Doucet, H., Eds. Springer International Publishing: Cham, 2016; pp 189-207.

6. Biswas, S.; Huang, Z.; Choliy, Y.; Wang, D. Y.; Brookhart, M.; Krogh-Jespersen, K.; Goldman, A. S. *J. Am. Chem. Soc.* **2012**, *134*, 13276-13295.

7. Choi, J.; MacArthur, A. H. R.; Brookhart, M.; Goldman, A. S. *Chem. Rev.* **2011**, *111*, 1761-1779.

8. Lawrence, M. A. W.; Green, K.-A.; Nelson, P. N.; Lorraine, S. C. *Polyhedron* **2018**, *143*, 11-27.

9. Kasera, A.; Biswas, J. P.; Ali Alshehri, A.; Ahmed Al-Thabaiti, S.; Mokhtar, M.; Maiti, D. *Coord. Chem. Rev.* **2023**, *475*, 214915.

10. Shafiei-Haghighi, S.; Singer, L. M.; Tamang, S. R.; Findlater, M. *Polyhedron* **2018**, *143*, 126-131.

11. Haenel, M. W.; Oevers, S.; Angermund, K.; Kaska, W. C.; Fan, H.-J.; Hall, M. B. *Angew. Chem. Int. Ed.* **2001**, *40*, 3596-3600.

12. Calimano, E.; Tilley, T. D. *Dalton Trans.* **2010**, *39*, 9250-9263.

13. Segawa, Y.; Yamashita, M.; Nozaki, K. *Organometallics* **2009**, *28*, 6234-6242.

14. Gupta, M.; Hagen, C.; Flesher, R. J.; Kaska, W. C.; Jensen, C. M. *Chem. Commun.* **1996**, 2083-2084.

15. Kundu, S.; Choliy, Y.; Zhuo, G.; Ahuja, R.; Emge, T. J.; Warmuth, R.; Brookhart, M.; Krogh-Jespersen, K.; Goldman, A. S. *Organometallics* **2009**, *28*, 5432-5444.

16. Rath, S. P.; Sengupta, D.; Ghosh, P.; Bhattacharjee, R.; Chakraborty, M.; Samanta, S.; Datta, A.; Goswami, S. *Inorg. Chem.* **2018**, *57*, 11995-12009.

17. Manzano, R. A.; Young, R. D. *Coord. Chem. Rev.* **2021**, *449*, 214215.

18. Maser, L.; Vondung, L.; Langer, R. *Polyhedron* **2018**, *143*, 28-42.

19. Kanzelberger, M.; Zhang, X.; Emge, T. J.; Goldman, A. S.; Zhao, J.; Incarvito, C.; Hartwig, J. F. *J. Am. Chem. Soc.* **2003**, *125*, 13644-13645.

20. Doyle, L. E.; Piers, W. E.; Borau-Garcia, J. *J. Am. Chem. Soc.* **2015**, *137*, 2187-2190.

21. Laviska, D. A.; Zhou, T.; Kumar, A.; Emge, T. J.; Krogh-Jespersen, K.; Goldman, A. S. *Organometallics* **2016**, *35*, 1613-1623.

22. Allen, K. E.; Heinekey, D. M.; Goldman, A. S.; Goldberg, K. I. *Organometallics* **2013**, *32*, 1579-1582.

23. Allen, K. E.; Heinekey, D. M.; Goldman, A. S.; Goldberg, K. I. *Organometallics* **2014**, *33*, 1337-1340.

24. Cheng, C.; Kim, B. G.; Guironnet, D.; Brookhart, M.; Guan, C.; Wang, D. Y.; Krogh-Jespersen, K.; Goldman, A. S. *J. Am. Chem. Soc.* **2014**, *136*, 6672-6683.

25. McBee, J. L.; Tilley, T. D. *Organometallics* **2009**, *28*, 5072-5081.

26. Parmentier, M.; Hartung, T.; Pfaltz, A.; Muri, D. *Chem - Eur. J.* **2014**, *20*, 11496-11504.

27. Nishimura, T. *Chem. Rec.* **2021**, *21*, 3532-3545.

28. Biya, E.; Neetha, M.; Anilkumar, G. *ChemistrySelect* **2021**, *6*, 10127-10140.

29. Bell, J. D.; Murphy, J. A. *Chem. Soc. Rev.* **2021**, *50*, 9540-9685.

30. Lee, C.-I.; DeMott, J. C.; Pell, C. J.; Christopher, A.; Zhou, J.; Bhuvanesh, N.; Ozerov, O. V. *Chem. Sci.* **2015**, *6*, 6572-6582.

31. Bary, G.; Jamil, M. I.; Arslan, M.; Ghani, L.; Ahmed, W.; Ahmad, H.; Zaman, G.; Ayub, K.; Sajid, M.; Ahmad, R.; Huang, D.; Liu, F.; Wang, Y. *J. Saudi Chem. Soc.* **2021**, *25*, 101260.

32. Functionalization of alkenes. In *Modern Methods of Organic Synthesis*, 4 ed.; Coldham, I.; Carruthers, W., Eds. Cambridge University Press: Cambridge, 2004; pp 315-369.

33. Kumar, A.; Goldman, A. S., Recent Advances in Alkane Dehydrogenation Catalyzed by Pincer Complexes. In *The Privileged Pincer-Metal Platform: Coordination Chemistry & Applications*, van Koten, G.; Gossage, R. A., Eds. Springer International Publishing: Cham, 2016; pp 307-334.

34. Fang, H.; Liu, G.; Huang, Z., Chapter 18 - Pincer Iridium and Ruthenium Complexes for Alkane Dehydrogenation. In *Pincer Compounds*, Morales-Morales, D., Ed. Elsevier: 2018; pp 383-399.

35. Yao, W.; Jia, X.; Leng, X.; Goldman, A. S.; Brookhart, M.; Huang, Z. *Polyhedron* **2016**, *116*, 12-19.

36. Crabtree, R. H.; Mihelcic, J. M.; Quirk, J. M. *J. Am. Chem. Soc.* **1979**, *101*, 7738-7740.

37. Baudry, D.; Ephritikhine, M.; Felkin, H. *J. Chem. Soc., Chem. Commun.* **1980**, 1243-1244.

38. Felkin, H.; Fillebeen-Khan, T.; Gault, Y.; Holmes-Smith, R.; Zakrzewski, J. *Tetrahedron Lett.* **1984**, *25*, 1279-1282.

39. Xu, W.-w.; P. Rosini, G.; Krogh-Jespersen, K.; S. Goldman, A.; Gupta, M.; M. Jensen, C.; C. Kaska, W. *Chem. Commun.* **1997**, 2273-2274.

40. Liu, F.; S. Goldman, A. *Chem. Commun.* **1999**, 655-656.

41. Punji, B.; Emge, T. J.; Goldman, A. S. *Organometallics* **2010**, *29*, 2702-2709.

42. Shi, Y.; Suguri, T.; Dohi, C.; Yamada, H.; Kojima, S.; Yamamoto, Y. *Chem - Eur. J.* **2013**, *19*, 10672-10689.

43. Göttker-Schnetmann, I.; White, P. S.; Brookhart, M. *Organometallics* **2004**, *23*, 1766-1776.

44. Yao, W.; Zhang, Y.; Jia, X.; Huang, Z. *Angew. Chem. Int. Ed.* **2014**, *53*, 1390-1394.

45. Nakayama, S.; Morisako, S.; Yamashita, M. *Organometallics* **2018**, *37*, 1304-1313.

46. Gordon, B. M.; Lease, N.; Emge, T. J.; Hasanayn, F.; Goldman, A. S. *J. Am. Chem. Soc.* **2022**, *144*, 4133-4146.

47. Calimano, E.; Tilley, T. D. *J. Am. Chem. Soc.* **2008**, *130*, 9226-9227.

48. Corre, Y.; Rysak, V.; Trivelli, X.; Agbossou-Niedercorn, F.; Michon, C. *Eur. J. Org. Chem.* **2017**, *2017*, 4820-4826.

49. Shinohara, K.; Kawabata, S.; Nakamura, H.; Manabe, Y.; Sakaguchi, S. *Eur. J. Org. Chem.* **2014**, *2014*, 5532-5539.

50. Park, S.; Brookhart, M. *Organometallics* **2010**, *29*, 6057-6064.

51. Uvarov, V. M.; de Vekki, D. A. *J. Organomet. Chem.* **2020**, *923*, 121415.

52. Morris, R. H. *Chem. Soc. Rev.* **2009**, *38*, 2282-2291.

53. Matsumura, Y.; Ogura, K.; Kouchi, Y.; Iwasaki, F.; Onomura, O. *Org. Lett.* **2006**, *8*, 3789-3792.

54. Xie, X.; Zhang, X.; Yang, H.; Ji, X.; Li, J.; Ding, S. *J. Org. Chem.* **2019**, *84*, 1085-1093.

55. Pérez-Torrente, J. J.; Nguyen, D. H.; Jiménez, M. V.; Modrego, F. J.; Puerta-Oteo, R.; Gómez-Bautista, D.; Iglesias, M.; Oro, L. A. *Organometallics* **2016**, *35*, 2410-2422.

56. Troegel, D.; Stohrer, J. *Coord. Chem. Rev.* **2011**, *255*, 1440-1459.

57. Riener, K.; Meister, T. K.; Gigler, P.; Herrmann, W. A.; Kühn, F. E. *J. Catal.* **2015**, *331*, 203-209.

58. Chalk, A. J.; Harrod, J. F. *J. Am. Chem. Soc.* **1965**, *87*, 16-21.

59. Sakaki, S.; Mizoe, N.; Sugimoto, M. *Organometallics* **1998**, *17*, 2510-2523.

60. Xie, X.; Zhang, X.; Gao, W.; Meng, C.; Wang, X.; Ding, S. *Commun. Chem.* **2019**, *2*, 101.

61. Wang, D.; Lai, Y.; Wang, P.; Leng, X.; Xiao, J.; Deng, L. *J. Am. Chem. Soc.* **2021**, *143*, 12847-12856.

62. Chianese, A. R.; Mo, A.; Datta, D. *Organometallics* **2009**, *28*, 465-472.

63. Nishibayashi, Y.; Segawa, K.; Takada, H.; Ohe, K.; Uemura, S. *Chem. Commun.* **1996**, 847-848.

64. Frölander, A.; Moberg, C. *Org. Lett.* **2007**, *9*, 1371-1374.

65. Chen, L.; Liu, Y.; Hou, G.; Song, H.; Zi, G. *Inorg. Chem. Commun.* **2013**, *29*, 141-144.

66. Cheng, C.; Brookhart, M. *J. Am. Chem. Soc.* **2012**, *134*, 11304-11307.

67. Corre, Y.; Werlé, C.; Brelot-Karmazin, L.; Djukic, J.-P.; Agbossou-Niedercorn, F.; Michon, C. *J. Mol. Catal. A: Chem.* **2016**, *423*, 256-263.

68. Faller, J. W.; Chase, K. J. *Organometallics* **1994**, *13*, 989-992.

69. Chen, T.; Liu, X.-G.; Shi, M. *Tetrahedron* **2007**, *63*, 4874-4880.

70. Johnson, K. R. D.; Hayes, P. G. *Organometallics* **2009**, *28*, 6352-6361.

71. Johnson, K. R. D.; Hannon, M. A.; Ritch, J. S.; Hayes, P. G. *Dalton Trans.* **2012**, *41*, 7873-7875.

72. Johnson, K. R. D.; Hayes, P. G. *Inorg. Chim. Acta* **2014**, *422*, 209-217.

73. Zamora, M. T.; Johnson, K. R. D.; Hänninen, M. M.; Hayes, P. G. *Dalton Trans.* **2014**, *43*, 10739-10750.

74. Webb, D.; Hayes, P., On the Coordination Chemistry of Bis- and Trisphosphinimine Containing Ligands. In *Comprehensive Coordination Chemistry III*, 2021; Vol. 1, pp 131-157.

75. Wheaton, C. A.; Hayes, P. G. *Catal. Sci. Technol.* **2012**, *2*, 125-138.

76. Hänninen, M. M.; Zamora, M. T.; MacNeil, C. S.; Knott, J. P.; Hayes, P. G. *Chem. Commun.* **2016**, *52*, 586-589.

77. MacNeil, C. S.; Glynn, K. E.; Hayes, P. G. *Organometallics* **2018**, *37*, 3248-3252.

78. MacNeil, C. S.; Hayes, P. G. *Eur. J. Chem.* **2019**, *25*, 8203-8207.

79. Cinellu, M. A.; Minghetti, G.; Cocco, F.; Stoccoro, S.; Zucca, A.; Manassero, M.; Arca, M. *Dalton Trans.* **2006**, 5703-5716.

80. MacNeil, C. S., Aborawi, A.A., Hayes, P.G. *Unpublished results*.

81. Yang, L.; Powell, D. R.; Houser, R. P. *Dalton Trans.* **2007**, 955-964.

82. Chisholm, D. T.; Hayes, P. G. *New J. Chem.* **2021**, *45*, 15043-15052.

83. Grushin, V. V. *Acc. Chem. Res.* **1993**, *26*, 279-286.

84. Viciano, M.; Poyatos, M.; Sanaú, M.; Peris, E.; Rossin, A.; Ujaque, G.; Lledós, A. *Organometallics* **2006**, *25*, 1120-1134.

85. Leis, W.; Wernitz, S.; Reichart, B.; Ruckerbauer, D.; Wielandt, J. W.; Mayer, H. A. *Dalton Trans.* **2014**, *43*, 12187-12199.

86. Lee, H.-B.; Maitlis, P. M. *J. Chem. Soc., Chem. Commun.* **1974**, 601-602.

87. Brayton, D. F.; Beaumont, P. R.; Fukushima, E. Y.; Sartain, H. T.; Morales-Morales, D.; Jensen, C. M. *Organometallics* **2014**, *33*, 5198-5202.

88. Martell, A. E., The Chelate Effect. In *Werner Centennial*, AMERICAN CHEMICAL SOCIETY: 1967; Vol. 62, pp 272-294.

89. Saikia, K.; Deb, B.; Dutta, D. K. *J. Mol. Catal. A: Chem.* **2014**, *381*, 188-193.

90. Brill, M.; Marrwitz, D.; Rominger, F.; Hofmann, P. *J. Organomet. Chem.* **2015**, *775*, 137-151.

91. Chen, F.; Sun, J.-F.; Li, T.-Y.; Chen, X.-T.; Xue, Z.-L. *Organometallics* **2011**, *30*, 2006-2011.

92. Smith, J. D.; Logan, J. R.; Doyle, L. E.; Burford, R. J.; Sugawara, S.; Ohnita, C.; Yamamoto, Y.; Piers, W. E.; Spasyuk, D. M.; Borau-Garcia, J. *Dalton Trans.* **2016**, *45*, 12669-12679.

93. Babbini, D. C.; Iluc, V. M. *Organometallics* **2015**, *34*, 3141-3151.

94. Choualeb, A.; Lough, A. J.; Gusev, D. G. *Organometallics* **2007**, *26*, 5224-5229.

95. Polukeev, A. V.; Marcos, R.; Ahlquist, M. S. G.; Wendt, O. F. *Eur. J. Chem.* **2016**, *22*, 4078-4086.

96. Riehl, J. F.; Jean, Y.; Eisenstein, O.; Pelissier, M. *Organometallics* **1992**, *11*, 729-737.

97. Krogh-Jespersen, K.; Czerw, M.; Summa, N.; Renkema, K. B.; Achord, P. D.; Goldman, A. S. *J. Am. Chem. Soc.* **2002**, *124*, 11404-11416.

98. McBee, J. L.; Escalada, J.; Tilley, T. D. *J. Am. Chem. Soc.* **2009**, *131*, 12703-12713.

99. Karshtedt, D.; Bell, A. T.; Tilley, T. D. *Organometallics* **2006**, *25*, 4471-4482.

100. Bruno, I. J., Cole, J. C., Edgington, P. R., Kessler, M., Macrae, C. F., McCabe, P., Pearson, J., Taylor, R. *Acta. Cryst. B.* **2002**, 389-397.

101. Leonard, N. G.; Williard, P. G.; Bernskoetter, W. H. *Dalton Trans.* **2011**, *40*, 4300-4306.

102. Lee, D. W.; Jensen, C. M.; Morales-Morales, D. *Organometallics* **2003**, *22*, 4744-4749.

103. Smith, J. D.; Chih, E.; Piers, W. E.; Spasyuk, D. M. *Polyhedron* **2018**, *155*, 281-290.

104. Hsiang, S.-J.; Hayes, P. G. *Unpublished results*.

105. Bennett, M. A.; Latten, J. L.; Ayers, L. J.; Thorn, D. L., An Iridium(III) Complex Containing Cyclometallated Triphenylphosphine Formed by Isomerization of an Iridium(I) Triphenylphosphine Complex. In *Inorg. Synth.*, 1989; pp 200-203.

106. Kulzick, M. A.; Andersen, R. A.; Muetterties, E. L.; Day, V. W. *J. Organomet. Chem.* **1987**, *336*, 221-236.

107. Huang, M.-H.; Zou, X.-R.; Liang, L.-C. *J. Chin. Chem. Soc.* **2020**, *67*, 353-360.

108. Sato, K.; Komuro, T.; Osawa, T.; Hashimoto, H.; Tobita, H. *Organometallics* **2022**, *41*, 2612-2621.

109. Weller, M.; Weller, M. T.; Overton, T.; Rourke, J.; Armstrong, F., *Inorg. Chem.* OUP Oxford: 2014.

110. Crabtree, R. H.; Mellea, M. F.; Mihelcic, J. M.; Quirk, J. M. *J. Am. Chem. Soc.* **1982**, *104*, 107-113.

111. Bantu, B.; Wurst, K.; Buchmeiser, M. R. *J. Organomet. Chem.* **2007**, *692*, 5272-5278.

112. Calimano, E.; Tilley, T. D. *Organometallics* **2010**, *29*, 1680-1692.

113. Calimano, E.; Tilley, T. D. *J. Am. Chem. Soc.* **2009**, *131*, 11161-11173.

114. Jover, J.; Cirera, J. *Dalton Trans.* **2019**, *48*, 15036-15048.

115. Meredith, J. M.; Robinson, R., Jr.; Goldberg, K. I.; Kaminsky, W.; Heinekey, D. M. *Organometallics* **2012**, *31*, 1879-1887.

116. Zuo, W.; Braunstein, P. *Organometallics* **2012**, *31*, 2606-2615.

117. Suginome, M.; Ito, Y., Activation of Si—Si Bonds by Transition-Metal Complexes. In *Activation of Unreactive Bonds and Organic Synthesis*, Murai, S.; Alper, H.; Gossage, R. A.; Grushin, V. V.; Hidai, M.; Ito, Y.; Jones, W. D.; Kakiuchi, F.; van Koten, G.; Lin, Y. S.; Mizobe, Y.; Murai, S.; Murakami, M.; Richmond, T. G.; Sen, A.; Suginome, M.; Yamamoto, A., Eds. Springer Berlin Heidelberg: Berlin, Heidelberg, 1999; pp 131-159.

118. Suginome, M.; Ito, Y. *Chem. Rev.* **2000**, *100*, 3221-3256.

119. Beletskaya, I.; Moberg, C. *Chem. Rev.* **2006**, *106*, 2320-2354.

120. Richers, C. P.; Roediger, S.; Laserna, V.; Hartwig, J. F. *Chem Sci* **2020**, *11*, 10449-10456.

121. Camerano, J. A.; Sämann, C.; Wadepohl, H.; Gade, L. H. *Organometallics* **2011**, *30*, 379-382.

122. Melen, R. L.; Gade, L. H., New Chemistry with Anionic NNN Pincer Ligands. In *The Privileged Pincer-Metal Platform: Coordination Chemistry & Applications*, van

Koten, G.; Gossage, R. A., Eds. Springer International Publishing: Cham, 2016; pp 179-208.

123. Sebest, F.; Lachhani, K.; Pimpasri, C.; Casarrubios, L.; White, A. J. P.; Rzepa, H. S.; Díez-González, S. *Adv. Synth. Catal.* **2020**, *362*, 1877-1886.

124. Barral, K.; Moorhouse, A. D.; Moses, J. E. *Org. Lett.* **2007**, *9*, 1809-1811.

125. Cotton, F. A.; Lahuerta, P.; Sanau, M.; Schwotzer, W. *Inorg. Chim. Acta* **1986**, *120*, 153-157.

126. Kuhn, K. M.; Grubbs, R. H. *Org. Lett.* **2008**, *10*, 2075-2077.

127. CrysAlisPRO. **2010**, Oxford Diffraction/Agilent Technologies UK Ltd, Yarnton, England.

128. Sheldrick, G. M. *Acta. Cryst. C.* **2015**, 3-8.

129. Sheldrick, G. M. *Acta. Cryst. A.* **2015**, 3-8.

130. O. V. Dolomanov, L. J. B., R. J. Gildea, J. A. K. Howard and H. Puschmann. *J. Appl. Cryst.* **2009**, 339-341.

131. C. F. Macrae, I. S., S. J. Cottrell, P. T. A. Galek, P. McCabe, E. Pidcock, M. Platings, G. P. Shields, J. S. Stevens, M. Towler and P. A. Wood. *J. Appl. Cryst.* **2020**, 226-235.